Effect of boundaries on swimming of *Paramecium multimicronucleatum*

Saikat Jana

Dissertation submitted to faculty of
Virginia Polytechnic Institute and State University
in partial fulfillment of the requirements for the degree of

Doctor of Philosophy
in
Engineering Mechanics

Sunghwan Jung, Chairman
John J. Socha
Mark A. Stremler
Mark R. Paul
Pavlos P. Vlachos

June 27, 2013
Blacksburg, Virginia

Keywords: micro-swimmers, locomotion, *Paramecium*, ciliates, Stokes flow.

Abstract

Microorganisms swimming in their natural habitat interact with debris and boundaries, which can modify their swimming characteristics. However, the boundary effect on swimming microorganisms have not been completely understood yet, and is one of most active areas of research. Amongst microorganisms, unicellular ciliates are the fastest swimmers and also respond to a variety of external cues. We choose *Paramecium multimicronucleatum* as a model system to understand the locomotion of ciliates.

First, we explore the effects of boundaries on swimming modes of *Paramecium multimicronucleatum* by introducing them in 2D films and 1D channels. The geometric confinements cause the *Paramecia* to transition between: a directed, a meandering and a self-bending behaviors. During the self-bending mode the cell body exerts forces on the walls; which is quantified by using a beam bending analogy and measuring the elasticity of the cell body. The first investigation reveals the complicated swimming patterns of *Paramecium* caused by boundaries.

In the second study we investigate the directed swimming of *Paramecium* in cylindrical capillaries, which mimics the swimming of ciliates in the pores of soil. A finite-sized cell locomoting in extreme confinements creates a pressure gradient across its ends. By developing a modified envelop model incorporating the confinements and pressure gradient effects, we are able to predict the swimming speed of the organisms in confined channels.

Finally we study how *Paramecium* can swim and feed efficiently by stirring the fluid around its body. We experimentally employ μ-Particle Image Velocimetry to characterize flows around the freely swimming *Parameicum* and numerically use Boundary Element Method to quantify the effect of body shapes on the swimming and feeding process. Results show that

the body shape of *Paramecium* (slender anterior and bulky posterior) is hydrodynamically optimized to swim as well as feed efficiently.

The dissertation makes significant advances in both experimentally characterizing and theoretically understanding the flow field and locomotion patterns of ciliates near solid boundaries.

Dedicated to Maa, Baba and Chiku

Acknowledgement

I would like to express my sincere thanks to Dr. Jung for taking me under his guidance and introducing me to the world of microscale locomotion. His guidance, encouragement and enthusiasm is the reason behind my successful investigations. I have vivid memories of my early days when he explained the theory behind Taylor's swimming sheet step by step to me and numerous discussions that we had in his office. I have been extremely lucky to have him as my advisor and mentor. No words can express my gratitude for him, that I feel in my heart.

I would like to thank Dr. Stremler, Dr. Socha, Dr. Paul and Dr. Vlachos for being in my committee and providing constructive comments on my work. I am grateful for your help and guidance during the different stages of my PhD work. I am grateful to Dr. Vlachos for asking me the challenging questions and providing guidance (with Dr. Jung) which led to completion of Chapter 5.

I have had the opportunity to work with many intelligent individuals during my research work. Matthew Giarra helped me with the data acquisition and analysis for the Particle Image Velocimetry project. Zhenning Cao, Suvojit Ghosh and Aschvin Chawan helped me trap *Paramecia* in drops and channels, in different collaborative projects. All of you have taught me many things; especially running experiments with precision, patience and laugh at the end of the day. A big thanks to Peng Zhang who ran simulations and provided me with the basis for comparing my experimental data.

Members of BIFLab Peng, Sean, Navish, Daniel and Brian, thank you for the lively atmosphere in the lab and the fun moments we had. My friends outside the lab: Suvojit, Souvick Chatterjee, Basu, Udit, Anupam, Wrik, Ravi; thanks for jokes and the late night rides. Thanks to my roommate Rohit and his girlfriend Swathi for the delicious food and

the lively discussions at the end of a tiring day.

A big hug to my parents and my brother Akash. All of you have constantly showered me with praises and encouragements in the most difficult of times and kept my confidence up. Mom and dad; you are the reason for me being successful, and I am truly grateful for all your affection. Thanks to Akash for reading my dissertation and commenting on it at such short notice. My grandfather late Basanta Kumar Jana and my uncle late Dhirendra Nath Samanta; I hope you are proud of my achievements and smiling from the heavens.

Contents

List of Figures

List of Tables

Chapter 1

Introduction

1.1 Microorganisms and the environment

The environment around us abounds a wide array of microorganisms; many of which innocuously cohabit with humans. They influence our life and ecosystem in different ways, for example phytoplanktons operate the biological pump [1] which helps in carbon fixation from atmosphere thereby redcuing the concentration of carbon dioxide from the the atmosphere, large masses of bacteria form biofilms on surfaces [10] that are very hard to clean or group of planktons exhibit blooms [1] or may cause seasonal red tides in estuaries or rivers[11] that may or may not be harmful to the ecosystem (Figure 1.1) .

1.2 Classification of Life

Typically all life can be classified into three domains Archea, Bacteria and Eukarya [12]. Archea refers to a class of single celled ancient bacteria supposedly from which most of the

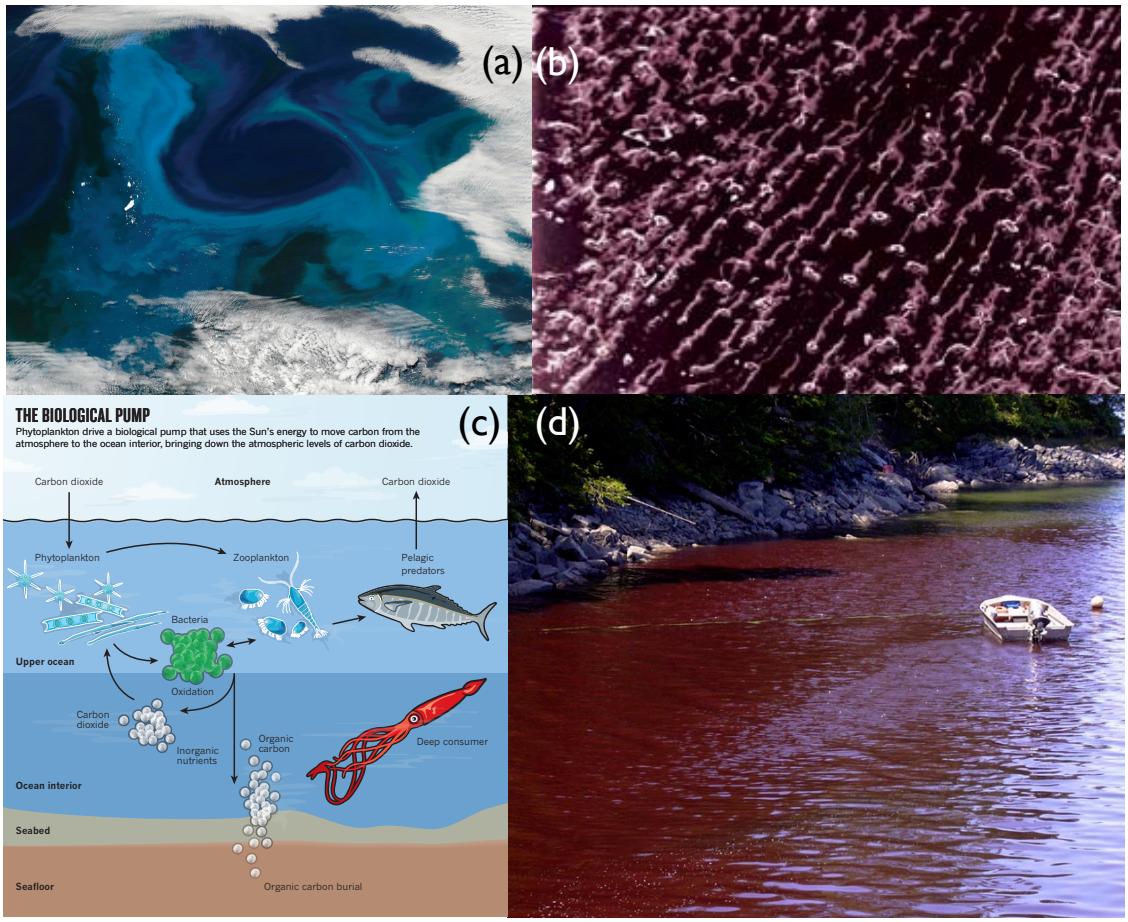

Figure 1.1: Images that describe how microorganisms affect our life. (a) Shows the phytoplankton bloom as seen from outer space through a cloud cover. (Taken from [1] with permissions from Nature Publishing Group) (b) Shows a bacterial biofilm formed in a high shear environment. Taken from [2] (with permission from Nature Publishing Group)(c) Shows a cartoon of the biological pump involving a variety of sea dwelling organisms. Taken from [1] (with permission from Nature Publishing Group) (d) Shows the red tide formed due to rapid growth and accumulation of the ciliate *Myrionecta rubra* in the Columbia river estuary during autumn season. Image courtesy of Stewards of George Harbor Society.

current life-forms have evolved. They are characterized by a rigid cell wall and contain no nuclei or membrane bound organelles and were able to live in the extremely hazardous environment [13].

Bacteria lack a nucleus or any other membrane bound organelle and have their intercellular

contents surrounded by a rigid cell wall[1]. They are unicellular and are vital for many nutrient cycles, and can also cause diseases within humans. These single cells represent the first step in evolution of larger multicellular organisms and hence present a key to understand the evolution of biological complexity.

Eukaryotes usually have a prominent micronucleus and several micronuclei which encapsulate their nuclear material and are much larger than the bacteria. Their outer covering is usually referred to as cytoskeleton which provides shape to the cell body which consists a complicated network of microtubules, microfilaments and intermediate filaments. Some of them are unicellular like *Paramecium* or *Chlamydomonas* while others are multi-cellular like *Volvox carteri* and their average size ranges from few microns to millimeter.

1.3 Introduction to *Paramecium*

Paramecium is a unicellular eukaryote commonly found in the freshwater ponds at the soil-water or water-air interface; especially near the ones that are close to decaying matter. They are divided into two different groups based on their body shape [14]: (a) The *aurelia* group which is characterized by a long slender body with almost a circular cross section and includes *P. aurelia*, *P. caudatum*, *P. multimicronucleatum* etc. In contrast (b) the *bursaria* species are known for its wide bodies and comparatively shorter lengths, e.g. *P. bursaria*, *P. trichium* .

Paramecium multimicronucleatum is the largest and fastest amongst the *aurelia* group and is easy to culture in the laboratory and handle thereby making it suitable for experimentation. Owing to its excitable membrane and high density of genetic material in the micronucleus it is a commonly used for research [15]. The organism is shaped roughly like that of a prolate

[1]before 1960 Bacteria and Archea were classified together as Prokaryotes

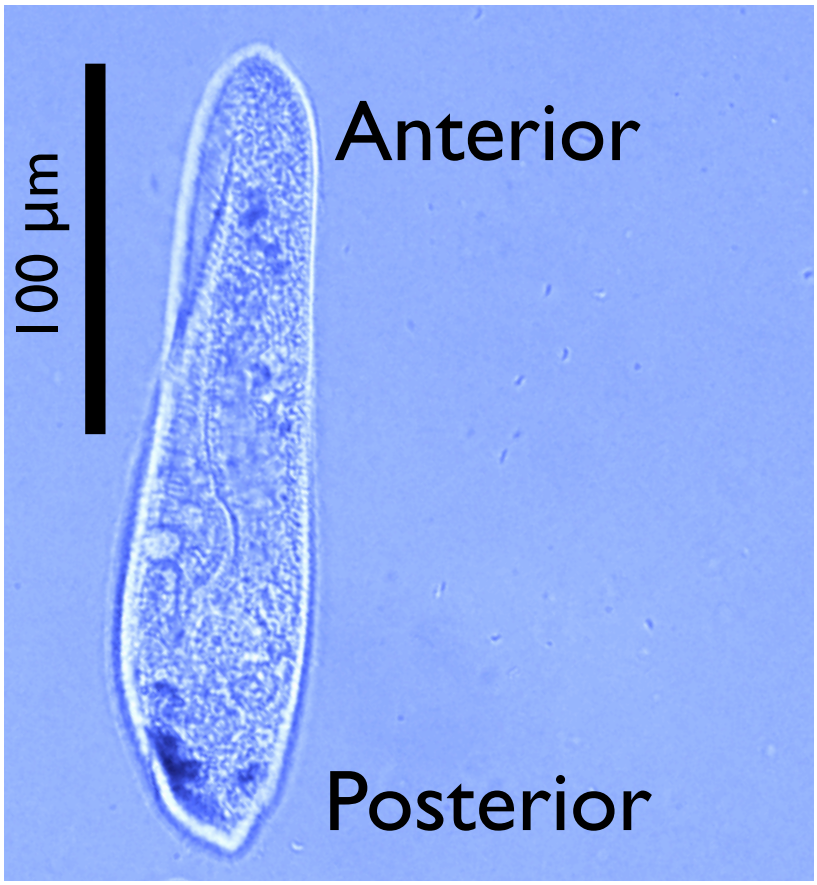

Figure 1.2: Snapshot of *Paramecium multimicronucleatum* showing the slender anterior end, the bulky posterior end and the slit close to anterior end. The slit represents the directions in which the oral groove points.

spheroid with the anterior(front) end being more pointed as compared to the posterior (back) end as seen in figure 1.2. At the center of the longitudinal axis there exists an opening which is called the oral groove that allows the organism to feed by creating suction. A slit that opens from the oral groove runs towards the anterior end (along the longitudinal axis) and merges with the anterior tip. The periphery of the cell body is lined with numerous cilia; however the length of the cilium and the beating frequency at different locations of the cell body are little different from each other. Cilia covering the body measure about 10 μm in length and beat at 10$\sim$20 Hz while those especially near the oral groove are found to be smaller in size. Those at the posterior end are considerably longer, less active, and measure

roughly 14 μm in length and usually remain together to form a tuft [14].

When an immobilized *Paramecium* is observed under a microscope one can observe the circulation of cytoplasm within the cell body (cyclosis). The streaming cytoplasm shows the circulation of variety of membrane bound organelles (except micronucleus) like micronuclei, contractile vacuoles etc and also helps in transport of nutrients and cargo within the cell. The cytoplasm is encased within a thick covering called as cortex. Starting from the interior of the cell the cortex consists of a thin layer of ectoplasm followed by a thick layer called pellicle and finally a layer of thin plasma membrane; together they form the rigid covering that provides a definitive shape to the cell. The cortex under an electron microscope shows hexagonal packing (Honeycomb like structure) [14] and provides a definite shape to the cell body; but it is flexible enough to allow changes in the body shape.

1.4 Ciliary beat and Metachronism

It is widely known that the ciliary beat is essential parameter in locomotion of *Paramecium*. Many researchers have tried to understand the nature of the ciliary beat around the body of the organism and how the beat helps in movement. The first observation was provided by Jennings [16], who speculated that cilia beat from the head to the anterior end to the posterior end (i.e. beat is planar) all along the length of the body. However such a simplistic assumption does not explain how the organism executes helical trajectory in unbounded fluid medium.

In quest for understanding the beat pattern many researchers started investigating how an individual cilium beats [3, 17] in a variety of organisms [18]. Using high speed imaging [19] they were able to resolve the different configurations of the ciliary beat as shown in the figure 1.3(c). The whole beat cycle is considered to be divided into two major phases: (a)

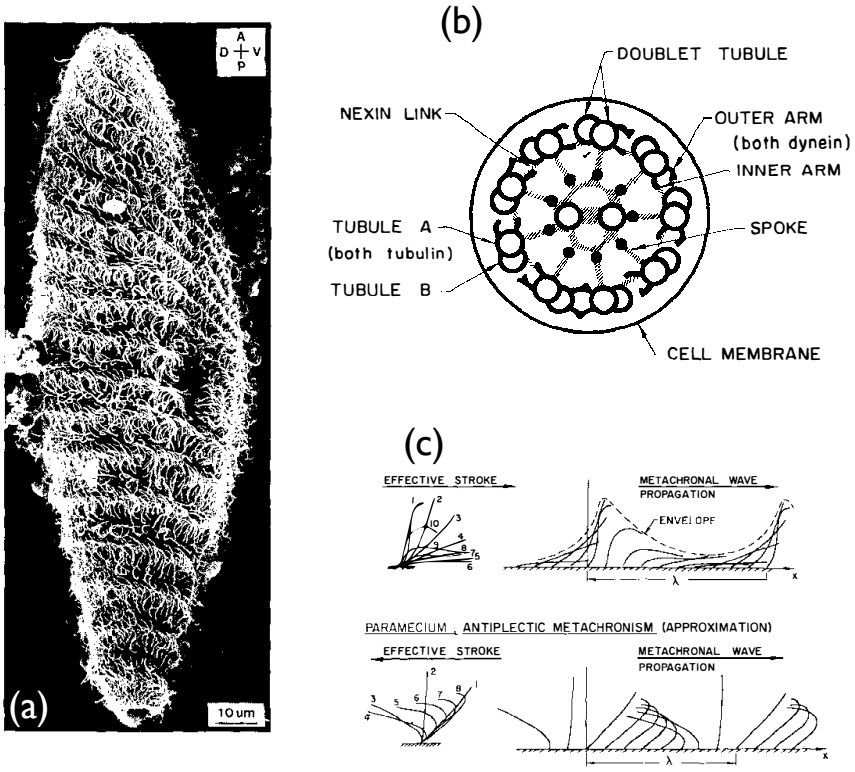

Figure 1.3: (a) Shows the spontaneous reorganization of the the cilia of the *Paramecium* cell. Taken from [3](under the academic use guidelines from Journal of Cell Biology and guidelines of the VT fair use analyzer) (b) Shows the internal structure of the individual cilium. Taken from [4](with permission from Annual Reviews and under guidelines of the VT fair use analyzer)(c) Shows a schematic of the symplectic and antiplectic metachronism. Taken from [4](with permission from Annual Reviews and under guidelines of the VT fair use analyzer)

Power stroke during which the cilia is extended while showing its full face and generates the maximum amount of power (b) Recovery stroke during which the cilia is curled up so that drag is minimal.

The individual cilium beat showed similar patterns; but the unison of cilia caused different direction of wave propagations for various organisms [20]. In the meantime scientists also observed the existence of waves all over the body of the *Paramecium* [21]. These have been hypothesized to arise due to the synchronization of the nearby out of phase cilium (albeit

unproved until recently) [22, 23]. The waves are termed as the metachronal waves and were initially thought to be propagating in a 2D plane: symplectic and antiplectic [4, 21]. During symplectic metachronism the power stroke direction of the cilia is the same as the metachronal wave propagation direction. In contrast during the antiplectic metachronism the power stroke direction is opposite to the metachronal wave propagation direction. Organisms like *Opalina* are observed to have symplectic metachronism while *Paramecium* is observed to have antiplectic metachronism. Further investigations revealed the existence of other classes of metachronism in which the waves propagate out of the plane [21]. Using rapid fixation methods Tamm et al [3] were able to provide us a glimpse into this kind of metachronism and about how the cilia reorganize all over the body of the organism. The picture of a forward swimming *Paramecium* shows (Figure 1.3(a)) that cilia arrange themselves into helical strands, spiraling over the surface of the body. The asymmetric nature of the beat provides us with a probable explanation of why *Paramecia* spiral as they swim around in the unbounded fluid.

1.5 Ionic Control of the ciliary beat

Albeit cilia beat to provide the *Paramecium* with propulsive power; their reorganization into metachronal waves have been a mystery. Fluid physicists often speculate that the synchronization is due to weak mechanical forces that transmit through the viscous medium [22]. On the other hand biologists often attribute the ciliary synchronization to the bio-electric control mechanism that lies within the cell [24]. *Paramecium* has thousands of ion channels distributed throughout the cortex which help in controlling the influx/ efflux of Ca^{2+} and K^{+} ions across the cell body [9]. The flux causes a difference in potential inside the body as compared to the ambient environment in which it is swimming. The first measurement

of potential difference inside the cell and as compared to the ambient environment was first reported by Eckart [24] in Ni^{2+} deactivated *Paramecia* (no ciliary activity), albeit his observations about the motion of the cilia are rather qualitative. An increase in Ca^{2+} inside the cell body causes the cell to be depolarized causing a reversal of ciliary beating and the cell to move backward or circle around with one of its end hinged.

In another variant of a similar experiment Naitoh [25] studied how mechanical stimulus contributes to the potential difference across the cell membrane. He held *Paramecia* in place and placed glass capillary electrodes inside the cell and in the ambient fluid. Then he touched different positions of the fixed cell and measured the potential difference across the membrane. While he touched the anterior end of the cell he found that the cell was depolarized thereby causing an increase in the potential inside the cell. Whereas when he touched the posterior end, the cell became hyper polarized and value of the potential dropped inside the cell. This provided insight into the ciliary actuation mechanisms, due to ionic imbalances across a electro-responsive membrane [26].

In an ingenious study Dryl and his associates studied the swimming patterns of *Paramecium Caudatum* in solution of various ionic concentrations [5]. He observed the existence of four different kinds of swimming modes namely: a) Forward left spiraling(FLS) b) Continuous ciliary reversal(CCR) c) Partial ciliary reversal(PaCR) and d) Periodic ciliary reversal(PCR) as shown in Figure 1.4. Forward left spiraling consists of left handed helical tracks while CCR consists of posterior swimming *Paramecia* with relatively straight tracks. PaCR swimming mode causes the organism to execute a series of forward and backward jerks resembling random motion of a particle; while PCR consists of swimming tracks that show regular circular patterns about a center that shifts diffusively in time. The experiment demonstrated the various kinds of swimming patterns that a simple organism like *Paramecium* can execute in ionic solutions of different chemicals and concentration.

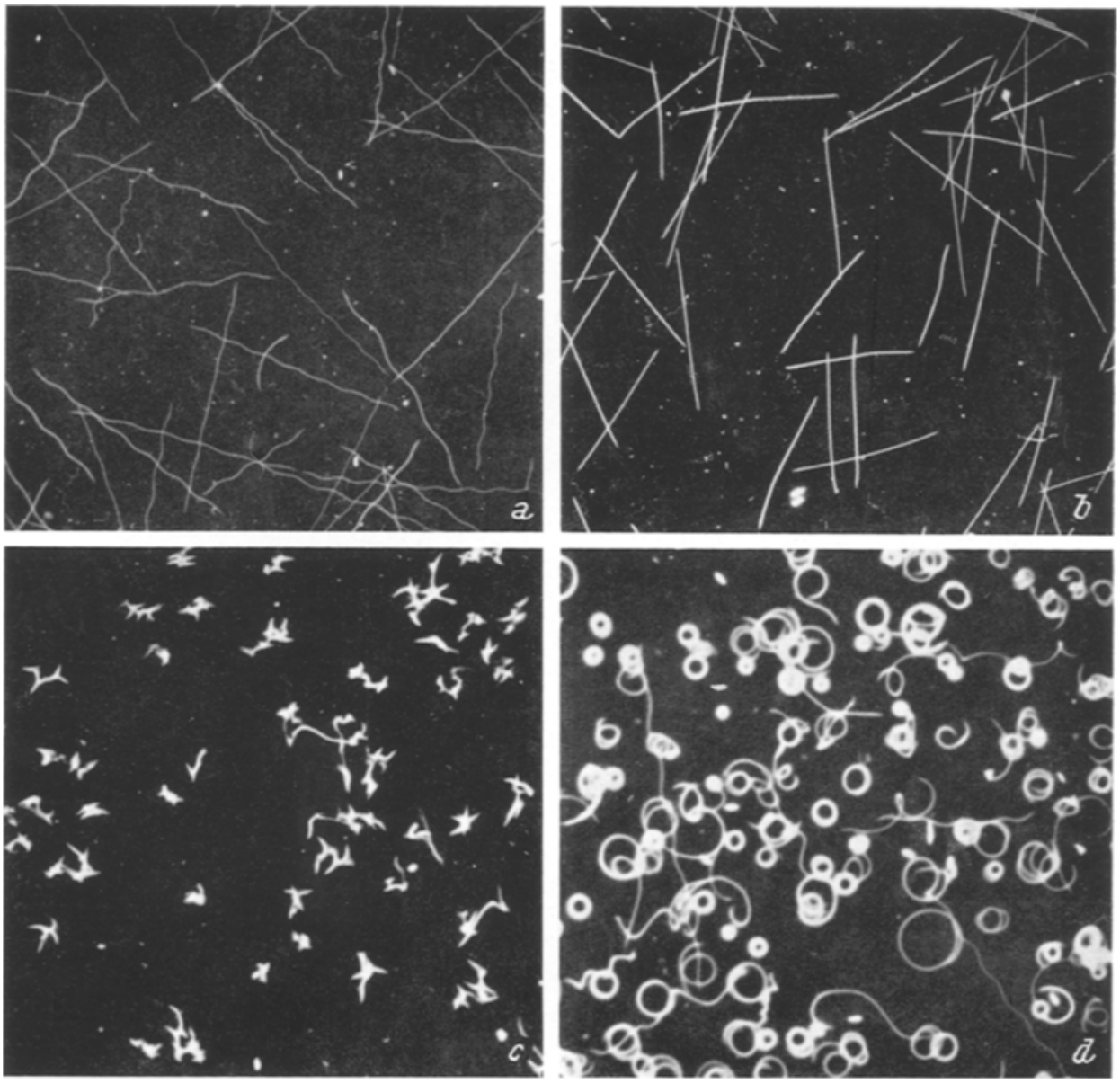

Figure 1.4: Shows different kinds of motion executed by the *Paramecium* in different solutions(of varying ionic concentrations) (a) Shows forward left spiraling. (b) Continuous ciliary reversal (c) Partial ciliary reversal (d) Periodic ciliary reversal. Taken from [5] with permission from Springer.

1.6 Experimental advances in microscale locomotion

The field of microscale locomotion was pioneered by Antoine van Leeuwenhoek whose letters to the Royal society [27, 28, 29] contains images that describe the motion of microorganisms in vivid detail. Since the early years of Leeuwenhoek microscale locomotion has advanced significantly in understanding the variety of swimming mechanisms used by organisms and the kinematics of the propulsive organelles. Such studies have undoubtedly contributed to our understanding however, many of these studies have not paid enough attention to the broader picture of organisms swimming near surfaces. The following section describes a variety of situations in which interaction with boundaries have caused changes in swimming patterns in a variety of organisms.

1.6.1 Spermatozoa

Investigation of motility of bull spermatozoa was one of the important markers in the history of microscale locomotion. Gray and Hancock together with Machin [30] described the various aspects of locomotion of spermatozoa in the bulk of fluid. However closer inspection in 1963 by Lord Rothschild [31] led to the observation of non-uniform distribution of spermatozoa in a drop of bull sperm. His best description of the situation was "sperm tended to stick to surfaces". The phenomena half a century later became attributed to the hydrodynamic forces involved due to orientation of the singularities near a wall. Brokaw's keen interest in the subject led him to investigate the bending waves [32] in detail using cinematography. He found that the tail contains regions bent like circular arcs followed by short unbent regions [33]; not nearly as sinusoidal as described by Gray. However such effect has little bearing on the speed or the energetics and most results complied to those put forth by Gray. Over the next two decades sperm became the most studied system both in terms of

the kinematics executed by the cell and the hydrodynamics associated with it. Sperm in a maze of microfluidic channels were found to swim in groups [34], caused by collision with the wall followed by re-orientation of cells. It was observed that in a group of swimming sperms initially out of phase can finally synchronize [35] which theoretically is found to be the most energetically stable state [36]. A result of the cooperation is manifested in increase in velocity of the group [37]. In the recent years Woolley's experimental study sperm cells [38] near surfaces led to observation of circular tracks. This lead to a surge of computational studies [39, 40] attributing such effects due to the hydrodynamics of the rotating head and the angle of approach of the cell near the boundary. Investigations have also attributed this phenomenon to non-linear buckling of the tail [41].

1.6.2 Bacteria

Many of the advancements in understanding bacterial locomotion is attributed to Howard Berg who discovered that the bacteria tend to swim helically [42] but their motion consists of "runs" during which multiple flagella synchronize together [43] or "twiddles" during which the flagella reorient randomly. Seeing the rapid switching between runs and twiddles(later came to be known as tumbles); Berg investigated the performance of the biological motor and studied its performance curves and its chirality [44]. Soon enough fluid physicists curiously observed the rotating motion of bacteria near boundaries and were able to predict the direction of circling near a boundary by knowing the chirality and the forces experienced near a boundary [45]. Bacteria are often termed as pushers (Force dipole like singularities) since the propelling device is located on the back side of cell body and are often observed to align parallel to surfaces owing to the stable orientation due to hydrodynamic effects [46]. In order to understand the behavior of bacteria in confined environments their motility was investigated in glass capillaries (of about 1.5 times the diameter of the cell) which revealed no

significant changes in the swimming velocities or turning angles when compared to swimming in unbounded fluid [47]. To investigate the effects of sub-micron confinements on the shape of the cells; they were made to grow in sub micron microfluidic structures which revealed that they can take anomalous shapes [48]. Their mobility is severely limited in such constrictions but they can render themselves motile by dividing and growing within these structures. Only recently it was found that bacteria placed in semi-solid agar gel deform themselves and by measuring the deformations optically a measurement of cell wall stiffness was predicted [49]. Using chemical gradients on agar gels *E. coli* were also made to swim along a specific direction [50] in microfluidic channels; thereby allowing scientists to selectively control the motion in a population of bacteria. Recent investigations into the flow field of the swimming bacteria have revealed closed dipolar flow patterns nearby the boundary (which otherwise were open far from boundaries) [51]. They also found that during long range interactions of organisms with the nearby walls hydrodynamic effects are of little consequence; but once the cell collides with the wall and reorients; hydrodynamic interaction may dominate and explain the long residence times of bacteria along the wall. The propulsive appendages of the motile cells can stir the fluid which interested the fluid physicists towards the problem of mixing arising in otherwise hard to mix viscous environments [52, 53]. Studies on 2D bacterial baths indicated that the long time dynamics of the tracer particles were super diffusive; indicating the occurrence of enhanced diffusion going on in such systems [54]. As the concentration of bacteria in the baths increased; scientists observed the transition from freely swimming to a jammed state and on further increasing the density observed local cooperation amongst bacteria although other also find an increasing order with density [55]. The cooperations manifested themselves as swirls or jets and was found to enhance the swimming velocity of a local group of bacteria [56]. The origin of such behavior is still under debate as some attribute this to chemotactic signaling while others think this might be due to the hydrodynamic cooperation between the cells [57]. A model of a cluster of self propelled rods has been

developed aims to explain the phenomena of jets and swirls by considering the hydrodynamic interaction between swimming cells [58].

1.6.3 Ciliates

Ciliary synchronization [22] and electro-responsive membrane [59] are important problems that have amused scientist over centuries. The problem of flow induced by a carpet of cilia in highly viscous fluids [60] has received significant attention owing to its similarity of human airways. Swimming characteristics of ciliates in tapered glass tubes [61] and in tubes coated with mucin [62] have revealed that they tend to slow down in confinements. Qualitative visualization of the flow field around the free swimmers have revealed Stokes quadrupole like flow patterns [63] and investigations under electric field have revealed anomalous velocities around the body [64]. Investigations into interaction of two swimming *Paramecia* have revealed the existence of hydrodynamic forces [65] that control the initial and the rebound angles of the organism. It can be concluded from the above investigations that hydrodynamics of individual cells as well as investigations involving effect of boundaries are rare in case of ciliates.

1.7 Theoretical advances in microscale locomotion

Owing to the rapid advances in experimental methods the necessity of quantitative methods to effectively describe the physics of the system became important. Theoretical techniques like small amplitude expansion of traveling waves; Resistive force theory for long slender tails etc. were developed to explain the relationship of velocities and power to the vital parameters of swimming. Development of singularity solutions of Stokes flow allowed description

of complicated flow patterns in various geometries and also allowed one to rationalize the hydrodynamic forces in the vicinity of the boundary.

Around early 50′s Sir G I Taylor started the analysis of swimming of microscopic organisms [66] in fluid recognizing that at such small scales viscous forces must be dominant as compared to inertia i.e., $Re = \rho V L/\mu << 1$. His videos show a macroscopic version of a model robot (executing time reversible motion) that fails to swim in very viscous fluids. He observed that many organisms (especially sperm) swim by propagating waves along their body and to mimic such motion he proposed the theoretical model of a swimming sheet in viscous fluid. By assuming that the deformations due to undulation are very small as compared to the body length, he did perturbation expansion to find that: (a) the first order swimming speed is zero (b) the second order swimming speed of the sheet is directly proportional to the square of the amplitude of the wave multiplied by the wavenumber. He also calculated the energy dissipated in such viscous environments and discussed the synchronization of two sheets which he attributes as the lowest energy and hence the most stable state.

One of the other notable works that happened concurrently was the development of the "Resistive Force Theory" by Gray and Hancock which describes the swimming of a spermatozoa by propagation of 2D bending waves [67]. They started off with a formulation of the forces experienced by the a small element on the tail and integrated it over the the length of the tail. Finally, by considering the fact that the net force exerted by the organism is zero they obtain the velocity of the tail is dependent on the parameters which is similar to the expression obtained by Taylor [66]. The two models opened up a world of opportunists amongst theorists who developed many variations of the problem [68, 69, 70, 71] to describe a wide array of swimming organisms and also allowed them to compare the results with the experimental observations.

In 1970s Purcell in his seminal paper on microscale locomotion describes the existence of a

kinematical constraint that prevents effective swimming in viscous environments [72]. He reasoned that when size of the organisms are very small ($Re << 1$) i.e. in highly viscous environments, if a swimmer executes time reversible motion of the swimming appendage there will be no net motion of the body (called as "Scallop Theorem"). He also explains that time is not explicitly important since the temporal effect cause instantaneous changes in the flow. He proposed the notion of a microscale scallop (2 link 1 (DOF) swimmer) swimming in an infinite fluid medium, which opens and closes its shell in a time reversible manner and hence cannot swim in highly viscous environments.

George Batchelor's paper on a stress system in force free swimming of particles [73] introduced a new method involving singularity solutions for modeling the motion of single particle or suspension of particle moving under stokesian conditions. Owing to the linearity of stokes flows the singularity method took advantage of using superposition method to model various kinds of problems [74, 75]. Variety of models for swimming microorganisms like flagellates and ciliates [76, 77] were developed which provided qualitative insights into the mechanics and the flow-fields caused due to these. Blake's introduction of image systems for singular solutions [78] provided a new impetus which paved the way for modeling of organisms far away [79] and near boundaries. These led to models explaining the hydrodynamics of spermatozoa swimming close to a boundary and reasons they show stable orientations when in a certain configuration [39].

The later part of 1990′s showed a re-emergence of theoretical investigations to explain the significant experimental advancements made during this period. Phase locking of swimming sheets were proved to have the minimal energy state and swimming sheet problem [36] was revisited and improvements were made to the perturbation series [80]. Models explaining the circular motion of spermatozoa and bacteria near the boundaries were developed to explain the corresponding observations in laboratory. Theoretical models of coupled oscillators

that simulate the metachronal waves were developed and investigations revealed that synchronization of cilia provide mechanical advantage in locomotion (albeit the effect is very small) [81, 82]. Numerical models of carpets of cilia have helped elucidate the mechanics of transport of highly viscous mucus on these highly relevant biological surfaces [83].

1.8 Helical Motion of Microorganisms

A wide array of organisms like bacteria, spermatozoa, spiroplasma, ciliates, rotifers, dinoflagellates etc. either utilize their propulsive organelle or the helical deformations of the body to execute helical tracks. In microscopic scales where symmetry breaking is imperative; traveling waves (helical or planar) is one of the methods to ensure net motion in the viscous environments. However when the tracks in a population of swimming cells the tracks of the organisms vary in the radius and the pitch of helix and has intrigued a few physicists.

Bacteria like *E. coli* have been long observed to swim by helical motion of the multiple flagella that synchronize together to propel the cell in a helical trajectory. Investigations however have revealed that the flagella push off-axis relative to the center of the cell body causing it to wobble and the extent of wobbling is controlled by the position at which the force is applied (dependent on orientation of flagellar bundle) [6]. Spiroplasma propagate helical bending waves along their body but can alter their helicity to cause kinks in their body which allow them to change directions as they swim. Magnetotactic coccoid bacteria also swim in helical trajectories under normal conditions; but their tracks can be altered by application of magnetic field that causes a reorientation of the magnetic chains. By varying the magnetic field the magnetic chains can reorient and cause additional forces and torques that change the usual motion of the cell.

Another classes of organisms are eukaryotic spermatozoa which propagate bending waves

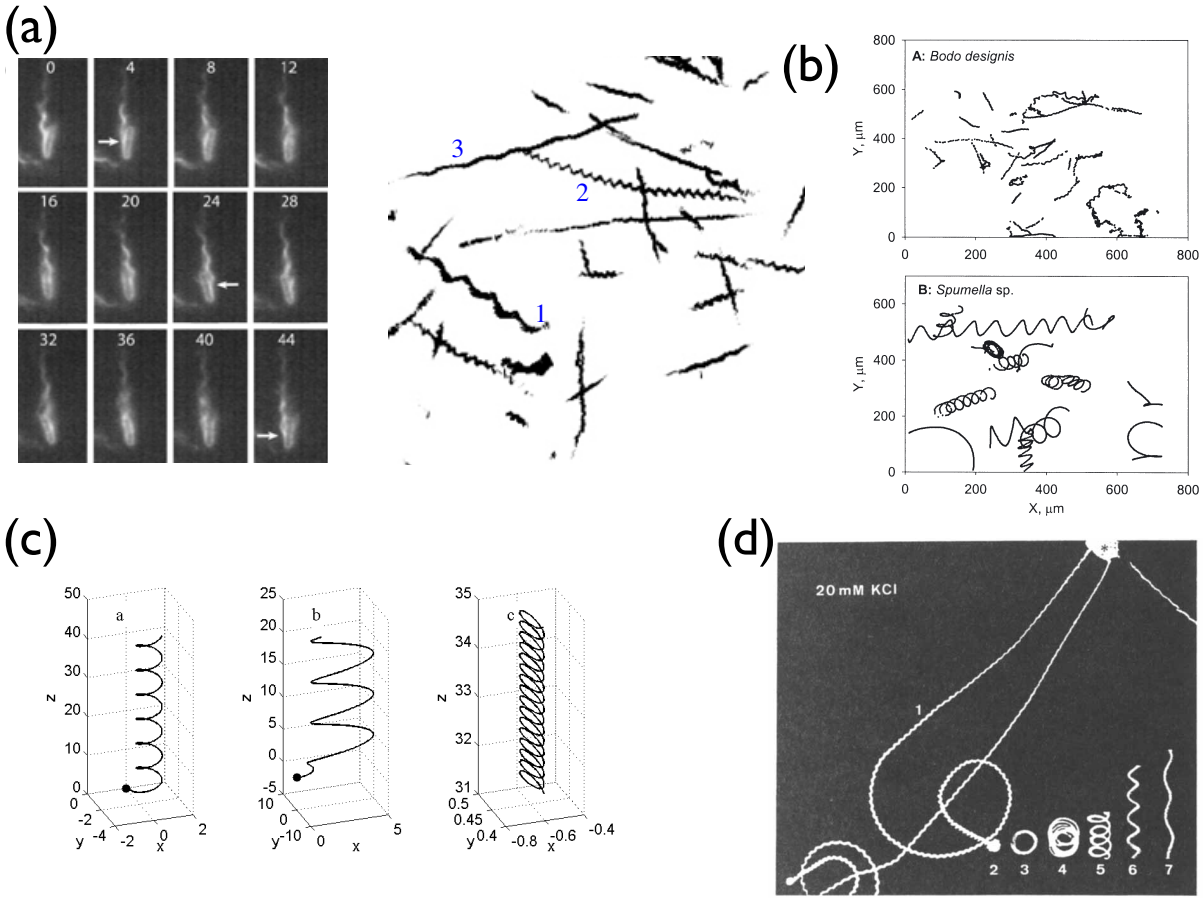

Figure 1.5: Figure shows the helical motion in a variety of organisms (a) Arrows point to the location of the flagellar bundles in different bacteria and the corresponding tracks executed by the bacteria. Taken from [6], under the guidelines of VT Fair use analyzer(b) Shows the different tracks executed by flagellates Taken from [7], under the guidelines of VT Fair use analyzer. (c) Shows simulation of helical tracks for flagellate swimming in shear flow. Taken from [8] with permission from Springer (d) Shows helical tracks of swimming *Paramecium*. Taken from [9] with permission from Elsevier.

by causing internal sliding of the microtubules. Sea urchin spermatozoa were often believed to execute planar bending waves when observed on the glass slides , albeit in reality their motion is helical in the bulk of the fluid. The fact was recognized by Brokaw which led to investigations into the rolling of the head and subsequently to understanding of the circular tracks executed by sperm near boundaries. Chwang undertook a theoretical analysis of the helical motion of tail and recalculated the power required during the motion [84] and also investigated an optimal tail to head size ratio. Recent imaging methods have revealed that human sperm predominately have helical modes of motion even in presence of the boundary [85]. To model the variety of helical modes of motion and circular tracks near a boundary a chemotaxis based model has been put forth [86].

Dino-flagellates propel themselves by swimming using two flagella perpendicular to each other which are also known as the longitudinal flagella(cis, located close to eyespot) and the transverse flagella(trans, comparatively far away from eyespot). The longitudinal flagella beats in a way that causes the translation of the cell while the beating of the transverse flagella causes the cell to rotate along its principal axes [87]. Since the cell body is highly asymmetric; the rotation induced along the three principal axes cause the organism to exhibit a helical trajectory. Such helical trajectory was observed by in study of prey induced changes in swimming characteristics of predators [88]; during the flagellate colonization of the sinking aggregates [7] and in the Levy walk analysis of the predation tactics of dinoflagellates [89]. A mechanistic model [8] based on Fenchel's description was also developed which suggests that helical swimming modes provide a greater robustness in upward transport when the cell is swimming in strong shear flows.

Ciliates especially *Paramecium* are recognized to have helical swimming tracks presumably due to their dexioplectic (out of plane) metachronal beat [5, 9]; which causes the cell to spiral around in the fluid. The varying amplitude and wavelength of the tracks are possibly due to a

geometric effect (asymmetric cell body shape) which causes rotation about the principal axes. To describe the helical motion of ciliates crenshaw proposes a minimal model [90] (1 degree of translation; 2 degrees of rotation) which he extends to describe the 6-DOF [91] (3 degree of translation; 3 degree of rotation) motion which may closely resemble the kinematics of *Paramecium*. By varying the different parameters(radius(r) and pitch of helix(p) etc.) in his equations of motion he demonstrates a variety of tracks that can be executed by the organism during chemotaxis [92]. He considers that the changes in the parameters are induced due to an external effect and just incorporates the numbers into his equations but doesn't provide any physical reason about why such tracks may be caused (asymmetric actuation of the cilia or the asymmetry of the body).

Phototactic marine annelid like *Platynereis dumerilii* posses equatorial ciliary bands that can be activated by the photoreceptors present in the organism. In the quest for understanding how photo-taxis steers the plankton [93]; the researchers tested the organism's response to light and found that the different region of ciliary bands produce different flows at different locations. Although they do not directly show how this difference causes helical motion; they modulate the cilia beat using a mathematical model in response to phototactic cue and find that the tracks align themselves to the light cues. They finally compare the tracks qualitatively from experiments and theory and attribute the reorientations of the cell to phototaxis.

1.9 Objective of Investigations

Interactions of microorganisms with the nearby environments is ubiquitous during navigation and foraging. Sperm/Bacteria swimming in circles near surfaces, accumulating parallel to the surfaces owing to hydrodynamic effects are some of the interesting examples that demon-

strate the various changes that can be caused in swimming parameters by the neighboring boundaries. Such investigations are nascent for most "model organisms" and particularly rare in case of unicellular ciliates. Unicellular eukaryotes like *Paramecium* occupy unique position amongst different organisms in terms of biological complexity. The biological functions are as simple (yet complicated) as that of a single cell; however thousands of cilia covering the body represents a complete departure from bacteria and sperm in terms of number of propelling appendages. The electro-mechanical responsiveness of membrane and synchronization of cilia has proven to be challenging puzzle for both biologists and physicists; while studies involving interactions with boundaries are rare.

The focus of this thesis will be on characterizing the motion of the ciliate *Paramecium multimicronucleatum* in a variety of artificial geometries, predicting the velocities in cylindrical confinements and quantifying the flows around the swimming cell.

Chapter 2

Experimental protocols

Initial cultures of *Paramecium multimicronucleatum* from Carolina Biological Supply (Part # 131540) were ordered for experiments. Carolina Biological obtained the initial cultures of ATCC 30842 *Paramecium multimicronucleatum Clone 203* in 1954 and the *Paramecia* have been in constant culture since that time. After obtaining the samples; the volume of the culture was thoroughly bubbled with a pipette and observed under the microscope to ensure that cells were sufficiently motile.

2.1 Culturing Method

Wheat seeds (Part # 132425) were boiled in spring water for 20 minutes at 350°C. It was ensured that the seeds boiled to an extent that their outer covering was cracked. Both glass (Kimble Kimax) as well as plastic petri-dishes were used for the culturing purpose. In plastic petri-dish (VWR25384 − 090) 5 ml of boiled water was poured followed by the introduction of $1 - 2$ boiled wheat seeds and the temperature of the solution was allowed to equilibrate to room temperature. Original cultures were centrifuged at 300 gs for 10 minutes

in microcentrifuge tubes (Grainger 11L818) and the resulting white residue at the bottom was picked up using a VWR Pipettor. The residue was then inoculated into the petridishes and the cultures were placed in a chilling incubator where the temperature was consistently maintained at 25°C. This culturing medium is known as the "double wheat medium" and provided superior cultures as compared to other methods used. It should be noted that the culture media should be placed in a container such that the surface area is maximized and the depth of the fluid volume should not be greater than 5-15 mm. Figure 2.1 shows the growth curve of *Paramecium* and it can be observed that at the end of 7∼10 days the growth curves reach a saturation indicating that new cultures should be placed every $14 - 21$ days.

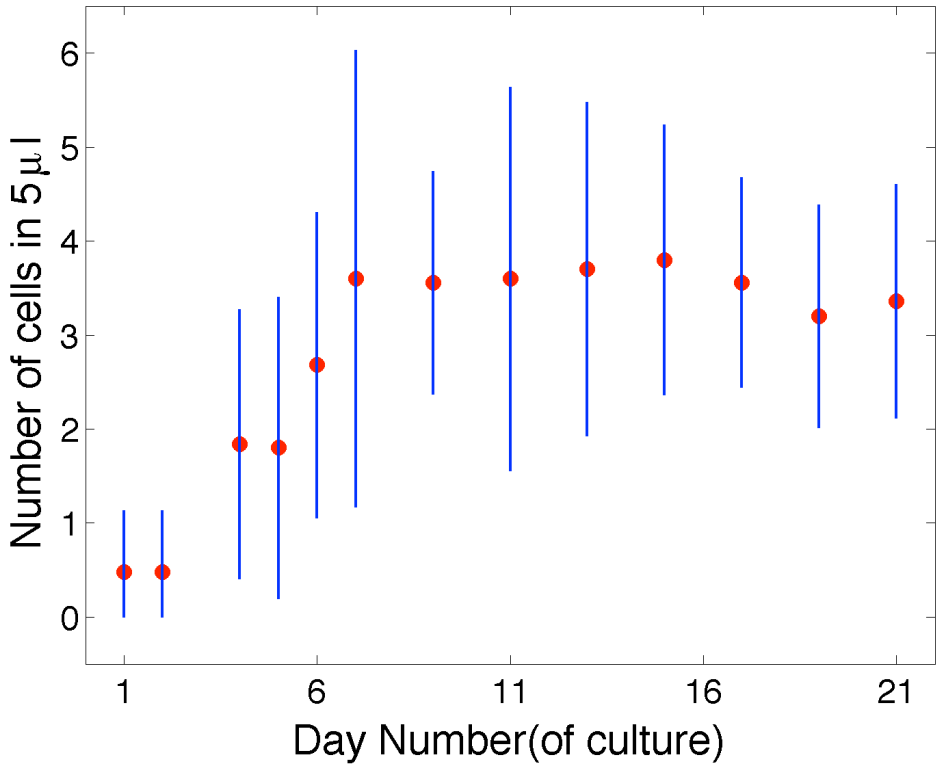

Figure 2.1: Figure showing the population curve of the *Paramecium* over a period of twenty one days

Other methods that were also used to culture was the "Hay medium" in which Hay strands were boiled in spring water followed by filtering of the debris. The resulting medium was

cooled and let to stand for two days after which *Paramecia* were inoculated into the medium. Cell death was observed two days after the inoculation, possibly due to the low pH values of the medium. Protozoan pellets boiled in water were also utilized for the cultures and cell death was also observed with this media.

2.2 Debris removal and Buffer solution

The cultures ideally need to be monitored every other day for abnormalities in shapes of the *Paramecium* and presence of excessive amount of foreign organisms. After a period of $6-7$ days one might observe the formation of biofilm at the air water interface. This is harmful as it may cut off the oxygen supply needed for the proper growth of the organisms. The food grains also start decaying and form mesh-like structures in which *Paramecia* grow in large numbers. In order to isolate the organisms from the culture and prepare them for experiments; it is advisable to give a gentle swirl to the fluid medium so *Paramecia* get untangled from the decaying food mesh. After the procedure they are made to pass through a 325 μm plastic mesh which removes the macroscopic food particles and debris from the medium.

Even after the filtration there are lot of microscopic debris and organisms that stir the flow. Hence it is advisable to centrifuge the cells and re-suspend them in a fresh medium. It has been observed that certain media(Tris buffer, PBS buffer) enhance the motility of the cells while maintaining almost isotonic conditions with respect to the cell body. A mixture of 9 mM $CaCl_2$ (0.998 g), 3 mM KCl (0.224 g) and 5 mM Tris HCl (0.788 g) is mixed in one liter of distilled water (Millipore, Dudek Lab). The resulting solution is titrated with 1mM NaOH and the pH is adjusted to 7.2. The pH of the titrated solution was confirmed using pH meter (Oakton pH 5 Arcon series) and pH test strips (ordered from Micro-world company).

Cells introduced into this medium showed renewed vigor and swimming activity. They were allowed to equilibrate for 20 min$\sim$1 hr before they were used in the experiments. The washing steps were repeated again to ensure that there are minimal debris in the background.

2.3 Immobilizing *Paramecia*

It was required that *Paramecia* be immobilized for certain experiments. In those cases an equal volume of hot water at 100°C was added to the culture which immobilized the cells. The cells were not entirely killed in the process; but their motility is severely limited by employing this method.

Another method to immobilize *Paramecia* is to trap them in agar gel. This method was employed to get a tomographic scan of the nano-particles inside the cell body; but was not pursued further owing to difficulties. Water was boiled to a temperature of 100°C and 0.5 g of agar gel was dropped into the water and stirred for about 2 minutes. The solution was stirred and allowed to cool in petridishes that have large surface areas. *Paramecia* cultures were dropped into the mixture just before solidifying and the mixture was stirred again. The result was that the *Paramecia* got trapped in the fibers of the solidified agar gel. If the original content of the agar is increased to a level greater than 0.5 g the mobility of the organisms was severely limited and if lowered the organisms tend to locomote by deforming its body.

2.4 Manufacturing of PDMS channels

Many of the projects required manufacturing microchannels for use in cell locomotion experiments. The first step in this process is to make a drawing in AutoCAD using closed

polylines. The drawing is usually sent out to a third party vendor like Stanford Microfluidics or collaborators at other universities who make the molds from the drawing and send it back to us. The mold master contains positive features (channel drawings); which can be easily imprinted on a polymer substrate. After the mold is received we prepare a 10:1 mixture of Polydimethylsiloxane (Sylgard 184, Dow corning) and its curing agent in small plastic cups. The compounds are mixed thoroughly which causes lots of bubbles to be introduced into the system. Separately the Mold master which contains drawing features developed on a silicon wafer is taken and cleaned with Iso propyl alcohol. A stream of compressed air is used to dry off the silicon wafer and then placed in a sterile petri-dish and then the polydimethylsiloxane (PDMS) mixture is poured over it. The petridish is placed in a desiccator connected to a vacuum pump which is degassed until all the bubbles have been eliminated. Then the dish is placed in an oven at 65°C and left overnight to bake.

PDMS chunks are cut out from the cured polymer and holes are punched in the inlet and outlet ports. The chunks are placed in the vacuum chamber of a plasma cleaner (Harrick Plasma) and treated for 2 minutes. Finally they are bonded onto the pre-cleaned glass slide and allowed to stand in a hot chamber at 65°C to enhance the bonding strength. The devices are then taken out of the oven and allowed to equilibrate at room temperature. Washed *Paramecia* can be injected into the inlets using the pipettes, but caution be taken to ensure that very high pressures are not exerted. Care should be taken so that cells are not subjected to extreme shear flow conditions. The flow of the liquid within the channel (due to imbalance of fluid levels) can be arrested by touching the ends of the devices with a Kimwipe which removes fluid by capillary action. Equilibrating the flow takes patience and time and should be done carefully as it is crucial for creating the quiescent flow conditions that most of the experiments require.

2.5 Vital Staining

Under a microscope the *Paramecium* cells manifest themselves as translucent/ transparent objects. While attempting to study their locomotion on hydrophobic/hydrophilic surface (colored white) we had to stain them in order to enhance the contrast from the background and be able to able to track them using a computer. Neutral red (1% aqueous) i.e. 1% by volume of water was ordered from Carolina biological and was diluted to 1/2500% by volume in spring water. Equal volumes of concentrated *Paramecia* cultures (previously washed two times using buffer) were mixed with this solution and allowed to stand for 15∼30 minutes. Time required to color the organism was determined visually by the extent of dyeing and varied for each of the runs.

It was observed that about 5% of cells died during the staining procedure. When the staining (enough red particles were ingested by the organism, giving it a red color) was deemed complete by the experimenter (refer to figure 2.2), the solution were immediately diluted with fresh buffer solution. Centrifuging was followed by resuspension in buffer solution, immediately after which experiments were performed in 2-6 hours. It was observed that the *Paramecia* retained their colors even after 2-3 days and there was little or no toxic effects as cell movements and populations seemed to behave similar to non- dyed *Paramecia*.

2.6 Manufacturing of Micron sized Glass devices

2.6.1 Glass Capillaries

A glass pipette was held onto one end of the holder and a small dead weight (paper clip or metal clip) was attached to one of its ends. The flame of the propane tank was adjusted

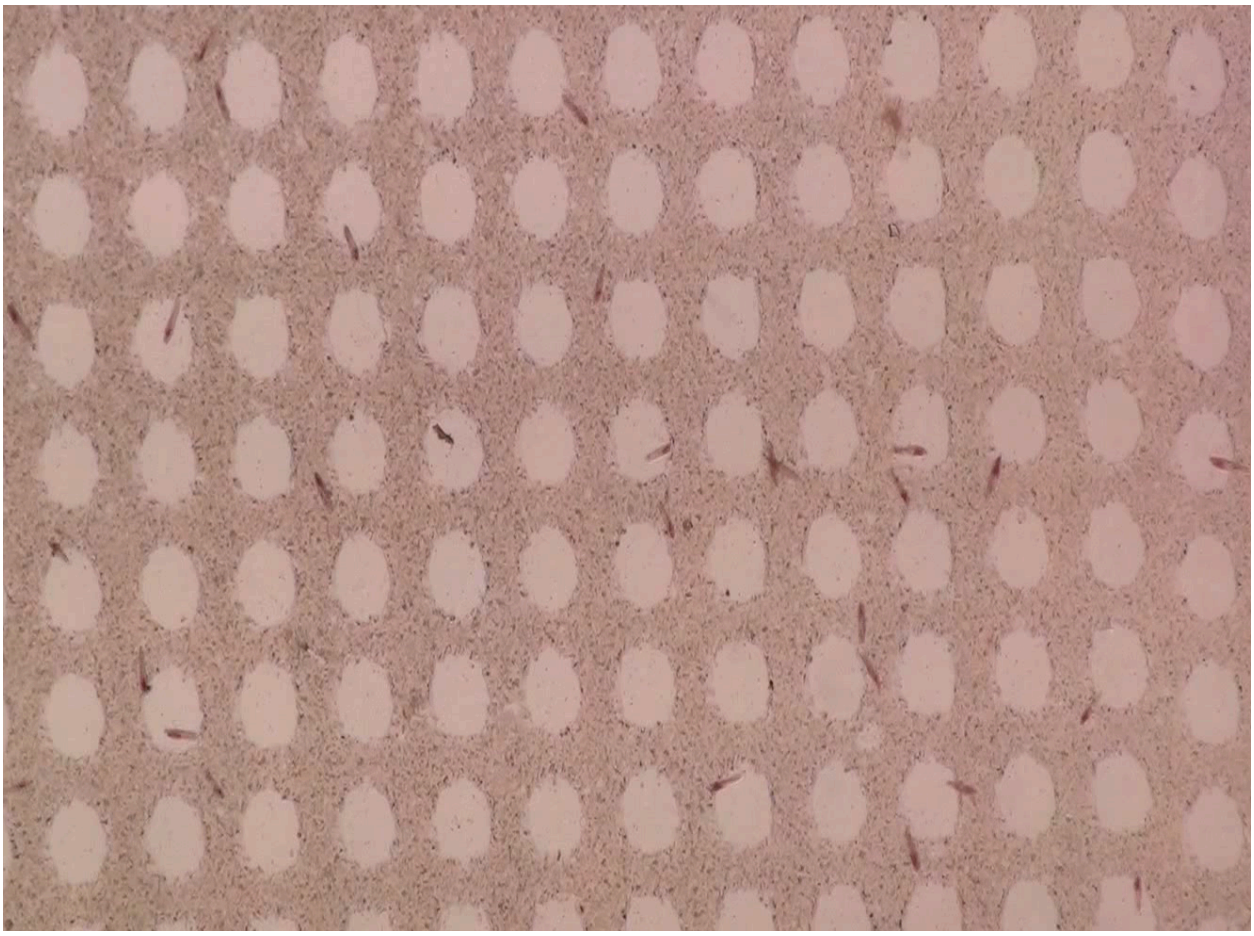

Figure 2.2: Figure shows *Paramecia* stained with Neutral red dye, swimming on surface with patterned wettabilities.

to its minimal level and held in close proximity to the tip of the pipette. By varying the distance of the flame from the glass surface; the tip was allowed to draw under the weight, which allowed us to obtain capillaries measuring 90 μm - 200 μm inner diameter.

2.6.2 Micro-pipette

Micro-pipettes were used to apply suction to *Paramecia* and hold them in place for the experiments involving determination of Young's modulus. Glass pipette tips were secured firmly the holder of Micro-forge (MF 900, Narishige Inc.) and heat was applied (using a

heated filament) to a particular section which caused the hollow section to be extruded under its own weight. Halfway throughout the length, where the diameter of the extruded section has become sufficiently low (∼20 μm); heat is applied so that the thin region bends and forms an angle with the vertical. This is done since the pipette will be held with a micromanipulator and the bend allows it to easily dip inside the fluid volume without fouling onto any other surfaces.

2.6.3 Micro-cantilever beams

Borosilicate glass rods(∼ 0.5 mm) were first extruded and then the tip was heated until a blob of glass formed at the tip of the rod. The heating coil was then brought in close proximity to the blob and the blob was stretched perpendicular to the thin section. The manufacturing process was adapted in a way that resulted in the diameter of the stretched section being close to 10 μm and the fiber is aligned perpendicular to the extruded region. The length of the stretched section was adjusted by clipping the fiber to a particular length so that the stiffness of the fiber lies within a particular range.

2.7 Sample preparation for Particle Image Velocimetry

For the set of experiments the *Paramecia* are made to swim in a particle laden fluid to get high contrast images that clearly distinguish between the particles and the background. We used polystyrene micro-spheres (Thermo-Scientific) of 1 μm diameter as the seeding particles. The suspending media of the micro-particles contains a surfactant which causes bursting of cells, hence when cells were put in this solution cell death happened in few minutes. To avoid this ill-effect the suspension of particles was centrifuged at 4.5 g for 4 minutes so that

the heavier particles settled at the bottom. The supernatant containing the surfactant was decanted and about 5.5 μl of the residual solution containing polystyrene spheres were re-suspended in 1.1 ml of the culture solution. *Paramecium* tends to swim freely in such solution without any change in their original swimming characteristics. However it was observed that the oral groove of the organism was clogged and the particles formed clusters at this region.

A sample was placed on the glass slide and two spacers were placed at the ends. Another glass slide was placed on top thereby creating a film of 754μm thickness. LED array (LED 12 from IDT; 11650 lumens) was mounted on top of a tripod and was placed at angle to the glass slide containing the sample. Evaporation due to intensity of light might be a issue; and was minimized by turning off the light periodically.

Chapter 3

Swimming patterns in confined environments.

Goal - To quantify the changes in swimming behavior of *Paramecium* in different geometries and understand the buckling of *Paramecium* in microchannels using beam bending theory.

3.1 Introduction

Motile microorganisms live in environments which are often interspersed with organic and inorganic boundaries [14]. While foraging in their native environment, microorganisms need to pass through and interact with crevices, obstacles or bio-flocs of various shapes and sizes [94, 95] and the need for understanding the interactions with boundaries. Prokaryotic bacteria like *B. subtilis* swim ballistically until hitting an obstacle and then back up along the same direction by reversing their flagella [96]; while ciliates like *Paramecium* do a slow back-up and gyrate their body followed by forward swimming [16]. Similarly, while swimming in labyrinthine channels *Spermatozoa* tend to align themselves along specific surfaces

[34]. Hence, when presented with an obstacle in their path; microswimmers tend to behave differently.

Swimming gaits [97] and body shapes are critical for identifying a microorganism. However, under varying external conditions which may present themselves as visual, hydrodynamic, physical or chemical cues; microorganisms either optimize their body shape or manifest a gait change. For example, bacteria in sub micron constrictions [48] and fabricated micro-structures [98] show adaptation by growing as well as dividing into anomalous shapes, and growth of yeast cells in small chambers cause them to buckle due to their increased elongation [99]. Large organisms like fish swim by undulating their body [100] and can also execute a C-shaped bending of body by using muscles in order to abruptly change the swimming direction [101]. At microscales, dinoflagellates change the radii and pitch of their swimming helix to hunt the prey [88], and *Paramecium* shoot out trichocysts and exhibit evasive maneuvers in response to a threat [102, 103]. Dilute suspensions of bacteria and spermatozoa exhibit accumulation near surfaces [39] or show circular swimming tracks due to hydrodynamic effects [38, 45].

The role of Calcium ion channels in controlling the motion of *Paramecium* by regulating the synchronization of cilia have been widely investigated [59]. Experiments have been performed showing that a stimulus to the anterior end of the *Paramecium* causes a change in the calcium ion gradients(inducing hyper-polarization); causing the cell to swim rapidly [25]. Stimulus on the posterior side causes the cell to depolarize and cause ciliary reversal thereby forcing the cell to swim in a straight line. Furthermore, swimming patterns in a variety of artificially created ionic solutions were investigated which showed that helical motion, swimming in circles and sudden jerky motions are possible under specific chemical conditions [5]. These trajectories are a stark contrast to helical swimming of ciliates; which is known to be the primary mode of locomotion.

To investigate the adaptation in swimming characteristics that arise in *Paramecium multimicronucleatum* we study its locomotion in a variety of confinements. We show that the trajectories of *Paramecium* transition from helical anterior motion to meandering when put in quasi 2D films of different thickness. While navigating channels of height 80 μm and certain width the meandering behavior gives way to bending; where *Paramecium* exhibits a half somersault by deforming its flexible body. The forces during the bending process is presumably derived from ciliary beating as the cell compression is observed to be minimal. This phenomena points to a new function of cilia apart from swimming/sensing or foraging and bending provides the cell with a navigational advantage by allowing abrupt change in direction of swimming in constrictions.

3.2 Swimming Characteristics in unbounded fluid

In previous experiments with *Paramecia* in capillary tube we found various kinds of swimming tracks executed by different organisms in the same population of swimmers. Spiraling motion as well as backward motion in straight lines followed by scanning around a single point were observed in capillary tubes while majority of the biologists only report about the helical motion of organisms. Physicists have also speculated on the change in behavior of the organism with the culture age; which was attributed to the changing food conditions in the navigating swimmers. To standardize our experimental protocols and eliminate the randomness we study the motion of the swimmers in the culture medium over a period of 21 days. We remove the organic debris by filtering it with a 325 μm mesh and washing them twice in Tris-Buffer solution. The washed cells were allowed to stand for at least 1 hour so that they get equilibrated and the effects of metal ions in causing de/hyper-polarization (and effectively change in swimming tracks) can be neglected. This allows us to eliminate

the effect of ions in changing the swimming patterns of the *Paramecium*. The equilibrated cells were then picked up by a pipette and then dropped onto a glass slide which resulted in formation of a thick film. Using a fiber optic light source we illuminated the sample with the light pointed in an oblique direction which resulted in dark-field images with the cells appearing as white spots on a dark background. The swimming tracks were recorded for very long times using a Sony Handy-cam fitted with a 4X macro lens which allowed us to have a very large field and depth of view. The movie were converted into black and white images and then using image analysis the paths of the cells were tracked. For each day around 60∼500 organisms were tracked so that good statistical measures can be obtained for a population of cells.

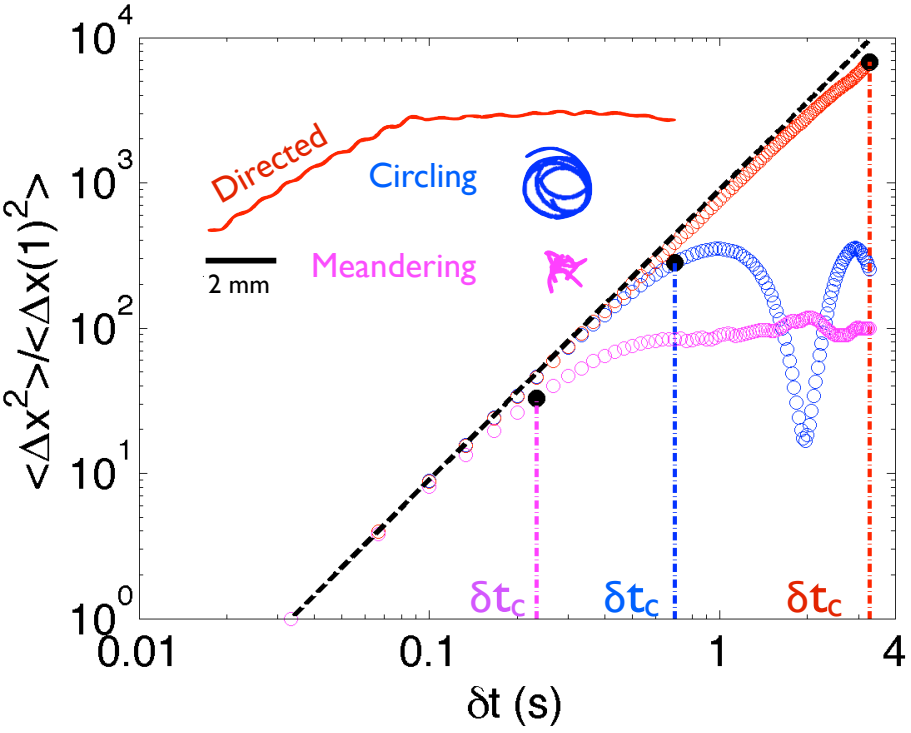

Figure 3.1: Inset shows different tracks executed by the *Paramecia* of the same population while swimming in unbounded fluid. The larger plot shows the normalized mean square displacement plot of the various tracks (color codes are the same in both the plots).

We observe three different kind of swimming modes (fig. 3.1) - directed, circling and meander-

ing. Directed motion manifests as unidirectional helical lines with small lateral undulations; during which the cell moves away very quickly from its original position without changing its direction abruptly. In contrast, during meandering motion *Paramecium* scans around a local position with very little displacements from its original position, but exhibits large number of abrupt turns. Although rare, circling motion is also observed during which the swimmer circles with variable radii around a local point. In order to categorize the different trajectories, we plot the normalized mean square displacement (MSD) vs. time difference (δt) [54] of the recorded tracks for the first 100 frames (T = 3.3 sec).

$$MSD_n = \quad < \frac{(x_{i+n} - x_i)^2 + (y_{i+n} - y_i)^2}{t_{i+n} - t_i} > \tag{3.1}$$

Figure 3.1 shows MSD plots for different trajectories executed by the *Paramecium* in unbounded fluid. The red dots corresponds to directed steady motion observed in experiments which closely follows the dotted black line denoting the ideal theoretical ballistic motion. It can be clearly observed that both meandering as well as circling motion show departures from the directed motion at much smaller timescales. We measure the absolute error $\eta = |\log(MSD_{ideal}) - \log(MSD_{calc})|$ for the trajectories, and at the instant when η deviates from 20% of the ideal ballistic case; is called the "Characteristic time". We will use the difference in Characteristic times to classify the swimmers as either "Ballistic"(δt_c >3.0 s) or "Meandering"(δt_c < 3.0 s). We plot the characteristic time during different days of the growth phase of micro-swimmers and make some interesting observations. First that given any particular day only 70% of the swimmers in the fluid are directed swimmers (as seen in Fig. 3.2) which means that they have large displacements from their initial starting points. Their tracks were observed to have varying helix radius and pitch; each characteristic of a single organism and the characteristic time is close to 3 s. On the other hand there are also 20% meandering swimmers which display diffusive like characteristics and have the charac-

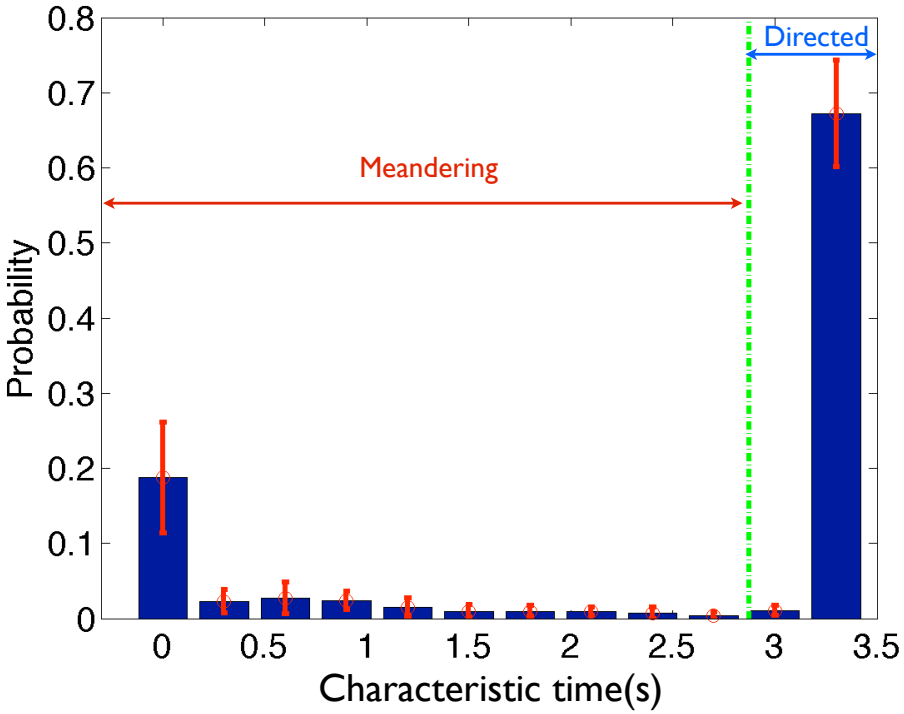

Figure 3.2: Figure shows the distribution of characteristic time for a population of swimming cells averaged over 17 days.

teristic times lying between 0.3 $\sim$ 3.0 s. The red error bars indicate the variation in the characteristic times over a period of 21 days indicating that directed motion is dominant swimming mode irrespective of the day in which the cells were harvested from the culture medium.

Another metric that is common measurement in bio-locomotion is the average velocities. We measured the swimming velocities through 21 days and found some variations. The average velocity of the swimmers across different days is close to 1500 μm/s but the standard deviation is about 600 μm/s; indicating that both fast as well as slow swimmers are present in the same population of cells. This is quite possible because the cultures placed from the originally ordered organisms were not clones and had mutated over time (cultures of Carolina were brought from ATCC in 1954 and have been in culture ever since).

3.3 Swimming characteristics in thick vs. thin liquid films.

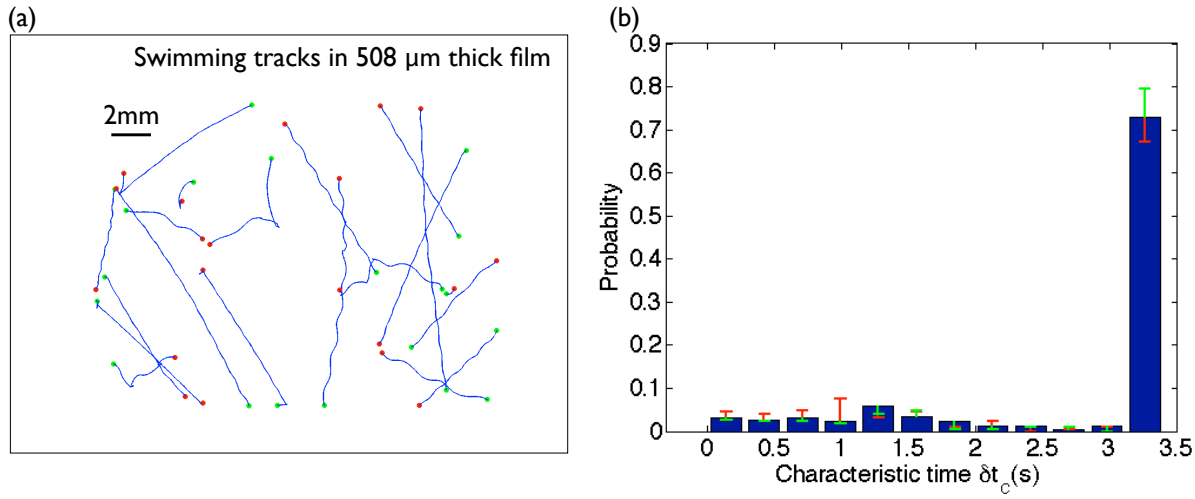

Figure 3.3: (a) Shows the swimming tracks of *Paramecium* 508 μm thick films. Most of the tracks are straight with varying pitch and radius of the helix. (b) Shows the distribution of the Characteristic times of the recorded tracks. Blue bars denote the characteristic time when $\eta = 20\%$ is chosen. The red line shows the variation from the values when $\eta = 25\%$ is chosen and green bar corresponds to $\eta = 15\%$

To understand the behavior of organisms we conducted experiments with fluid films of seven different thicknesses (H = 50, 76, 127, 254, 317, 381 and 508 μm) sandwiched in between two glass slides. The thickness was controlled by plastic spacers which were placed in between two glass slides. Care was taken so that the fluid film didn't penetrate the spacers which can affect the accurate control of gap thickness. *Paramecium* were made to swim in these thin films and their tracks were recorded with a Handy-cam fitted with a 4X macroscopic lens. The recorded tracks were then categorized using the criteria describes in the previous MSD plots. We find that for the case of 508 μm film, as shown in Figure 3.3 about 77 % of the swimmers exhibit directed swimming like characteristics; which represents the helical motion of *Paramecium* in an unbounded domain. The results are similar to the

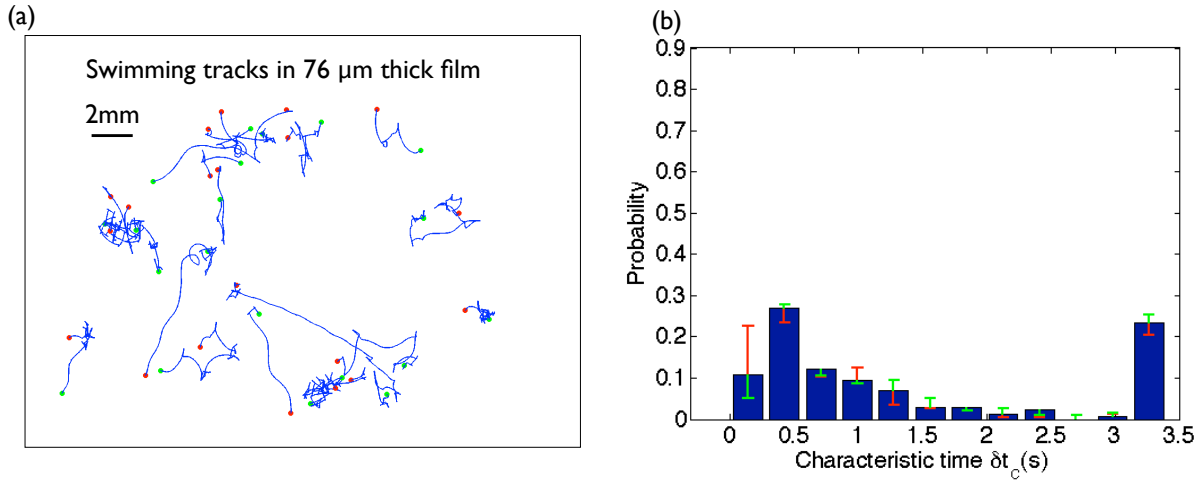

Figure 3.4: (a) Shows the swimming tracks in 76 μm films which appear to be quite random. (b) Shows the plot of the characteristic times of the swimming tracks recorded in thick 76 μm films. Blue bars denote the characteristic time when $\eta = 20\%$ is chosen. The red line shows the variation from the values when $\eta = 25\%$ is chosen and green bar corresponds to $\eta = 15\%$

characteristics of organisms in the unbounded fluid. We utilize the similar analogy of Mean Square Displacement for characterizing the swimming tracks; the plot shows a singly peaked curve with the peak at around 3 s.

In a total contrast, for the case of 76 μm gap thickness; about 78 % of the swimmers display meandering like characteristics showing lower values of characteristic times ($\delta t_c < 3.0$ s) as shown in Figure 3.4. A similar analysis of the Mean square displacement shows that the plot has a double peak; with one peak at around 0.3 s and the other at 3.0 s. This clearly denotes the fact that the tracks transition from directed swimming to meandering in small gap thicknesses.

Further analysis of the videos in the small gaps shows certain peculiar characteristics. While swimming in such small gaps; the *Paramecia* executes forward as well as backward swimming. The two phases of swimming are interspersed with frequent turns. This can possibly be explained by the hyper-polarization and de-polarization of the membrane due to frequent

collisions with the wall which shows the jerky movements. While in the directed swimming case the swimmers tend to scatter away from the wall if there is a collision with wall but don't show the jerky motions while compared to small gap thickness case.

Fig. 3.3 and Fig. 3.4 show that there is a change in the motion from directed swimming to meandering for the films of smaller thickness and it can be seen that the characteristic time peak shifts, from large value of 3.3 s (total track time) to a doubly peaked curve with maxima at around 0.3 s in smaller gaps. We also measure the average number of turns for the swimming tracks recorded and find that in smaller gaps the number of turns is about four times higher than those compared to the large gap thicknesses in Fig. 3.5. To measure this quantity we define a normal to the track at time t_i and at time t_{i+1} and if the difference is larger than 60° we define this as a turn of the organism. We count the number of turns executed by the organism for each track and average them over the population of swimmers for each thickness.

3.4 Characteristic times in different gaps

It would be interesting to understand how the swimmers change their behavior in different gaps and if there is a smooth shift of the peaks as expected in different gaps. Analysis of the mean characteristic time $\delta t_c^* = \overline{\delta t_c}/T$ shows an increasing trend confirming that directed motion is dominant in larger gap thicknesses and very less umber of turns in the smaller gaps as seen in Figure 3.5.

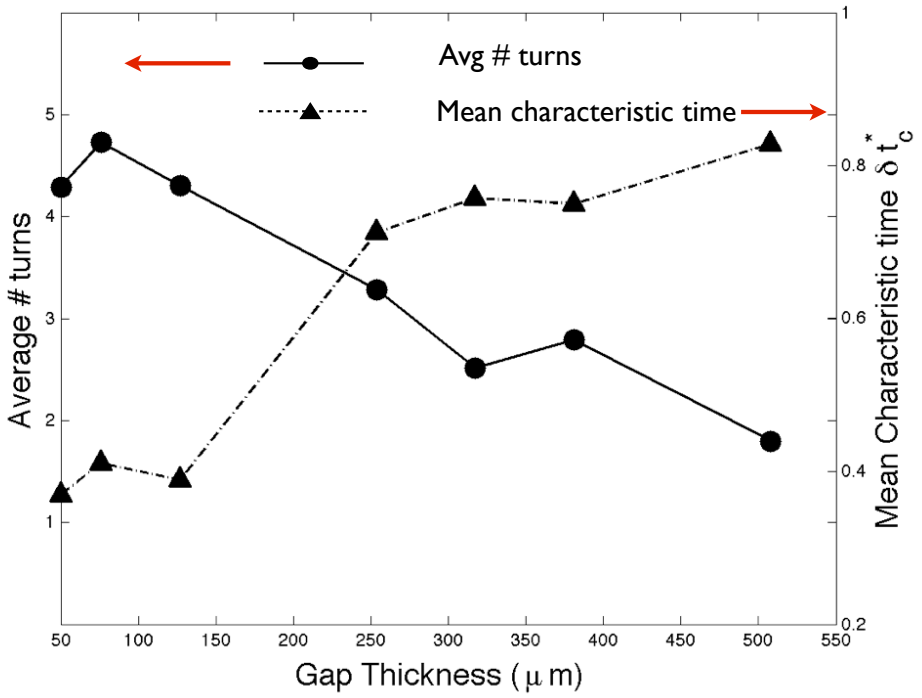

Figure 3.5: Figure shows the number of turns executed by the swimmers averaged over a population and also the distribution of mean characteristic time over different gap thickness.

3.5 Swimming characteristics in Channels

We also studied the transition of swimming gaits from quasi-2D to 1D confinements in PDMS channels manufactured from the mould master (ordered from Stanford Microfluidics Foundry) [104]. PDMS channels of various widths (W= 120-180 μm) and fixed heights (h = 80 μm) were used to test the confinement effect on the organism. Cases of directed swimming and meandering were observed reminiscent of swimming in 2D films; however in certain cases it was observed that *Paramecium* execute a half somersault to change its direction of motion (Fig. 3.6).

This can be attributed to the confinement which constrains *Paramecia* to touch and exert forces on the walls causing it to bend itself in the channel. Probability plot in Fig. 3.7

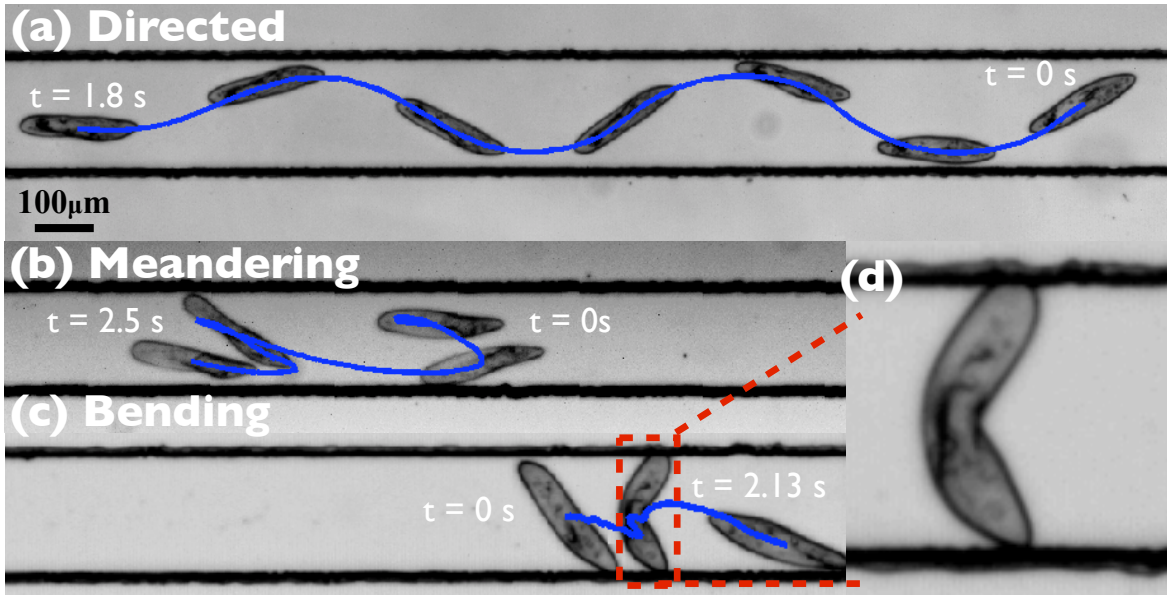

Figure 3.6: Three different kind of swimming trajectories seen during locomotion of *Paramecium* in confined channels: (a) directed swimming without changing direction, (b) meandering motion, (c) sudden bend to change its direction of swimming, and (d) zoomed-in image for self-bending.

shows that in the optimal range of $1.6 < L/W < 2.0$ values for which bending events are more probable. For larger channel widths ($L/W < 1$), *Paramecium* cannot touch both walls simultaneously and therefore cannot bend. While in smaller channels ($L/W \gg 1$) it is possible that the energetic cost of bending the cell body outweighs the forces generated by cilia.

This surprising self-bending of this unicellular body allows it to change its locomotion direction in extremely confined environments; where 2D meandering would not be feasible. A new fact comes to light that body flexibility and deformability can allow the organism to navigate complicated environments. Experimental observation of the bending phenomena shows that first the cell touches and slides along both the walls, and then hinges about the posterior end. Further, the anterior region keeps on sliding toward the posterior end while

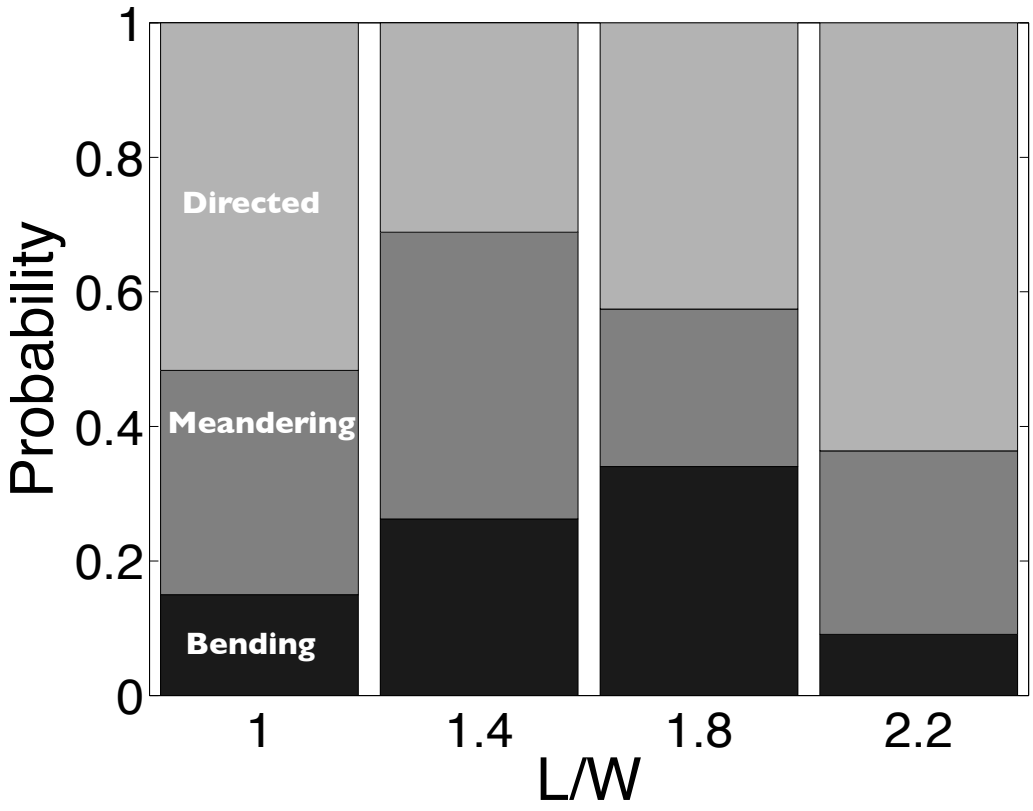

Figure 3.7: Probability plot of the three different swimming modes in PDMS channels; it is observed that the bending events peak when the geometric factor $1.2 < L/W < 2.0$

the posterior end remains almost fixed. Due to the active sliding of the anterior end, the cell body buckles like a bent bow. Since the cell compression (elongation or contraction of the body) is negligible, the power required for this process might be derived from the coordinated beating of the ciliary hairs. In organisms like *Euglena* there are protein strips which allow contraction and expansion of the pellicle [105]; however in *Paramecium* the existence of such strips is still in debate and no consensus exists.

To estimate the forces exerted during self-bending, the stiffness of the cell body is required. The Young's modulus of *Paramecia* was measured using a force-deflection technique [106] in which the organism is modeled as a cantilevered beam. The *Paramecium* was rigidly

held at one end, and a flexible glass fiber was placed in contact with the free end. The base of the glass fiber was displaced a distance δ_{base}, and the tip of the fiber in contact with the paramecium displaced a distance δ_{tip}. The force applied to the paramecium F was determined from the glass fibers deflection (δ_{base} -δ_{tip}) and stiffness k_F, where stiffness is defined as the force per unit deflection. The Young's modulus (E) of the *Paramecium* was then calculated based on the equation:

$$E = \frac{Fb^3}{3I\delta_{tip}} \tag{3.2}$$

where b is the distance of the applied force from the fixed end, and I is the area moment of inertia. Because the radius of the paramecium is not constant along its length, the moment of inertia was determined using the equation:

$$I = \frac{\pi}{4L}\int_0^L r(x)^4 \tag{3.3}$$

where the expression for the radius as a function of position $r(x)$ was determined for each organism tested and L is the length measured for each of the *Paramecium*. The function $r(x)$ were determined by selecting points along the upper edge of the *Paramecium* and curve fitting them with a 4th order polynomial. We assume that *Paramecia* have a circular cross section and are symmetric about their long axis. Equation 3.2 assumes that the cytoskeleton behaves as a linear elastic and homogenous material.

Just prior to experiments, *Paramecia* were killed by adding hot water (100°C) to a small volume containing paramecium (approximately 50:50 volume ratio). Paramecia were viewed using a fixed stage transmitted light microscope (Zeiss Axioskop) with 10X eyepieces and a 40X (0.75 NA) water immersion objective. Two micro-manipulators were used to position a

glass micro pipette to hold the *Paramecium* and a flexible glass fiber to deflect the cell body. *Paramecium* were picked up from one end with the micro pipette (20 μm inner diameter) and firmly held in position by suction. Suction was manually applied using a 60 mL syringe and maintained by closing a syringe valve.

3.6 Measurement of Elastic modulus of *Paramecium*

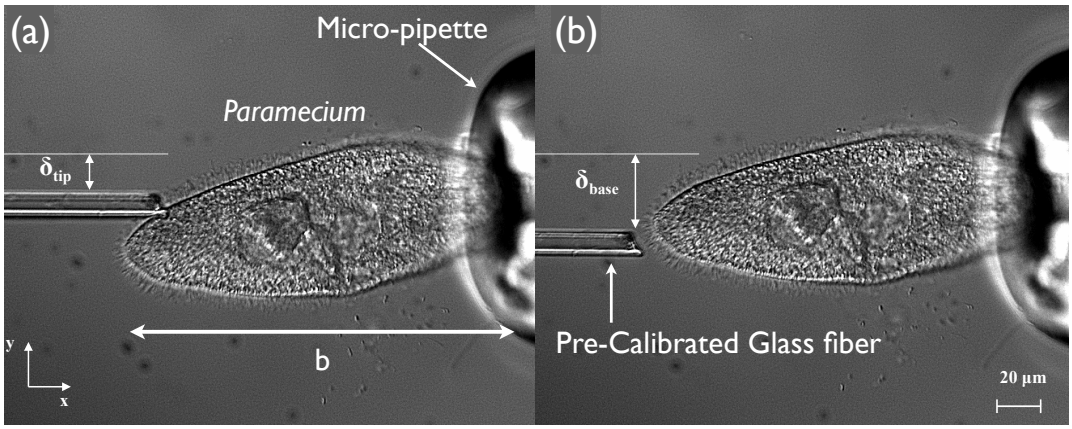

Figure 3.8: A snapshot of the force-deflection technique used to measure the Youngs modulus. The *Paramecium* is held at one end by a micro pipette and the tip of a flexible glass fiber contacts the free end. The horizontal white line indicates the position of the fiber in contact with the *Paramecium* prior to deflection. (a) The base of the flexible fiber is moved downward (y-direction), and the deflection of the fiber's tip (δ_{tip}) is measured. (b) The fiber is moved away from the *Paramecium* (x-direction) allowing the fiber to straighten and then the fibers base deflection (δ_{base}) is measured.

With the *Paramecium* firmly held at one end, a flexible glass fiber was brought into contact with the free end of the organism such that the long axes of both the organism and the fiber were parallel. The base of the glass fiber was displaced downward (y-direction), bending both the cell body and the fiber as seen in figure 3.8. The *Paramecium* was held in the deflected state several seconds before the fiber was moved away from the cell body (x-direction). The fiber then straightened so that the y-position of the tip equaled that of the base and the

total base deflection could be measured.

Videos of the *Paramecium* deflection and release were recorded using a high speed digital camera (Zeiss AxioCam HSm). Deflections of the *Paramecium's* free end (δ_{tip}) and the fiber base (δ_{base}) were extracted from the video in from of sequence of images. The range of δ_{base} was measured to be around $25 \sim 88$ μm, δ_{tip} was measured to be $7 \sim 40$ μm, and the applied force (F) was found to be $19 \sim 63$ nN. Care was taken to ensure that the *Paramecium* was rigidly held by the pipette (resembling a clamped cantilever beam). Measurements were discontinued if any sliding or rotation of the suctioned end was observed when a force was applied to the free end.

The flexible fiber was made from a borosilicate glass tube. The heating element of a micro-forge was used to pull a fine fiber from the tubes tip that was perpendicular to its shaft. The fiber had an outer diameter of 10.3 μm and was trimmed to a length of 4.8 mm. The stiffness of the glass fiber k_F was measured by applying small weights (glass beads) to the fiber and modeling it as a cantilevered beam with multiple point loads. Glass beads $210 - 250$ μm in diameter (Polysciences, Inc.) were statically attached to the horizontally positioned fiber. Using the micro-forge (35X magnification) with an eyepiece reticle, the vertical deflection of the fiber tip (δ_{tip}), the fibers length (l), the bead diameters, and the distance of the beads from the fiber tip (a) were measured. The weight of each bead (W_i) was determined from the beads diameter and known density ($2480 kg/m^3$). The fiber was calibrated four times yielding an average stiffness and standard deviation of $1,275 \pm 34$ pN/μm.

$$k_F = \frac{\sum_{i=1}^{N} W_i (1 - \frac{3a_i}{2l} + \frac{a_i^3}{2l^3})}{\delta} \tag{3.4}$$

For each *Paramecium* tested, multiple force-deflection trials were performed with applied

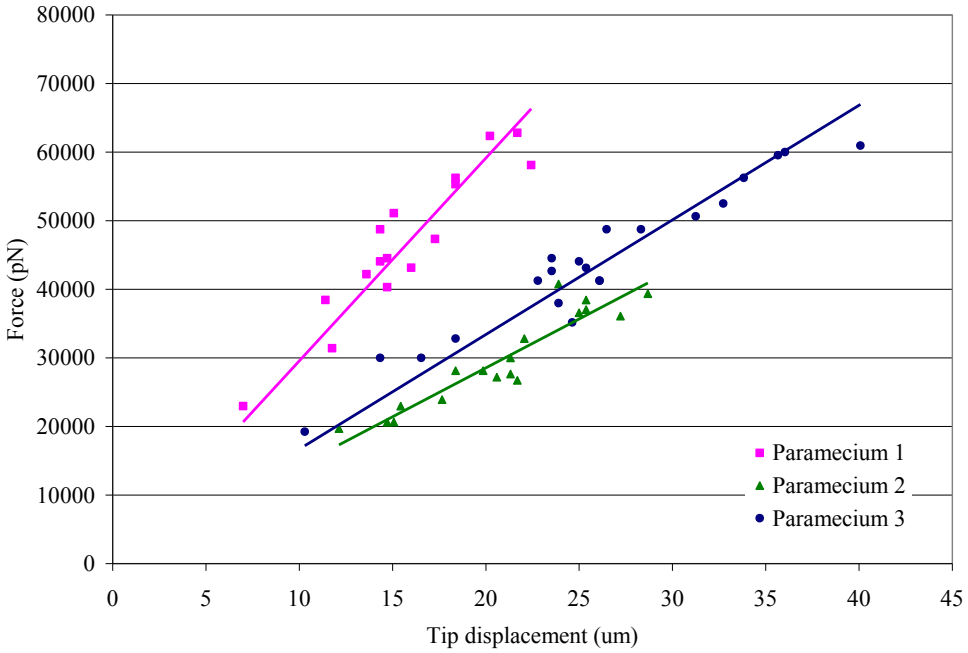

Figure 3.9: Graph of applied force vs. tip displacement. Multiple force deflection trials were performed for each *Paramecium*. The organism demonstrated linear elastic behavior in the range tested. Solid lines show linear regressions with the following equations: *Paramecium* 1: y = 2957x ($R^2 = 0.86$), *Paramecium* 2: y = 1427x ($R^2 = 0.87$), *Paramecium* 3: y = 1671x ($R^2 = 0.91$). The stiffness (slopes) depends on length and hence varies for each of tested *Paramecium*.

forces ranging from approximately $20 \sim 60$ nN. Plots of applied force vs. tip deflection for each organism demonstrated that the *Paramecia* are linear elastic in the range tested(refer to Fig 3.9). Linear regressions of the force vs. deflection plots yielded R^2 values ranging from $0.86 - 0.91$. The Young's moduli were determined for each force deflection trial and the average determined for each *Paramecium*. Average values, standard deviation and number of trials are given in the Table 3.1. We found the average elastic modulus for all the trials to be in range of 4.1 ± 0.4 kPa [107]; which is significantly lower than the cell wall of the prokaryotic bacteria *E. coli* [49, 108] and cilia [109] as well.

Table 3.1: Young's Modulus for different *Paramecia*

Paramecium No.	Number of Runs	Young's Modulus(Pa)
1	16	4349±467
2	18	4254±717
3	21	3622±369

3.7 Analysis of the bending profiles

3.7.1 Shapes and analysis procedure

In order to predict the deformed shapes of the organism in the channel (as shown in fig 3.10), we consider the total deformation energy of the cell. The aspect ratio of the *Paramecium* is 3∼4 which allows us to model these micro-swimmers as long cylindrical beams and allows us to easily estimate the forces required for the bending purpose. Visual observation of the images confirm that the stretching or compression of the cell is negligible. Therefore we neglect the compression energy and only consider the bending energy ($\mathcal{E}_B$).

The bending energy is given by $\frac{1}{2}\int EI\kappa^2 ds$ where κ is the centerline curvature, E is the elastic modulus of the cell, and I is the moment of inertia. Since the cell touches the walls we can write the total energy subject to the channel constraint as:

$$\mathcal{E} = \mathcal{E}_B + \lambda W = \int_0^L \left[\frac{1}{2}EI\left(\frac{\partial\theta}{\partial s}\right)^2 + \lambda\cos\theta\right] ds \tag{3.5}$$

By taking the variational derivative of the above equation and finding the maxima of energy, we get a quasi-static equation describing the static shape of the cell which is given by $\frac{d}{ds}\left(EI\frac{d\theta}{ds}\right) = -\lambda\sin\theta$ where λ denotes the force exerted by the organism on the channel walls during bending processes.

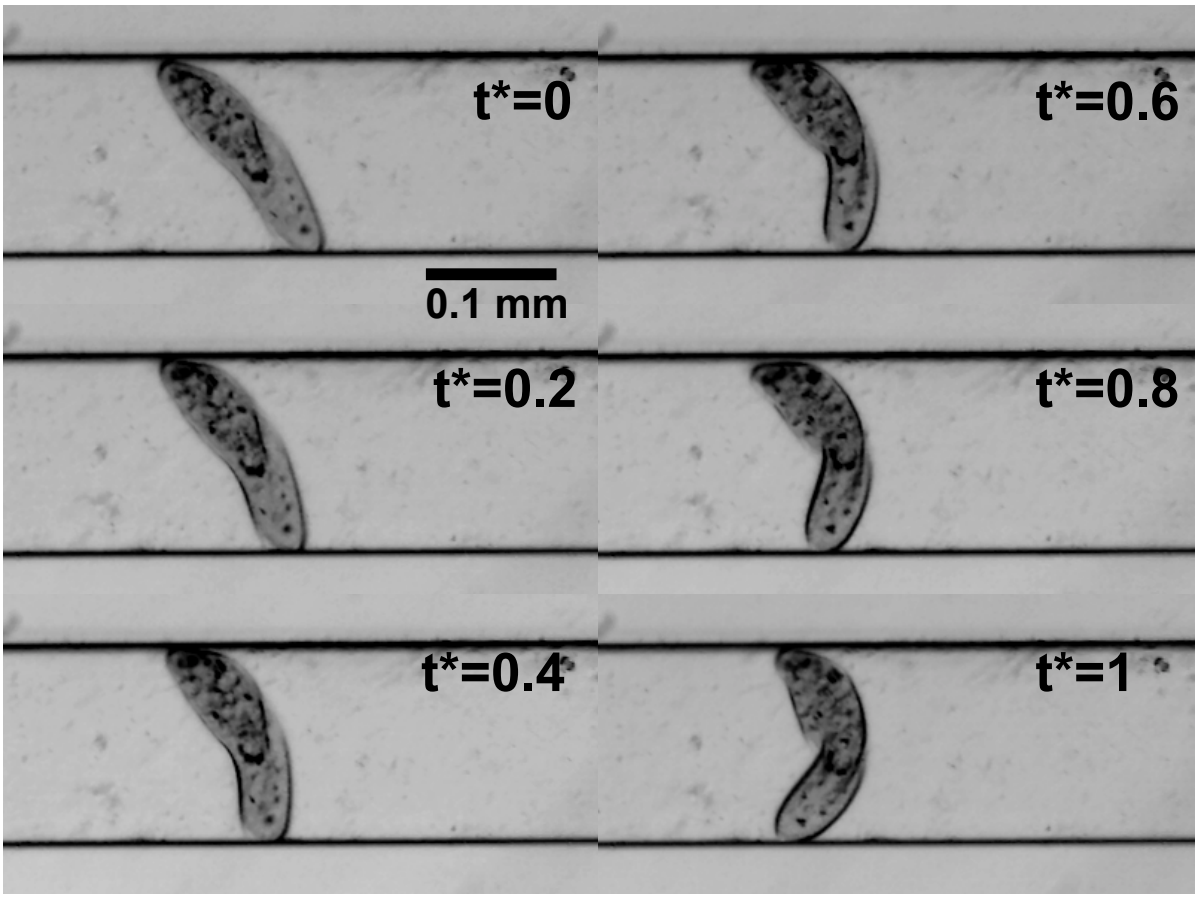

Figure 3.10: Figure shows the successive bent states of the *Paramecium* in the channel. $t^* = 0$ denotes the state during which the *Paramecium* just starts touching the wall and $t^* = 1$ denotes the state in which the organism has bent into a half crescent shape.

3.7.2 Fitted shapes

As shown in Fig. 3.10 , the *Paramecium* usually hinges its body on on one of the walls, and hence we assume zero bending moment at this end. This leads to the moment free boundary condition, $\frac{d\theta}{ds}|_{s=0} = 0$. The length of the *Paramecium* within the channel is also constant(i.e. no stretching or compression of the cell membrane) which is a physical constraint obtained from the shape of the organism. We use Runge-Kutta Method in MATLAB to solve the beam equation using the first moment free boundary condition and impose the condition of constant length on the *Paramecium*. By guessing the initial values of the forces one can

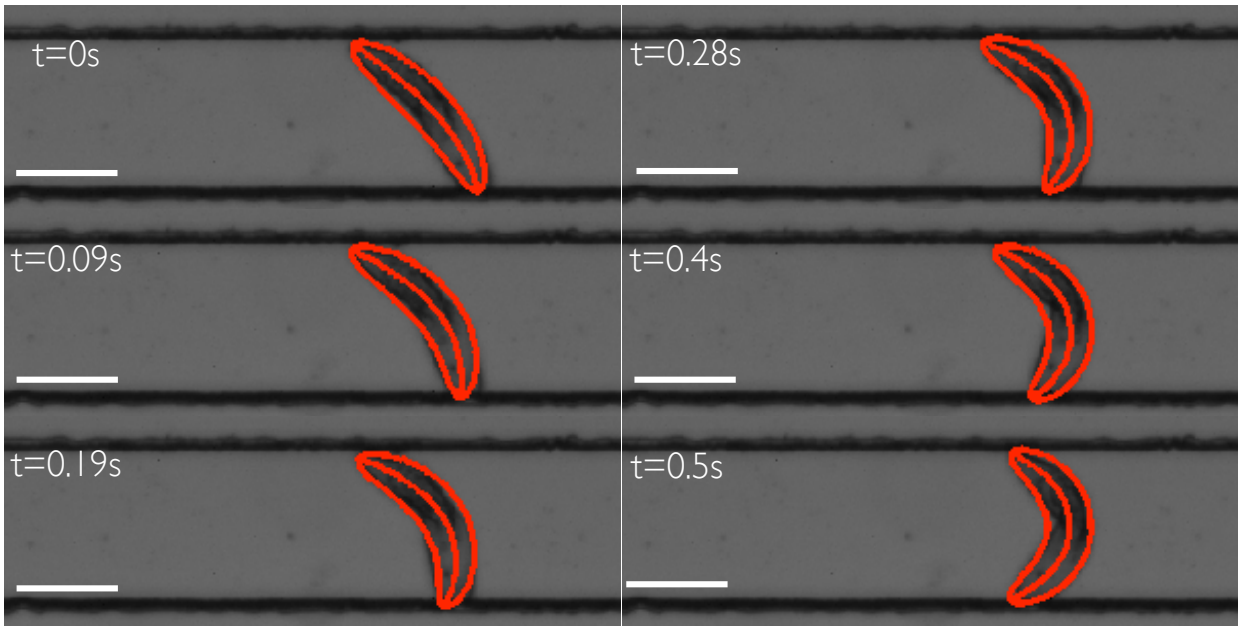

Figure 3.11: Figure shows the plot of the theoretical shapes on top of the images . Red lines show the shapes predicted by the theoretical equation.

match the bent shapes as predicted by the theory.

By comparing the experimental bent shapes of *Paramecium*, the forces (λ) at different instant are evaluated for the given elastic modulus. We fit the best possible shape on top of the images as shown in figure 3.11 to get the forces at each of the quasi-steady time steps.

3.7.3 Force exerted during the bending process

Two distinct regimes are observed in the bending process; the first stage involves touching both the walls ($t = 0$) so that the body is anchored. This regime is characterized by very little bending of the cell body and force values remain relatively low and constant as the cell is observed to slide around in the channel. The time to anchor varies in individual organism and is influenced by factors like roughness of walls and local adhesion between cilia and wall. The onset of the bending regime (t_b) (Fig. 3.12) is characterized as the single

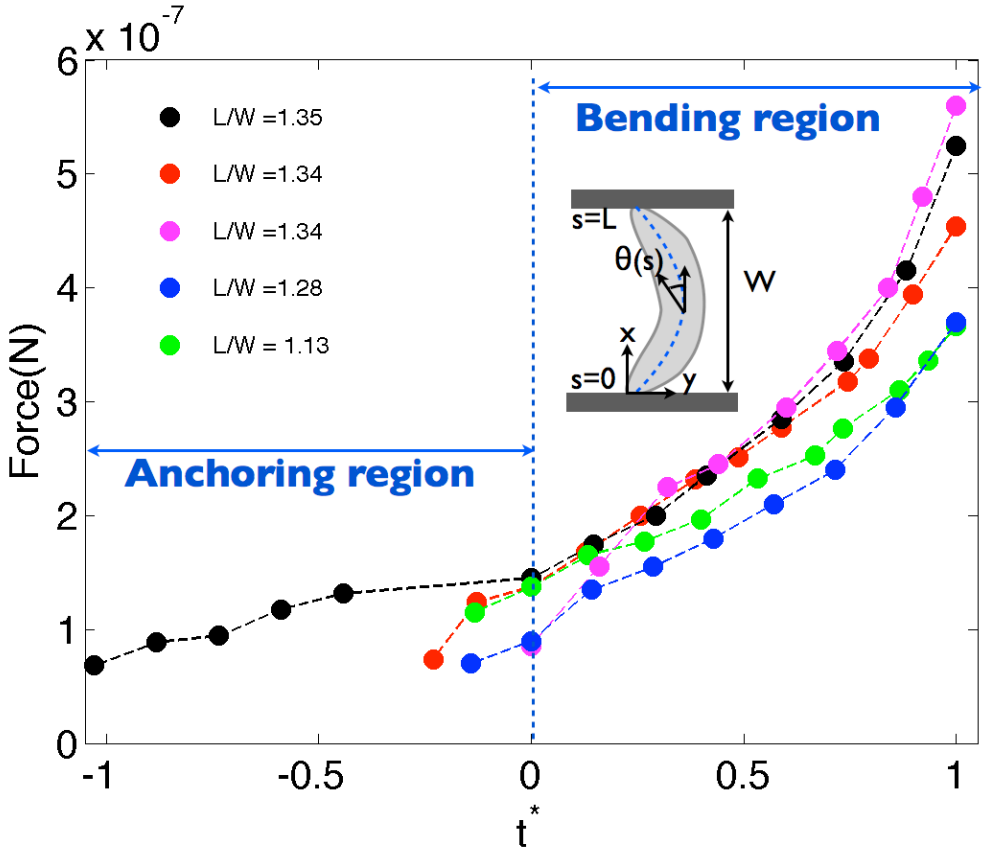

Figure 3.12: Inset shows the schematic of the theoretical model used for modeling. The plot shows the force exerted by the ends of *Paramecium* on the substrate at each different time-steps starting from the onset of bending($t^* = 0$). At initial time steps($t^* < 0$) it is observed that the force exerted is very small but increases rapidly as the organism bends into a crescent shape.

event when both ends of the organism touch the wall and there is a significant deformation of the body until the crescent shape is achieved (t_{end}). Figure 3.12 shows the plot of the forces exerted by the organism on the walls under varying confinement (denoted by different colors) at different instances of non dimensional time $t^* = (t - t_b)/(t_{end} - t_b)$. The plot shows a non-linear increasing trend until the end of bending regime after which the cell resumes swimming or prepares for another bending event.

3.8 Conclusion

The experimental investigations showed that physical confinements in a fluidic domain drastically alter the swimming patterns of *Paramecium*. From quasi-3D to 2D, the ciliate frequently switches swimming directions. Such 2D meandering behavior in confinements tend to give way to self-bending in a confined channel. For the case of *Paramecium* the cell body itself is softer than propulsive organelle cilia. The cell itself being more soft than the propelling organelle; allows it to deform while locomoting in extreme confinements. The beating of propulsive organelles which causes the buckling of cell body possibly points to another class of biological functions that the cilia can perform. Our work points to the direction that body deformability can be an important criteria for locomotion in complicated environments and possibly in complex fluids and gels.

Chapter 4

Velocities and swimming patterns in glass capillaries

Goal- To quantify the motion of helical swimmers in capillary tubes of different diameters and develop a model to understand the velocity of the swimmers in cylindrical tubes[1].

4.1 Introduction

Microorganisms use a variety of propulsion mechanisms [110] to swim around in their habitat for predator evasion [111] or to gather food by swimming towards favorable gradients [112]. The locomotory behavior and performance is usually controlled by chemical [113] or hydrodynamic cues [88] arising due to interaction with the local environment. Although boundaries are usually neglected, introducing them in the fluidic system have revealed surprising effects in different organisms; for example sperm swimming near surfaces execute

[1]Parts of this work has been published in S. Jana, S. Um, and S. Jung. "*Paramecium* swimming in capillary tube." Physics of Fluids, 24(4), Apr 2012.

circular/curvilinear trajectories [38] and bacteria tend to aggregate near solid surfaces [45]. Boundary effects on bacterial swimming speed/direction, tumbling probability and turn angle in capillaries have been characterized [47, 114] while similar studies in ciliary organisms are rare. Motility of cells and the morphological changes in body shape due to restrictive geometries are active areas of investigation [48, 115]. These examples show that organism surface interactions can be critical and cause the organism to exhibit varied swimming characteristics/gaits as compared to swimming in ideal unbounded fluid conditions.

In ciliates propulsion is achieved by coordinated motion of cilia which helps in propagating metachronal waves [17]. Millions of ciliary hairs in mammals help in mucus transport [83] and also function as sensory organelles that help in maintaining balance; signifying the importance of cilia in various systems. The control of ciliary beat in Paramecium is an interesting phenomena and has been studied extensively from point of view of Ca^{2+} ion efflux/influx through the ion channels, while the role of hydrodynamic synchronization in beating arrays of cilia is being currently explored [82]. Experiments have been conducted to gain insights into the chemical-physiological [24] effects that cause changes in the ciliary beat [9] and trajectories as well as taxis of ciliates in solutions of varied ionic concentrations have been categorized [5]. The effect of high viscosities on the locomotory traits of Paramecium especially with regards to changes in wave velocities, amplitude and wavelength of the metachronal waves have been extensively documented [21]. Experiments on swimming of ciliates in vertically aligned tapered glass tubes [61] have contributed to understanding of drag acting on the bodies.

Theoretically a 2D wavy sheet can be used to describe simplified swimming motion in many micro-swimmers; which provided one of the first theoretical framework for modeling microorganisms, by considering small amplitude expansions of the propagating wave [66]. Further studies extended the 2D sheet model to include effect of planar boundaries and revealed

propulsive advantages for specific beat patterns at certain distances from the boundaries [116]. As thousands of cilia in *Paramecium* beat just out of phase to propagate waves in fluid; they have been modeled as infinitely long cylinders [68] or spheres [69] with surface undulations or as a spheroid with slip velocity [63]. These models were also used to validate swimming velocities in variety of ciliates and to develop a boundary layer theory for predicting the near and far field velocities of ciliary microorganisms in the unbounded fluid [117].

In most cases, experiments have involved measuring the average velocity; however, various trajectories executed by *Paramecium* have not been studied. While theoretical studies involving swimming *Paramecium* have mostly focused on infinite models without consideration of the boundary effects. We present a unifying experimental and theoretical approach to reveal the locomotive patterns of *Paramecium multimicronucleatum* and rationalize the pressure gradient effects, on the swimming velocities in confined spaces. In Sec. 3.2, we explain the experimental methods of introducing the organisms in confined geometries like the capillary tubes and the techniques used to visualize their motion. A theoretical model incorporating pressure gradient is developed to understand the effect of boundaries in Sec. 3.3. In Sec. 3.4, we compare the predicted swimming velocity with the experiments, and in Sec. 3.5 we discuss other important parameters that might affect locomotion of ciliates close to the boundaries.

4.2 Experiments

4.2.1 Procedure

Paramecium used in the experiments was found to have a long and slender structure with

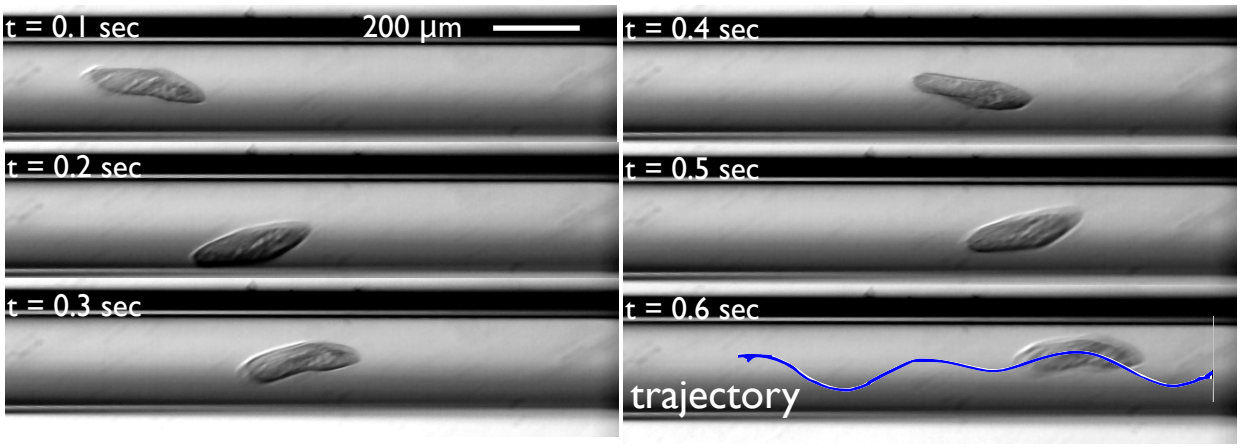

Figure 4.1: Snapshots of *Paramecium* swimming in a helical trajectory in a capillary tube. The blue line denotes the centroid of the organism at each of the recorded frames and is plotted on top of one of the representative frames.

axial length around 212±14 μm and diameter around 57±5 μm (shown in Fig. 4.1). We introduced the organisms into the glass capillaries by using the capillary action of the fluid and measured their velocities in capillary tubes of different diameters. *Paramecium* swimming in buffer (isotonic solution) were put into the capillary tubes which caused them to be confined in small circular geometry. We recorded the tracks of the swimming organisms using Leica DMI 3000B microscope in the bright-field mode with a MotionXtra N3 camera at 100fps. A generic code written in MATLAB was used to track the motion of these organisms and their velocities were calculated using the equation 4.1.

$$V_{swim} = \frac{\sum_{i=0}^{n-1} \sqrt{(x_{i+1} - x_i)^2 + (y_{i+1} - y_i)^2}}{\Delta t} \tag{4.1}$$

The experimental runs consisted of manufacturing over 500 capillary samples and helical tracks of over 250 organisms were recorded. At times there were multiple organisms in the tube which needed to be discarded to avoid external effects introduced by the neighboring organism. The tracks recorded showed different kind of motion; helical straight line and swimming along the posterior end. The experimental analysis only considered the cases

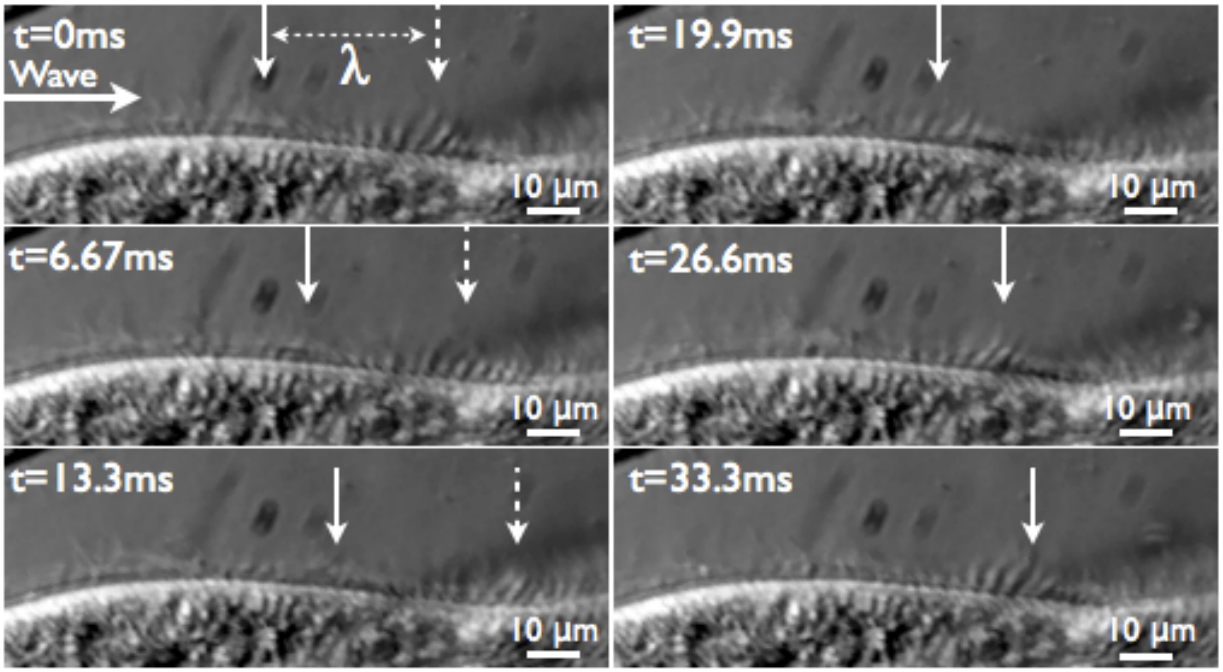

Figure 4.2: The metachronal waves propagated by the cilia of the *Paramecium* over a period of 33.3 ms. The sweep of the cilia and the direction of propagation of the wave can be visualized. Arrows follow the peak amplitude of the waves.

in which the tracks were helical and hence only 119 of the recorded tracks were deemed useful. Imaging of round capillaries under microscope caused optical distortions which leads to recording of altered amplitudes and velocities. We directly took images of the cross-section of various capillaries to get a relation between the true and the observed inner diameters of the tubes, which was further used to correct the observed amplitude and velocities of the organisms.

4.2.2 Metachronal wave parameters

In order to measure the vital parameters for swimming; we captured the cilia motion in semi-infinite fluid domain with the high speed camera at 300 fps, which allowed us to visualize the metachronal wave propagation over the organism. We assume that the cilia are so closely

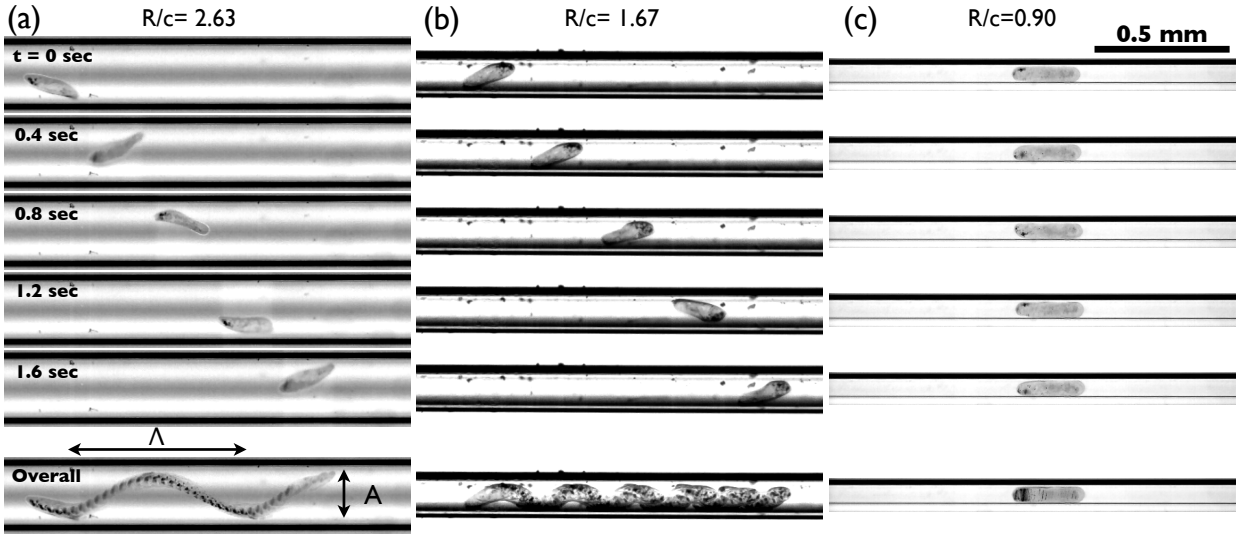

Figure 4.3: Swimming of *Paramecium* in tubes of different diameters. Λ denotes the wavelength and A the amplitude of the helical trajectory traced by organism in different diameter tubes. (a) shows swimming in large tube ($R/c = 2.63$) where the trajectory of the motion is helical. In swimming inside tubes of intermediate diameters ($R/c = 1.67$) small wavelength helices are seen. In very small tubes ($R/c = 0.9$) as shown in (c) *Paramecium* swims in a straight line.

packed that the fluid does not penetrate the material wave, thereby allowing no slip boundary condition to hold good. Each cilium was found to be 10$\sim$12 μm in length and 0.2 μm in diameter and beats slightly out of phase compared to the nearby cilium, thereby causing a traveling wave to pass over the surface of the organism. The typical wavelengths of the metachronal waves measured from five different videos of *Paramecium* (Fig. 4.2) in semi-infinite fluid medium were found 27$\pm$3 μm, half of peak to peak amplitude measured around 4.2$\pm$0.2 μm and the frequency of the beat being around 30 Hz . These vital parameters for swimming are assumed to be constant for the swimming *Paramecium* in variety of constrained geometries.

4.2.3 Observations

In tubes of extremely small diameter the swimming velocity of the organism was very low with almost a straight line motion with variable rotation rates. Whereas in tubes of larger diameter the organism was seen to move in a helical path instead of straight line motion. We applied a correction factor for the path of the swimming organisms, as the image analysis only revealed the 2D projection of the helix. It is observed that the *Paramecium* swims slowly as the tube diameter is decreased. This can be attributed to the increased drag felt by the organism due to the proximity of the boundaries. For the capillary tubes whose diameter were very close to the diameter of the *Paramecium*, the swimming velocity was close to zero but the organism seemed to be rotating about its axis.

To compare the velocities in various tubes and in semi-infinite fluid domain (a drop of fluid on the glass slide); we diluted the suspension of swimming organisms and recorded the tacks of single organisms in the field of view. Their velocity was found to be 1534 $\pm$ 278 μm/s; their amplitudes 21.6 $\pm$ 3.2 μm and the wavelengths of the swimming tracks being 217 $\pm$ 24 μm.

In tubes of smaller diameter ($R/c \sim 1.5$) we observed that a backward (posterior) swimming *Paramecium* executed a helical swimming trajectory with small amplitude wavelengths as shown in Figure 4.3. Such swimming gait have not been reported before [5, 118]. In this range of tube diameters and considering the forward swimming *Paramecium*, little helical motion of the organism is observed.

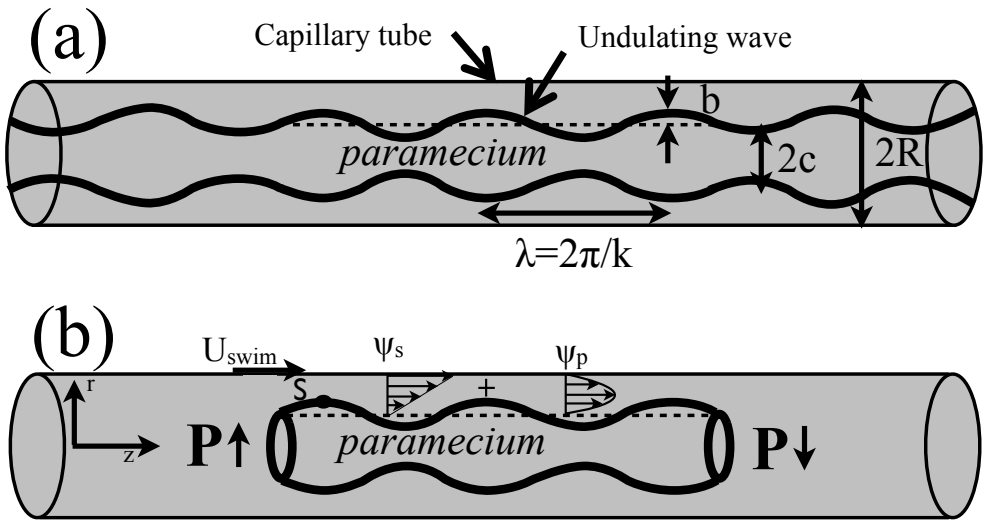

Figure 4.4: Schematic of a wavy (a) infinite cylinder or (b) finite cylinder swimming inside the cylindrical tube. It is assumed that the organism is swimming in the negative z direction with a velocity U_{swim}. By transforming the coordinate system to one, where the organism is swimming with velocity U_{swim} we get the current schematic with the descriptions of the velocities on the walls of capillary.

4.3 Theoretical model

The governing equations for very low Reynolds number flows ($Re \ll 1$) are the Stokes equations:

$$\nabla p = \mu \nabla^2 \mathbf{u}, \nabla \cdot \mathbf{u} = 0 \tag{4.2}$$

Since these organisms have a large length to diameter ratio; they can be possibly modeled as cylinders. As seen in the Figure 4.2 the cilia create synchronized motion to produce metachronal waves; to an observer this seems like a material wave propagating on the surface of the organism. Under the assumption that no fluid penetrates the wave of cilia tips since they are densely packed all over the surface of the organism, the concept of envelop model can be applied to the physical system. To simplify the model we assume that the metachronal

wave propagates from the head to the tail all along the length of the body. The boundary in this case is the circular capillary tube; thus the problem reduces to modeling a cylinder with a wavy surface swimming inside a cylindrical geometry.

Figure 4.4 shows the schematic of the organism swimming the tube with a velocity U_{swim}. In previous studies *Paramecium* has been modeled as an infinitely long cylinder so that there is no pressure gradient at the front and the back while swimming in the unbounded fluid. Similar infinite models can be developed for a *Paramecium* swimming inside a tube [68]. However, due to the presence of the confined spaces the finite length *Paramecium* creates a pressure gradient at its ends that influences its locomotion within tubes. Considering the propagating wave on the surface of the organism to be of frequency ω,wavelength λ, radial amplitude b, transverse amplitude a, and wave number $k = \frac{2\pi}{\lambda}$; any material point S on the undulating surface can be written as:

$$r_s = c + b\sin(kz - \omega t), \quad z_s = z + a\cos(kz - \omega t + \phi) \tag{4.3}$$

where ϕ is the phase difference between the two waves.

The velocity of the material point S on the wave can be written as:

$$u_r = -b\omega\cos(kz - \omega t), \quad u_z = a\omega\sin(kz - \omega t + \phi) \tag{4.4}$$

We work in the frame in which the organism is swimming with a velocity U_{swim}. In the small amplitude limit, the boundary conditions of the surface of the organism at $r = c$ can be written as:

$$u_r|_{r=c} = -b\omega\cos(kz - \omega t), \quad u_z|_{r=c} = a\omega\sin(kz - \omega t + \phi) \tag{4.5}$$

and the boundary conditions at $r = R$ in the frame of the swimming velocity of the organism can be written as

$$u_r|_{r=R} = 0, \quad u_z|_{r=R} = U_{swim} \tag{4.6}$$

As the *Paramecium* swims inside the capillary effects of pressure gradient due to finite spaces as well as shearing motion (due to swimming) need to be taken into account. The boundary conditions employed are analogous to the case of peristaltic pumping; where the velocities are enforced in the similar fashion and pressure gradient is assumed constant at the ends of the length of the organism [119, 120].We assume similar conditions for the swimming *Paramecium* with the pressure gradient being constant between the anterior and the posterior end. The swimming problem can thus be envisioned as sum of pressure driven flow and shear flow in the narrow annulus that surrounds the *Paramecium*. We seek a solution in terms of the axisymmetric streamfunction ψ such that $\psi = \psi^{(p)} + \psi^{(s)}$ where $\psi^{(p)}$is the streamfunction corresponding to pressure driven flow and $\psi^{(s)}$due to the the shear flow. Using cylindrical co-ordinates and axisymmetric stream function we can write the velocity components to be $u_r = -\frac{\partial \psi}{r \partial z}$,$u_z = \frac{\partial \psi}{r \partial r}$.

First let us consider the pressure driven flow and substitute the equations for the velocities into the stokes equation. By solving considering the stationary boundaries we find the streamfunction for the pressure driven flow to be:

$$\psi^{(p)} = \frac{1}{4\mu}\frac{\partial p}{\partial z}\left[\frac{R^2 - c^2}{\ln \frac{R}{c}}\left(\frac{r^2}{4} - \frac{r^2}{2}\ln\frac{r}{c}\right) + \left(\frac{r^4}{4} - \frac{c^2 r^2}{2}\right)\right] \tag{4.7}$$

For the shear flow part we can substitute the velocity components in the Stokes equation and by taking curl we end up with an equation of the form $\left(\frac{\partial^2}{\partial r^2} - \frac{1}{r}\frac{\partial}{\partial r} + \frac{\partial^2}{\partial z^2}\right)^2 \psi^{(s)} = 0$.

Rewriting coordinate systems as $\eta = kr$ and $\zeta = kz - \omega t$ and using separation of variables in η and ζ we can obtain a streamfunction solution of the form:

$$\psi^{(s)} = \frac{U_{swim}\eta^2}{2k^2} + \sum_{i=0}^{m} F_n \sin(\zeta) + \sum_{i=0}^{m} G_n \cos(\zeta) \tag{4.8}$$

where,

$F_n = \eta \left[A_n K_1(n\eta) + B_n \eta K_2(n\eta) + C_n I_1(n\eta) + D_n \eta I_2(n\eta)\right]$

$G_n = \eta \left[\alpha_n K_1(n\eta) + \beta_n \eta K_2(n\eta) + \gamma_n I_1(n\eta) + \delta_n \eta I_2(n\eta)\right]$

and $A_n, B_n, C_n, D_n, \alpha_n, \beta_n, \gamma_n, \delta_n$ are the constants to be determined from the boundary conditions and I and K are modified Bessel functions of the first and second kind.

We seek perturbation expansions of the velocities $u_r = -k^2 \frac{\partial \psi}{\eta \partial \zeta}$ and $u_z = k^2 \frac{\partial \psi}{\eta \partial \eta}$ derived from the stream function to the $O^0(bk)$ and $O^1(bk)$ and compare the velocities with Equation 4.6. The calculations of the zeroth order radial velocities yields the following set of the equations (after comparing the sine and cosine terms from both sides of the equation) at the surface of the *Paramecium*:

$$\begin{aligned} A_1 K_1(\eta_c) + B_1 \eta_c K_2(\eta_c) + C_1 I_1(\eta_c) + D_1 \eta_c I_2(\eta_c) &= \frac{b\omega}{k^2} \\ \alpha_1 K_1(\eta_c) + \beta_1 \eta_c K_2(\eta_c) + \gamma_1 I_1(\eta_c) + \delta_1 \eta_c I_2(\eta_c) &= 0 \end{aligned} \tag{4.9}$$

while at the surface of the capillary tube we get the following set of equations:

$$\begin{aligned} A_1 K_1(\eta_R) + B_1 \eta_R K_2(\eta_R) + C_1 I_1(\eta_R) + D_1 \eta_R I_2(\eta_R) &= 0 \\ \alpha_1 K_1(\eta_R) + \beta_1 \eta_R K_2(\eta_R) + \gamma_1 I_1(\eta_R) + \delta_1 \eta_R I_2(\eta_R) &= 0 \end{aligned} \tag{4.10}$$

where $\eta_c = kc$ and $\eta_R = kR$ where c is the mean radius of the organism and R denotes the radius of the capillary tube. The calculations and comparison of sine and cosine components

of the zeroth order longitudinal velocities yields the following set of the equations at the surface of the organism:

$$\begin{aligned}
\frac{k^2}{\eta_c}(-A_1\eta_c K_0(\eta_c) - B_1\eta_c^2 K_1(\eta_c) + C_1\eta_c I_0(\eta_c) + D_1\eta_c^2 I_1(\eta_c)) &= a\omega\cos\phi \\
\frac{k^2}{\eta_c}(-\alpha_1\eta_c K_0(\eta_c) - \beta_1\eta_c^2 K_1(\eta_c) + \gamma_1\eta_c I_0(\eta_c) + \delta_1\eta_c^2 I_1(\eta_c)) &= -a\omega\sin\phi
\end{aligned} \tag{4.11}$$

By comparing the constant terms we find that $U_{swim} = 0$; which shows that the zeroth order swimming speed is zero i.e. the organism doesn't move. Following the same analysis and at the surface of the capillary tube we get the expressions:

$$\begin{aligned}
-A_1\eta_R K_0(\eta_R) - B_1\eta_R^2 K_1(\eta_R) + C_1\eta_R I_0(\eta_R) + D_1\eta_R^2 I_1(\eta_R) &= 0 \\
-\alpha_1\eta_R K_0(\eta_R) - \beta_1\eta_R^2 K_1(\eta_R) + \gamma_1\eta_R I_0(\eta_R) + \delta_1\eta_R^2 I_1(\eta_R) &= 0
\end{aligned} \tag{4.12}$$

Since the zeroth order swimming speed is zero; at the surface of the *Paramecium* we can undertake a 2nd order expansion of the form:

$$u_z = u_{z(\eta_c,\zeta)} - \frac{\partial u_z}{\partial\eta}|_{(\eta_c,\zeta)} bk\sin\zeta - \frac{\partial u_z}{\partial\zeta}|_{(\eta_c,\zeta)}(ak\cos\phi\sin\zeta + ak\cos\zeta\sin\phi) \tag{4.13}$$

Comparing the sine, cosine and the constant terms we have the set of following three equa-

tions:

$$
\begin{aligned}
-A_1K_1(\eta_c) - B_1\eta_cK_0(\eta_c) + C_1I_0(\eta_c) + D_1\eta_cI_1(\eta_c) \\
-\frac{\eta_c b}{2\mu k^2}\frac{\partial p}{\partial \zeta} + \frac{b(\eta_r^2-\eta_c^2)}{4\mu k^2 \ln\frac{\eta_R}{\eta_c}}\frac{\partial p}{\partial \zeta} = \frac{a\omega\cos\phi}{k^2} \\
U^{(1)}_{swim} - \frac{bk^3}{2}(A_1K_1(\eta_c) + B_1\eta_cK_1(\eta_c) + C_1I_1(\eta_c) + D_1\eta_cI_0(\eta_c)) \\
-\frac{a\omega k^2}{2} - \frac{abk\cos\phi\eta_c}{4\mu}\frac{\partial p}{\partial \zeta} + \frac{abk\cos\phi}{8\mu k}\frac{\eta_R^2-\eta_c^2}{\ln\frac{\eta_R}{\eta_c}}\frac{\partial p}{\partial \zeta} = 0 \\
A_1K_1(\eta_c) + B_1\eta_cK_2(\eta_c) + C_1I_1(\eta_c) + D_1\eta_cI_2(\eta_c) = \frac{b\omega}{k^2}
\end{aligned}
\tag{4.14}
$$

The above three equations 4.14 coupled with equations 4.12 gives us a set of five equations and six unknowns $A_1, B_1, C_1, D_1, U_{swim}, \frac{\partial p}{\partial z}$.

To solve the set of equations we note that in the stationary frame the swimming *Paramecium* squeezes out a volume of fluid through the annulus which is given by $Q = U_{swim}\pi c^2$ where c is the radius of organism. Also in the translating frame we can calculate flux which can be given by $Q' = \int\int u_z r d\theta dz$. Both the fluxes thorough the annulus should be the same which gives us a relation between U_{swim} and $\frac{\partial p}{\partial z}$.

$$
\frac{\partial p}{\partial \zeta} = \frac{8\mu c\eta_c^2 U_{swim}}{(\eta_r^2-\eta_c^2)^2(1+\frac{1}{\ln\frac{\eta_r}{\eta_c}} - \frac{2\eta_r^2}{\eta_r^2-\eta_c^2})} \tag{4.15}
$$

Which when substituted back to the equations allow us to get a set of five equations and five unknowns which can be solved to find out the constants(A_1, B_1, C_1, D_1) and the swimming velocity U_{swim} of the organism. The expression for swimming velocity of the *Paramecium*

comes out to be:

$$U_{swim} = \frac{k^3 b}{2} F_n(\eta_c) + \frac{a^2 k\omega}{2} + \frac{abk\eta_c \cos\phi}{8\mu} \frac{\partial p}{\partial \zeta} - \frac{abk\cos\phi}{8\mu\eta_c} \frac{\partial p}{\partial \zeta} \frac{\eta_R^2 - \eta_c^2}{\ln \frac{\eta_R}{\eta_c}}$$

where $\eta_R = kR$ and $\eta_c = kc$.

The above expression shows that the swimming velocity is directly dependent on $(ak)^2$ and also the pressure gradient terms. For the infinite boundaries case with no pressure gradient the above equation reduces to the following expression:

$$U_{blake} = \frac{\omega k}{2} \left[\frac{(K_0^2 - K_1^2)b^2}{K_1^2 - K_0 K_2} - \frac{2K_1^2 ab\cos\phi}{\eta_c (K_1^2 - K_0 K_2)} - a^2 \right] \tag{4.16}$$

which is same as in [68].

4.4 Results

The motivation of the study was to rationalize the behavior of the organisms in close proximity to the boundaries. As the *Paramecium* swims inside the tube it traces out a helical path with the length of the body being aligned in the swimming direction. Figure 4.5 shows the variation of the amplitude of the helical path of organism as it swims in capillary tube of different diameters. As the radius of the capillary increases the *Paramecium* also increases the diameter of the helix in which it swims. However in case of semi-infinite fluid the swimming amplitudes are much smaller as compared to the largest tube.

Theoretically we considered the small amplitude expansions for the waves and hence the expression derived for the swimming velocity would only be valid for smaller capillary tubes in which there is very less off axis movement. From the plot above and the constraints

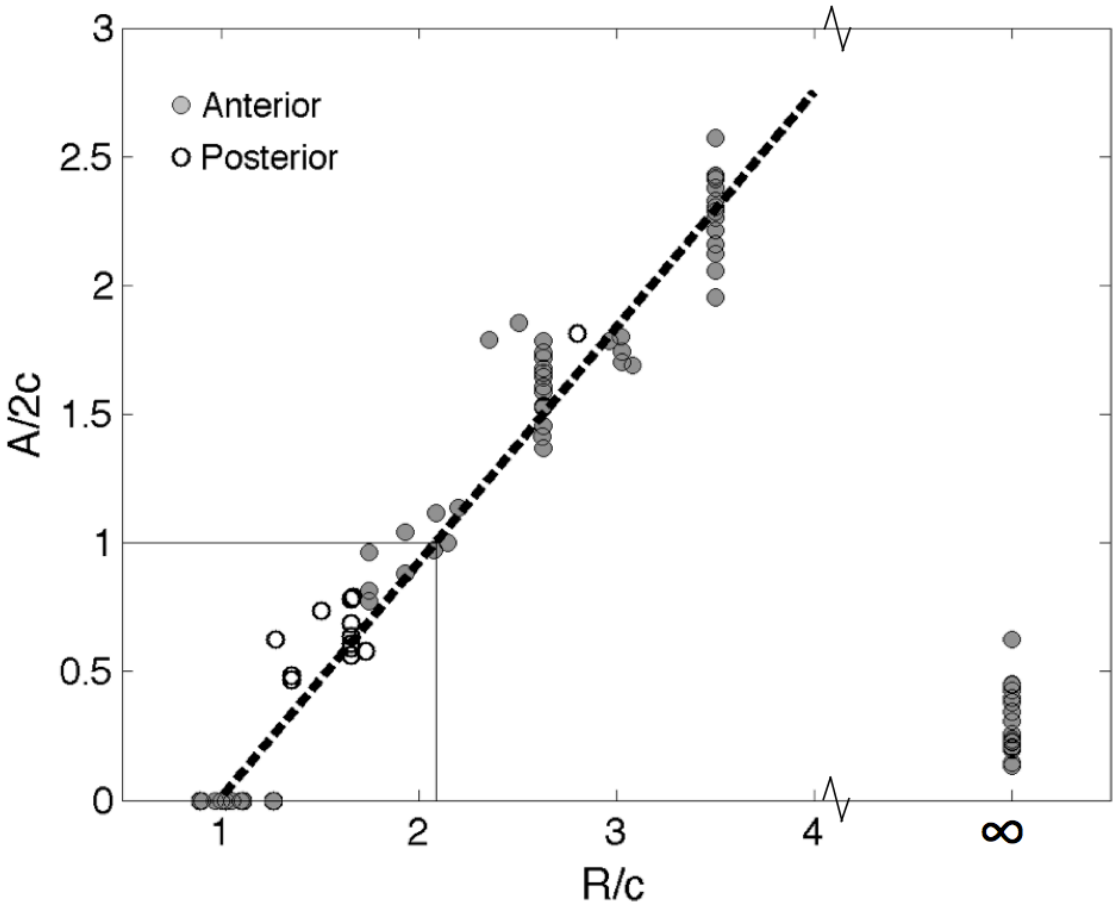

Figure 4.5: Plot of the non-dimensional amplitude of the helical path vs the non-dimensional radius of the tube. The plot shows a linear variation which increases with the radius of the tube.

on the amplitude of swimming of *Paramecium* we can conclude that for $A/(2c) < 1$ our experimental and theoretical results would remain valid. This gives us corresponding value of the non-dimensional radius of the capillary tube $R/c < 2.1$.

Figure 4.6 shows the variation of velocity with the radius of the capillary tube. The dotted line shows the swimming velocity when no pressure gradient effects are considered and the solution converges very quickly to the case in which the boundaries are at infinity. In the experiments we observe a slowly increasing trend of velocity. For a finite size *Paramecium* swimming inside a restrictive geometry there is a finite pressure gradient at the front and the

back. The plot of the swimming velocity considering finite pressure gradient is shown by the solid line. It shows a slowly increasing trend and finally converges to the infinite boundary and no pressure gradient case for very large R/c values. We observe that the velocities in the semi-infinite domain are a little higher as compared to the swimming values in the largest tube.

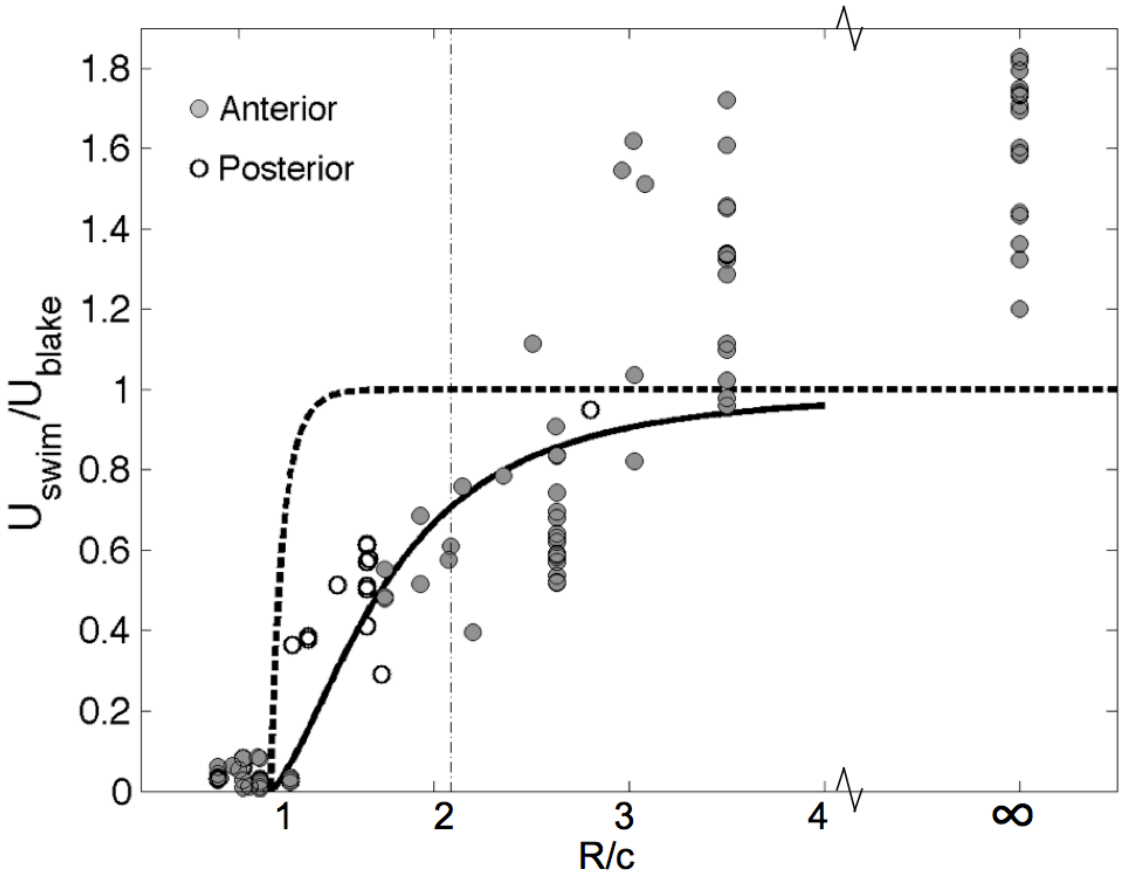

Figure 4.6: Plot of normalized swimming velocity vs. the non-dimensional radius of the tube. Two different cases are compared, one with the dotted line shows the model of an infinite ciliate swimming in capillary tube. The solid line shows the velocity variation of the finite sized *Paramecium* inside confined geometries. Dots represent the experimental result and compares well with the finite pressure gradient model due to the restrictive environment.

It can be seen that for $R/c < 2.1$ both the experiments and theory show an increasing trend and predictions match quite well. For the larger R/c we see that the velocities are

much larger as opposed to that predicted value for the infinite boundary case. From the experiments we see that the organism follows the surface of the glass capillary as it swims in helical path in tubes of different diameter.

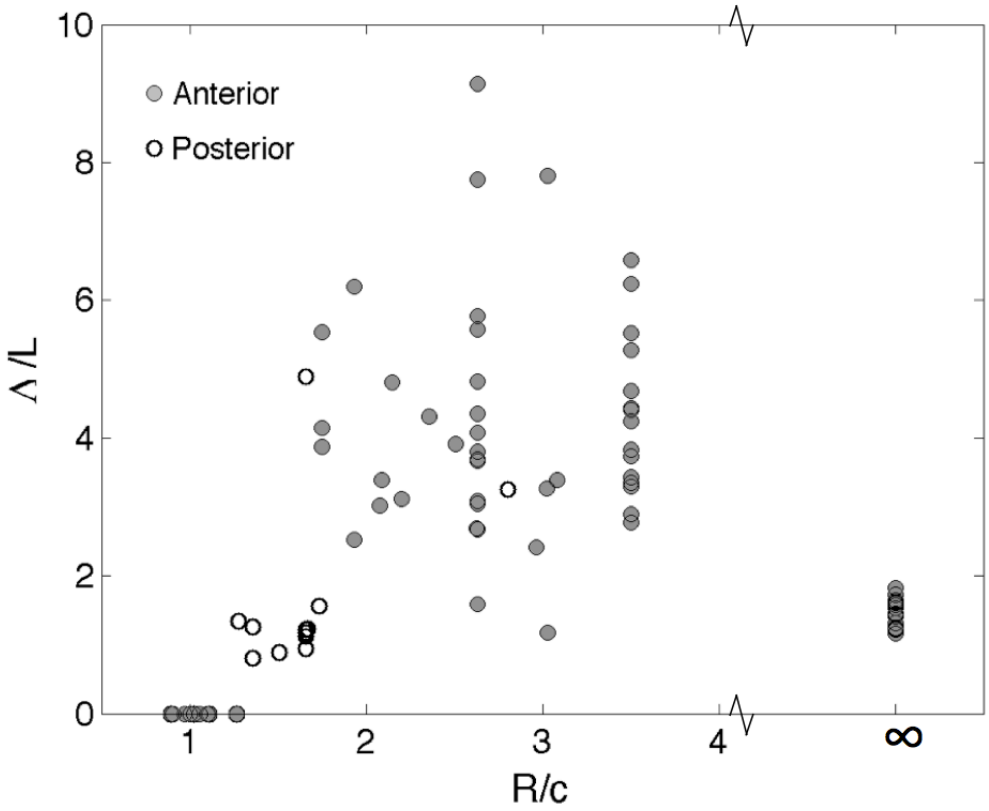

Figure 4.7: Plot of the non-dimensional wavelength vs. non-dimensional radius of the tube. No apparent trend is seen with increasing radius of the tube. In contrast while swimming in the semi-infinite domain the *Paramecium* has well defined wavelengths of the helical path.

Figure 4.7 shows the variation of wavelengths of the helical path while they are swimming in the tube. The wavelengths also show a linearly increasing trend for the limit $R/c < 2.1$. In this limit the helices of the swimming are well defined and periodic wavelengths are observed. While swimming in tubes of larger diameter ($R/c > 2.1$) it was observed many times that the organism did not execute a full helix.

In order to compare the swimming efficiency (η) of *Paramecium* in different diameter tubes (in which they might swim in a helix or a straight line); we estimate an efficiency parameter

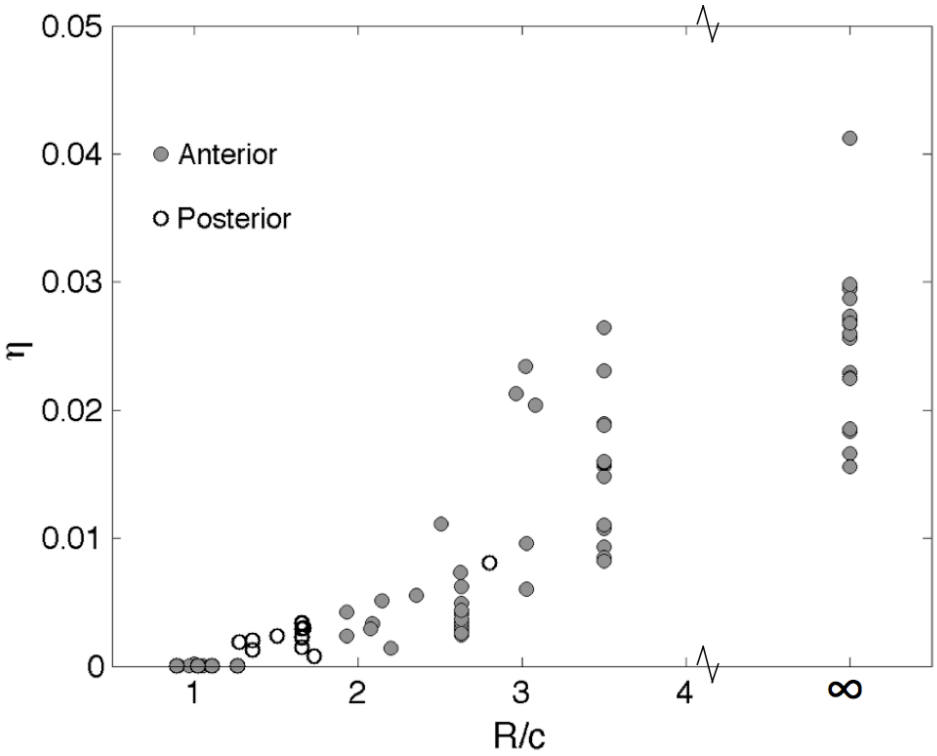

Figure 4.8: Plot of the efficiency of the various trajectories inside the tube from experiments as compared to a *Paramecium* swimming in semi-infinite fluid domain.

$\eta = U_{swim}T/P$ where T denotes the thrust force by the organism $T = \mu U_{swim}/\lambda$, U_{swim} is the swimming velocity obtained experimentally, λ is the wavelength of the metachronal wave [68]. P denotes the power generated by the undulating wavy *Paramecium* when it is swimming in the unbounded fluid; which has been derived by Blake for an infinite model [68]. This is a good reference for comparison because we are calculating the efficiency in different level of boundedness; from extremely confined to infinite fluid case. As observed from Fig. 4.8 for the infinite fluid cases the efficiency is close to 3% however in confinements where $R/c < 2.1$ the efficiency is lower than 0.5%. It suggests that the swimming efficiency of *Paramecium* in smaller tubes are lower as *Paramecium* experiences more drag from confinements.

4.5 Discussion

We investigated the locomotion of ciliary organisms in confined geometries. As the boundaries close on the organism, more viscous effects are felt by the cilia. The swimming velocity of *Paramecium* decreases due to the effect of close boundaries. Also in such confined spaces a finite sized organism feels a pressure gradient across the ends. This pressure gradient affects the swimming velocity and needs to be considered while modeling similar self propelling objects in restrictive geometries. Our experiments confirm this observation which show a slowly increasing trend of velocities. One remark is that swimming velocities in the semi-infinite domain are under-predicted by theoretical model. It might be due to the simplifying assumption in which we consider the beat pattern as a simple 2D sinusoidal whereas the ciliary beat in *Paramecium multimicronucleatum* is 3D diexoplectic. It is also observed that there are very few cases in which *Paramecia* tend to swim in straight lines with the velocity values being in the lower range of the swimming values obtained for the case of helical swimming. It can be concluded from these data that amplitude of the trajectory of the *Paramecium* has very less bearing on the velocity in the tubes where $R/c < 2.1$.

Many interesting questions arise from this study especially about the amplitude of the waves propagated by the *Paramecium*. In a restrictive channel the beat of the waves is limited by the dimensions of channel and the size of organism. Due to the proximity, do the amplitudes of the beat change to provide a locomotory advantage?

The helical path traced out by the *Paramecium* with the anterior portion of the body aligned towards the local swimming direction is also an interesting locomotory trait. It was also observed that as the radii of the capillary tube increased the radius of the swimming helix also increased. It was also found that anterior swimming *Paramecium* can execute well defined helical paths when put inside capillary tubes of certain diameter. This is in contrast

to the freely swimming *Paramecium* which has very small radii of helical trajectories. In semi-infinite fluid domain the radii of the helix is very small (almost seems like a straight line motion) whereas in capillaries they swim with the radius similar to that of capillary tube.

Chapter 5

Swimming and fluid uptake (feeding) by *Paramecium* in thick fluid films

Goal - Experimentally characterize the flow-field around the asymmetric body of *Paramecium* and estimate the swimming and feeding efficiencies due to top-bottom asymmetry of the body.

5.1 Introduction

The macroscopic world animals usually have mouth/tongue that serves the purpose of feeding/drinking, and hands/feet that help the animal to run or swim under a variety of conditions. In microscopic cilia/flagella are the most important organelles that help the organism achieve motility, transport the nutrients to the body of the organism. Such organelles are present int bacteria are called flagella that bundle at the back of the cell body which helps it to push the fluid swim helically during its run phase (also called pushers). While, Chlamydomonas has two flagella at the front that helps it to pull its body through the viscous

environment (called pullers). The appendages exert force on the fluid and their beating configuration determines the characteristic of the flows around the body of the organism. In micro-world where steady state flow is commonly observed; the beating cilia/flagella can create dynamic flows around a microorganism.

While flows around microorganisms have long been a constant source of theoretical investigation amongst physicists, it is only recently that flows around "microorganisms" have started to be quantified experimentally thereby allowing us to quantify the flow perturbations created by the propelling appendages. Since the regime of fluid flow is Stokesian the flow field around the swimmers can be theoretically investigated by superposition of singular solutions [121]. The singular solutions have a property of decaying over large distances meaning their effects can be felt far away from the source. Such signals can be picked up by other swimmers (the exact sensory mechanism is still unknown), for e.g. either preys or predators and can trigger a change in their swimming characteristics [88]. It was recently revealed that bacteria during their "run" phase swim with almost a steady motion of the flagella that generates steady dipolar flow field around the organism [51]. Flagellates like "Chlamydomonas" beat the two flagella synchronously, similar to breaststroke of humans which allows them to generate time dependent flow-field (quasi steady) around the body [122]. These investigations have caused a renewed interest in the area of hydrodynamics of cells especially for the case of cells swimming near boundaries and how the boundaries affect the flow structures and the forces experienced by the organism near walls.

Unicellular ciliates provide challenge in mapping the flow fields since the beating pattern of the cilia is controlled via the ionic potentials across the cell membrane. The changes in the beating pattern of the cilia can be brought about by the change in ambient ionic concentrations of the fluid media or due to physical touch by a nearby organism or even due to nearby boundaries as discussed in the previous sections. These parameters need to

be precisely controlled in the experimental setup; to get meaningful data that describes the swimming characteristics. If the dynamic nature of the beating pattern of the cilia around the body is different; the effective motion of the cell in the fluid media might show a variety of different configurations. Consequently the flow fields around the organism can look quite different and has been illustrated by hand drawings in his book by Jennings [16]. In order to model the flow fields around *Paramecium* Keller and Wu provided a nice theoretical basis by considering superposition of Stokeslets and Source-doublet and imposing a prescribed velocity on the cilia layer to capture the essence of the flows around the ciliates. They also took low resolution photographs with extended shutter times to show the streak patterns around a sedimenting as well as swimming *Paramecium* and find a qualitative agreement with theoretical predictions [63]. Kim et al do a low resolution μ Particle Image Velocimetry around *Tetrahymena Pyriformis* swimming inside a microfluidic chamber [64] and find cases of strong and weak tangential velocities on body surfaces that give rise to strong or weak swirls around their body; possibly for the cases of meandering motion of the cell in confinements as has been described in the previous chapter. While several investigations have tried to decipher the flows around *Paramecium*, quantitative high-resolution experimental data describing the flows around their body is still lacking.

While some scientists attribute the primary function of the cilia to be swimming; its importance in the feeding process cannot be ignored. Especially for the case of *Paramecium* fluid is transported into the oral groove by the beating of the cilia; which causes the formation of food vacuoles inside the body (possibly through Rayleigh plateau instability). Investigations of the coupled swimming and feeding processes using simulations has revealed that the swimming strokes helps in ideal distribution of nutrients around the cell body of bi-flagellates [123]. A recent study on the colonies of Choanoflagellates by Roper et al. [124] discusses how the hydrodynamic cooperations as a group allow the colony to generate stresslet like

flow pattern which provides a larger flux of fluid per cell and possibly nutrients. Such investigations albeit nascent in Stokesian Regime are common in somewhat larger animals like the copepods.

The goal of this chapter is to experimentally quantify the flow fields around swimming *Paramecia* and use the insights to numerically simulate the flows around the organism and gain understanding into competition between swimming and feeding in *Paramecium*.

5.2 Singular solutions of Stokes flow

In the microscopic world where viscous forces are dominant; the Navier-Stokes equations after scaling reduce to stokes equation:

$$\nabla \cdot \mathbf{u} = 0 \qquad \nabla p = \mu \nabla^2 \mathbf{u} + \mathbf{f} \tag{5.1}$$

where $\mathbf{u}$ denotes the fluid velocity and $\mathbf{f}$ represents the point force perturbing the fluid in a particular way. The solution to equation 5.1 is called a Stokeslet and represents a point force perturbing the fluid. The flow-field $\mathbf{U}_s$ and the pressure P_s corresponding to this fundamental solution is given by:

$$\mathbf{U}_s(\mathbf{x};\boldsymbol{\alpha}) = \boldsymbol{\alpha}/R + (\boldsymbol{\alpha}\cdot\mathbf{x})\,\mathbf{x}/R^3$$

$$\mathbf{P}_s(\mathbf{x};\boldsymbol{\alpha}) = 2\mu\boldsymbol{\alpha}\cdot\mathbf{x}/R^3$$

where α denotes the direction of the point force and $R = |\mathbf{x}|$ is the distance from the origin.The stokeslet exerts a net force on the fluid but no torque.

Since the stokes equations are linear; higher order derivatives of the Stokeslet are also solu-

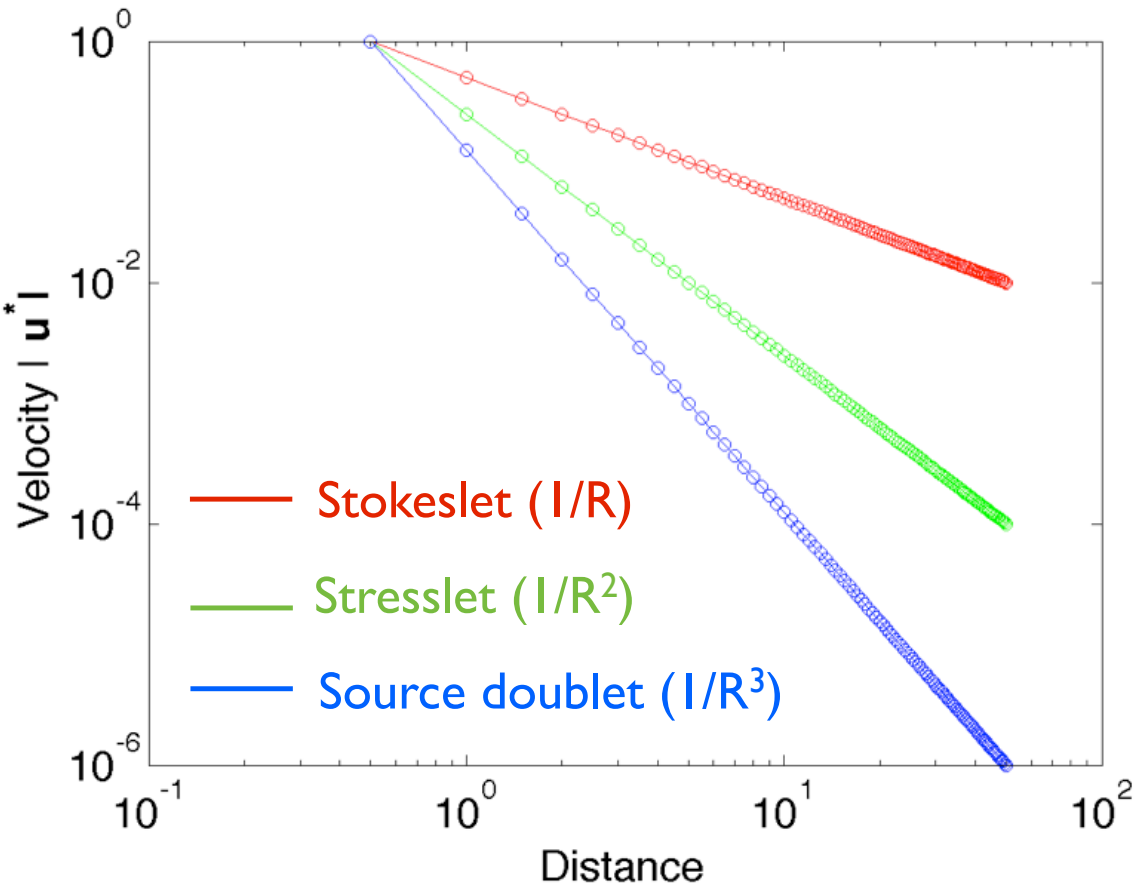

Figure 5.1: Figure shows the decay rates of velocities for the different singularities placed at origin ($\mathbf{u}^* = |\mathbf{u}|/u(1)$) along their equatorial line. Stokeslet shows a line with -1 slope, stresslet a line with -2 slope and source dipole a line with -3 slope on a log log plot.

tions of the equation 5.1. The first order derivatives also known as force dipoles consist of a symmetric component called as Stresslet and an anti-symmetric component called Rotlet. The velocity corresponding to a stresslet is:

$$\mathbf{U}_{ss}(\mathbf{x};\boldsymbol{\alpha},\boldsymbol{\beta}) = \left[-\frac{\boldsymbol{\alpha}\cdot\boldsymbol{\beta}}{R^3} + 3\frac{[(\boldsymbol{\alpha}\cdot\mathbf{x})\,(\boldsymbol{\beta}\cdot\mathbf{x})]}{R^5}\right]\mathbf{x}$$
$$\mathbf{P}_{ss}(\mathbf{x};\boldsymbol{\alpha},\boldsymbol{\beta}) = 2\mu\left[-\frac{\boldsymbol{\alpha}\cdot\boldsymbol{\beta}}{R^3} + 3\frac{[(\boldsymbol{\alpha}\cdot\mathbf{x})\,(\boldsymbol{\beta}\cdot\mathbf{x})]}{R^5}\right]$$

The stresslet exerts no net force and no torque on the fluid. The antisymmetric component

is rotlet; which exerts no net force but a finite torque on the fluid. The velocity and pressure expressions for rootlet singularity is given as:

$$\mathbf{U}_r(\mathbf{x};\boldsymbol{\gamma}) = -\frac{\boldsymbol{\gamma}\times\mathbf{x}}{R^3}$$
$$\mathbf{P}_r(\mathbf{x};\boldsymbol{\gamma}) = 0$$

where $\boldsymbol{\gamma} = \boldsymbol{\alpha}\times\boldsymbol{\beta}$, indicates the net direction in which the torque vector points.

Another important singularity is Source dipole which is a second order derivative of the Stokelet or a first derivative of source [125]. The velocity and pressure corresponding to this singularity is given by:

$$\mathbf{U}_{sd}(\mathbf{x};\boldsymbol{\gamma}) = -\frac{\boldsymbol{\delta}}{R^3} + \frac{3\left(\boldsymbol{\delta}\cdot\mathbf{x}\right)\mathbf{x}}{R^5}$$
$$\mathbf{P}_{sd}(\mathbf{x};\boldsymbol{\gamma}) = 0$$

Of particular interest is the decay rate of the singularities $(1/R, 1/R^3)$ as shown in figure 5.1. By experimentally measuring the velocity decay in experiments and comparing the theoretical decay rates one can determine what singularities have a dominant contribution for the fluid flow.

5.3 Experiments

The sample containing the *Paramecia* and polystyrene microspheres was prepared and placed on a pre-cleaned glass slide. Two plastic spacers of $\sim$ 750 μm were placed on sides and a glass slide was placed on top of the fluid. The sample was placed on top of the microscope (Leica DMI 3000B) stage and was observed at 15X magnification. A LED array (LED 12

from IDT, 11650 lumen) was used to shine light externally and the angle was adjusted so that the sample was lighted in a way that the particles shine brightly on a dark background. It was also observed that ciliates tended to cluster together in the particulate medium which makes the recording of tracks of single cell difficult without any external influences. Imaging was undertaken using a IDT MotionXtra camera recording the swimming tracks at 100 Hz for 4 or 5 s. The light was switched off after each run to prevent the sample from heating thereby reducing the evaporation of the fluid. Over 88 gigabytes of data was recorded out of which only 8 gigabytes was deemed usable; owing to the variety of swimming patterns executed by the *Paramecium*. We only consider the cases of *Paramecium* swimming along a directed path as it represents the naturally observed swimming mode in infinite fluid medium with the cells being subjected to little or no external stresses.

5.4 Results

5.4.1 Experimental Results

To understand the flow fields around the swimming body we use μ-Particle image velocimetry to quantify the flows generated due to swimming of *Paramecium*. The average sinusoidal swimming velocities for the case of thirty different swimming *Paramecium* is found to be 1300 ± 493 μm/s and the average length of the major axis is found to be 270 ± 10 μm and the minor axis to be 50 ± 3 μm. Prana PIV processing software, courtesy from Dr. Vlachos's lab (AETHER) was used to process the acquired images. The average pixel displacements per frame close to the body of *Paramecium* was observed to be around $10 - 12$ pixels per frame which led us to select a 64X64 pixel interrogation window size for the PIV process. Since the particles near the body are displaced by a large amount while the particles in

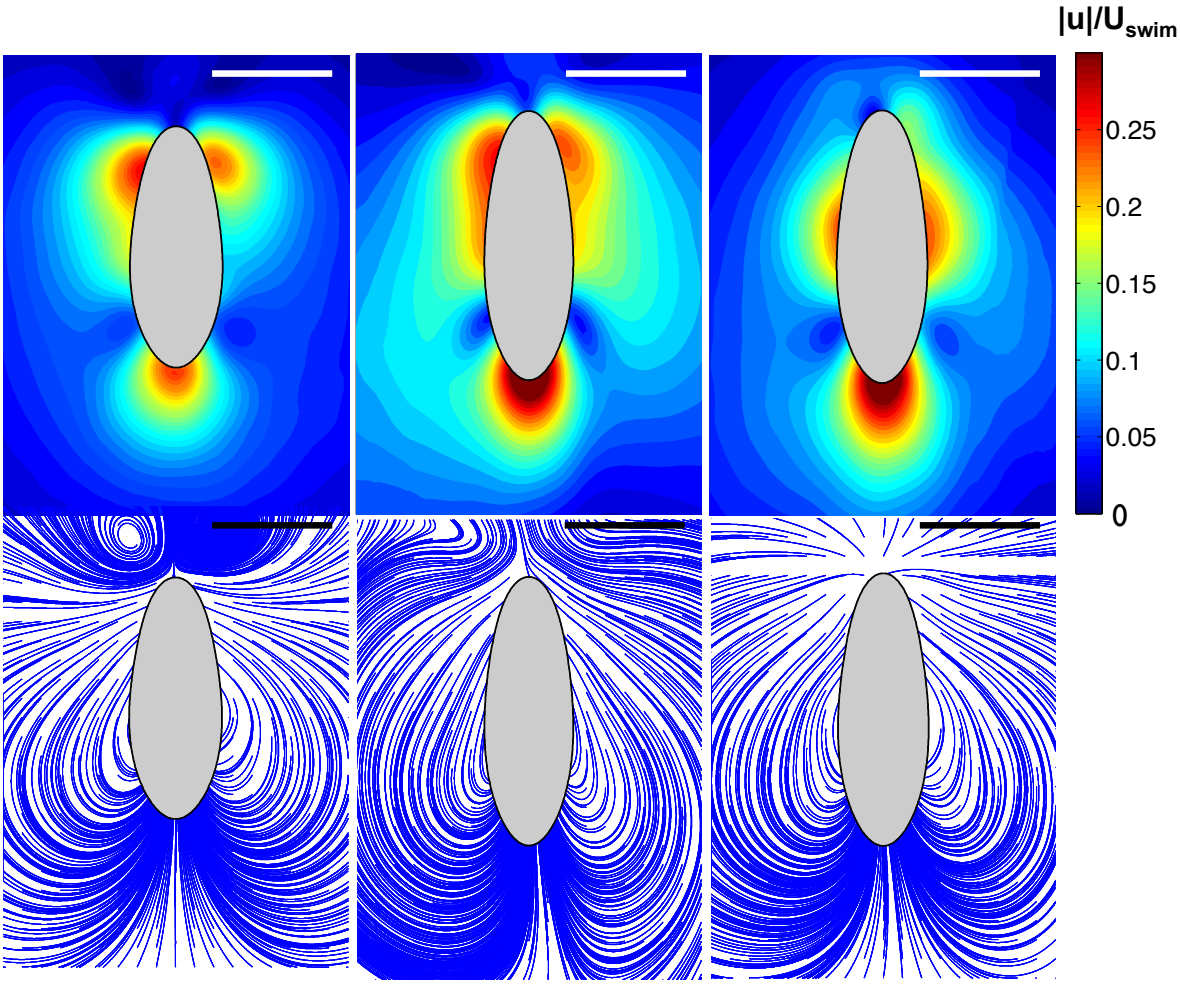

Figure 5.2: Figure showing the magnitude of velocity around the body and the corresponding streamlines. All scale bars are 100 μm.

the far-field have little or no displacement Multi-grid Multi-frame method with frame step of 5 was used to resolve the flows. Since the *Paramecia* are swimming along their anterior end in arbitrary directions we reorient them in a way that their anterior end is always aligned along the positive y direction. After the alignment we average out the vectors at the corresponding grid points and plot the magnitudes of velocity and streamlines around the body of *Paramecium*.

About 16 cases of directed swimming was observed amongst the various recorded tracks;

some of which are shown below. The flows represent similar qualitative characteristics, the region of highest magnitude of velocities are mostly found at posterior end or on the either side of body close to the anterior end of the organism but is not exactly the same for each of the organism. The streamlines for the different cases show left right symmetry in almost all the organisms. However if we look at the fore-aft end of the flow-field we find that the streamlines around the *Paramecia* are bent mostly towards the aft side. The flow field bears a striking resemblance to the source dipole except from the fact that that the fore-aft asymmetry is not preserved.

5.4.2 Experimental Shapes of *Paramecium*

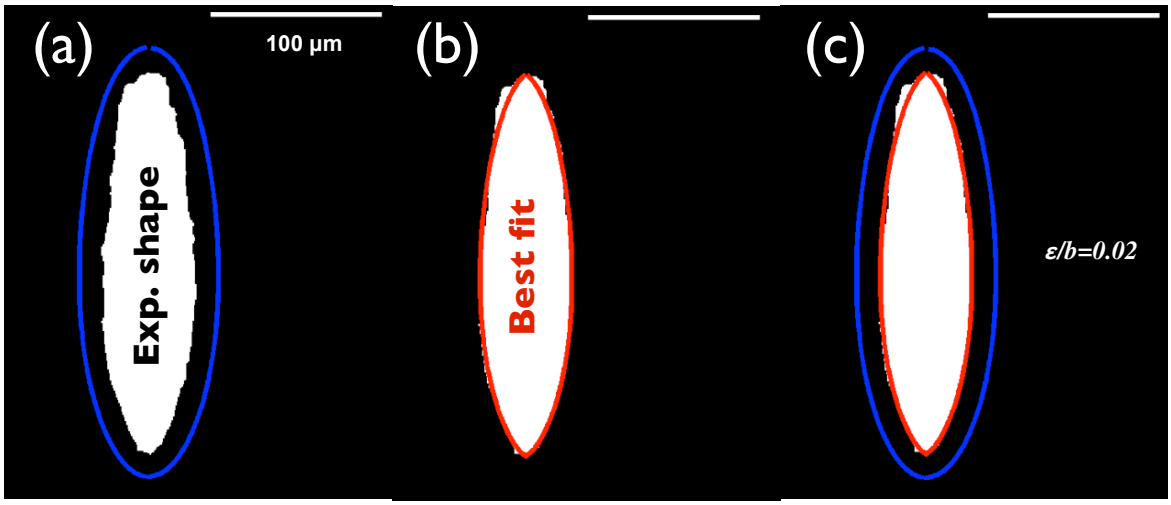

Figure 5.3: Plot shows the best fits shapes of the cilia/ body layer obtained from fitting the parameters (a) Shows the cilia layer around the body of the *Paramecium* (b) Shows the best fit of the theoretical shape on the experimentally obtained body shape. (c) Shows the both the layers around the body.

To understand the effect of this asymmetry we first look at the body shape of *Paramecium*. *Paramecium* has previously been considered to be prolate spheroidal in shape and described by the equation $z^2/a^2 + r^2/b^2 = 1$ which assumes anterior posterior asymmetry. The param-

eters a denotes the major axis length and b denotes the minor axis length; both inclusive of the cilia layer thickness. In reality the posterior end is bulky as compared to the slender anterior end. To capture this effect we can modify the equation describing the *Paramecium* as:

$$r(z) = b\left[(1 - z^2/a^2)^{1/2} - \frac{\epsilon}{b}\sin(\pi z/a)\right], \tag{5.2}$$

where the parameter ϵ/b is the non-dimensional deformation parameter and describes the asymmetric shape of the *Paramecium* in the experiments.

To measure this parameter we go back at the real experimental shapes obtained during the experiments. In the recorded images we find that the cell body reflects light strongly but the cilia lining the body doesn't do so. Hence we cannot measure the length a directly from experiments; but can measure the major axis length of the cell body. Assuming that the cilia layer is of constant thickness of about 14 μm we can find the constant parameter which is the major axis length (a) of the *Paramecium*. We vary the parameters b and ϵ/b and generate the different theoretical shapes. Finally we find the minimum of the difference between $|A_{experimental} - A_{theoretical}|$ to get the optimal parameters. In case the area minimization yielded two minimum optimal parameters a mean was chosen.

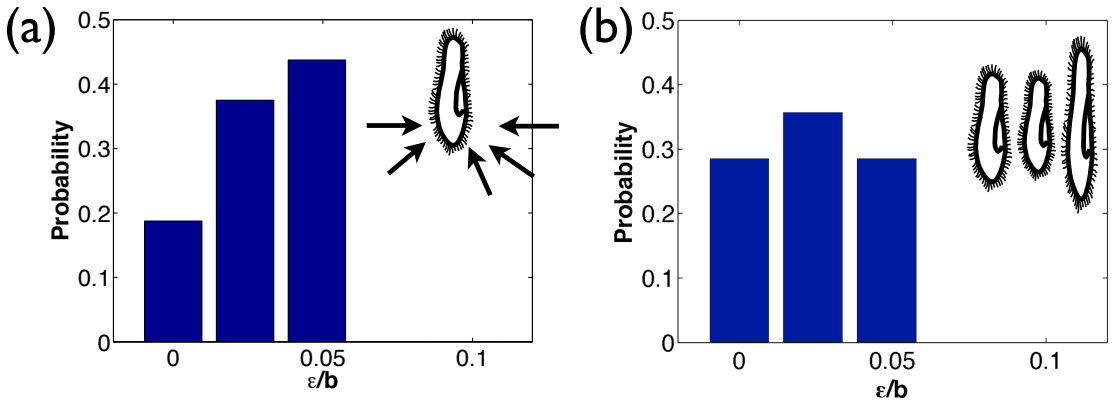

Figure 5.4: Plot showing the variation of (a) ϵ/b for the different profile views (b) ϵ/b for the different organisms

We carried out the optimization process for the average images obtained from the measurements of 16 different *Paramecia*. The mean and standard deviation for the different organisms were found to be $\epsilon/b \sim 0.043 \pm 0.023$. The *Paramecium* rotates as it moves in a sinusoidal path in the fluid medium; hence the different profile views can have different deformation parameters. The deformation parameter is found to be $\epsilon/b \sim 0.047 \pm 0.023$, signifying the fact that the posterior end of the *Paramecium* is deformed albeit on an average about 4% of the major axis length.

5.4.3 Decay rates of velocity

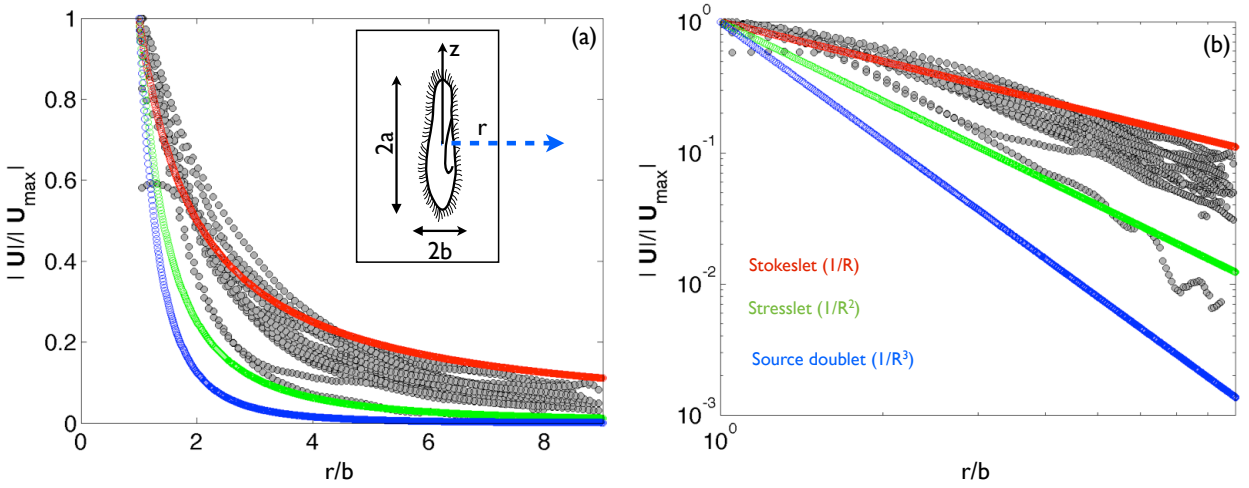

Figure 5.5: Plot showing the decay of velocity along the radial direction (z=0) (a) linear plot (b) Log-log plot for different cases. The three different colored lines: red, green and blue show the decay rates of velocity for stokeslet($1/R$), Stresslet ($1/R^2$) and the source doublet ($1/R^3$) in the linear or log-log plots are plotted as reference for comparison.

To understand the swimming of microorganisms in terms of forces exerted on the fluid elements, it is ideal to look at the decay of velocities from the body. By studying the decay rate of the velocities combined with the pattern of the flows, an understanding of singularities causing the flows can be determined. The inset of figure 5.5 shows the axisymmetric coordi-

nate system around the body of the *Paramecium*. Figure 5.5(a) shows the decay rate of the velocities along the equatorial plane of the prolate spheroid shaped organism in a linear plot and 5.5 shows the decay in a log-log plot. The velocity decay rate in the near field of the body ($r/b < 2$) follows a line of slope -1.1 and in the far-field the rate of decay is -1.6.

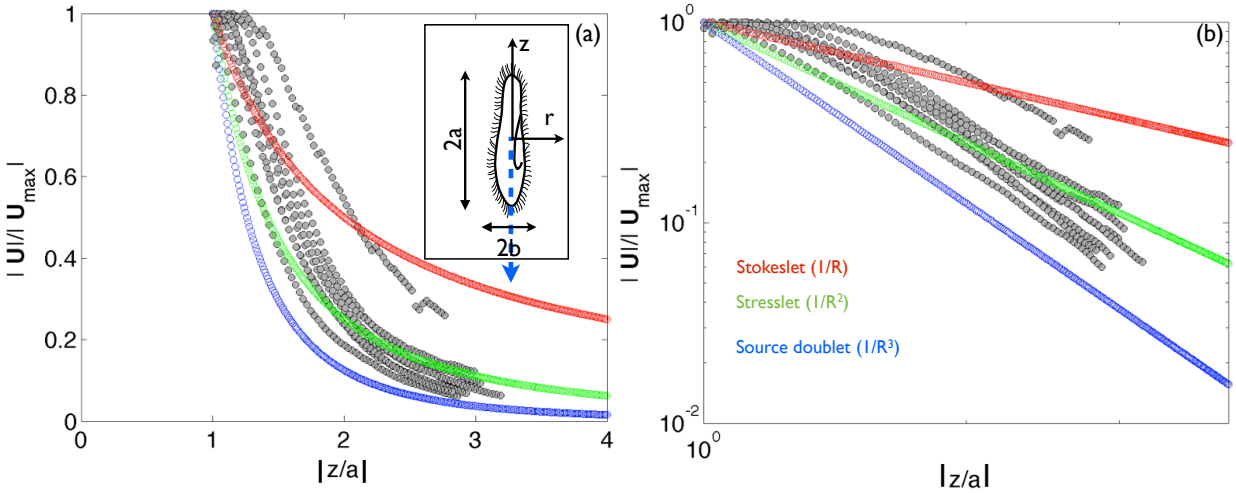

Figure 5.6: Plot showing the decay of velocity along the posterior (r=0 & z <0) (a) linear plot (b) Log-log plot for different cases. The red, green and blue dots corresponds to lines of $-1, -2$ and -3 slope on the log log plot.

We can also look at decay of the velocities at the posterior end of the *Paramecium*; which reveals a near-field($z/a < 2$) decay rate of -1.2 and a far-field decay rate of -2.6. The far-field decay rate in this case indicates that the source dipole might play the role of the dominant singularity. The streamline patterns around the body also points to this fact.

5.4.4 Normal and Tangential Velocities on the cilia layer

The cilia of the *Paramecium* create the necessary perturbation in the fluid that help the organism to locomote in the fluid. It is assumed that the cilia organize into metachronal waves within the cilia layer and impart velocity to the fluid. Previous theoretical work has

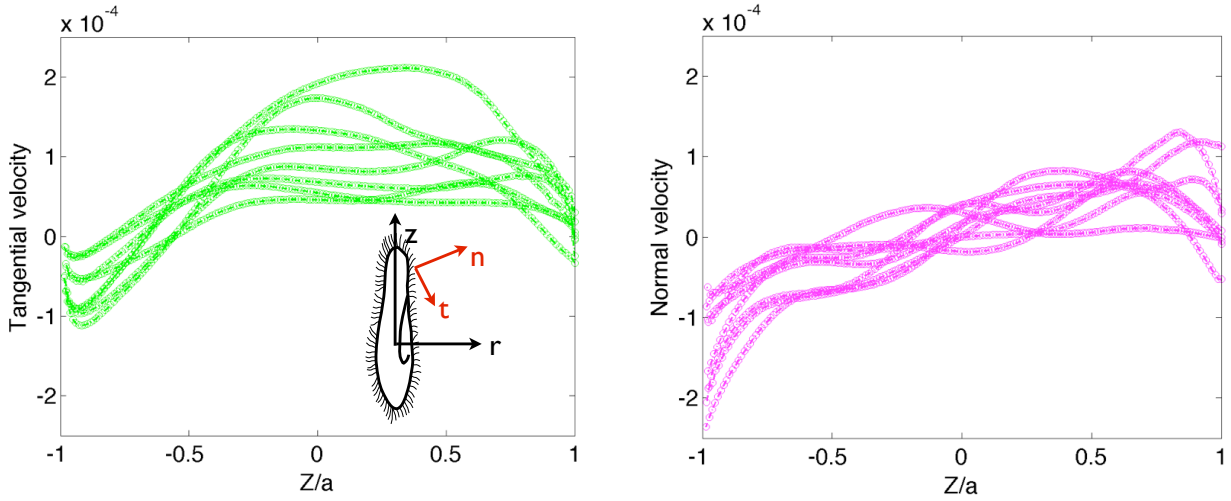

Figure 5.7: (a) Tangential and (b) Normal components of the velocities along the deformed body of the *Paramecium*; the normal and tangential coordinate directions are shown in the inset .

intuitively (yet accurately) assumed the existence of the normal and tangential velocities to be functions of cosine and sine, however experimental data for the real swimming is non-existent. Since we have already determined the shape of the cilia layer around the body of the organism, it becomes easier for us to calculate the velocities on this layer from the experimental data of the flow-field. For the given shape of the cilia layer (bulky posterior) we can compute the normal and tangential coordinates along the cilia layer and interpolate the experimental velocities onto this layer.

Figure 5.7 shows the values of the normal and tangential components of the velocity along the cilia layer. The tangential velocities at the upper half of the body $z/a > 0$ are higher as compared to the posterior part indicating that the cilia along the anterior end stir the fluid faster. In most cases it is assumed that the cilia create transverse (shear) flows; but the plot 5.7(b) shows the existence of the normal velocity. The effect of normal velocity possibly comes from the slender anterior and bulky posterior which will be discussed in the next section.

5.4.5 Formulation of the *Paramecium* swimming problem

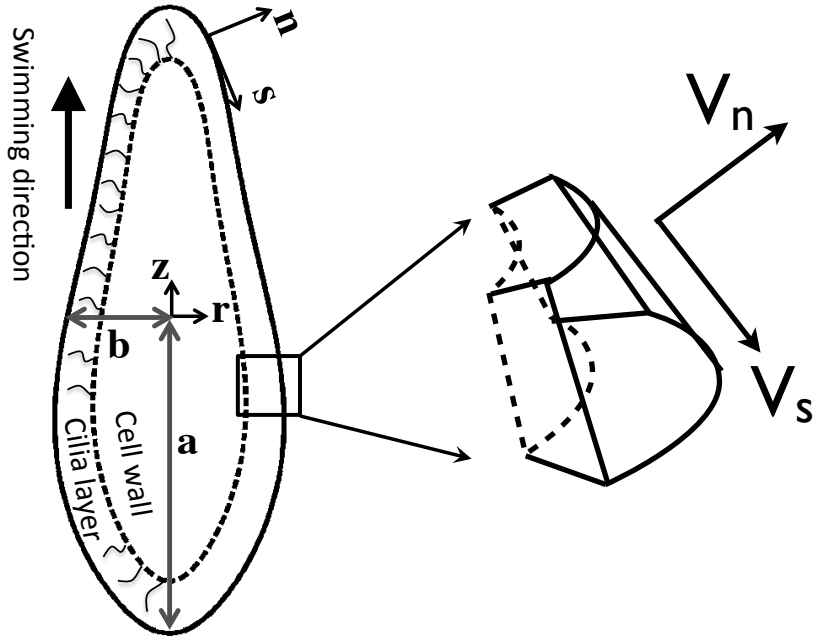

Figure 5.8: Figure (a) indicates the cell-body layer, cilia layer of a *Paramecium* (b) shows a sectional view of the cilia layer on the anterior portion of the body.

To develop a model we assume that *Paramecium* covered uniformly with the cilia all over their body. In the previous sections we worked inn the frame of reference attached to the laboratory, we now change over the frame which is attached to the center of the moving cell body. If the *Paramecium* is swimming with a constant translational speed U_{swim} along the z direction, then the surface velocity in the moving frame can be written as:

$$\mathbf{u}_s = \mathbf{u} - U_{swim}\mathbf{e_z} \tag{5.3}$$

We assume that all cilia work in unison at a constant rate and create surface velocity on the cilia layer. At the anterior end the tangential velocity is zero and the maximal value occurs at the equator of the body. Such assumptions were also used by Keller and Wu [63]

to obtain the flow profile around a symmetric *Paramecium*.

However for our case we find that deformation parameter $\epsilon/b \sim 0.04$, which indicates that the anterior part is more slender as compared to posterior . We use this difference in body shape to find the normal velocity on the ciliary layer for the case of a deformed *Paramecium*. f we take a cross-section on the anterior section of the body we find that area of the cross-section at the top is lesser as compared to the area at the bottom as seen in figure 5.8(b). Assuming that cilia work at a constant rate to pump the fluid in this layer the flux of the liquid through this cross-section should be constant. Using continuity across an infinitesimally small cross section we find that the tangential and the normal velocity takes the form:

$$\mathbf{V_s} = -v_s \left(\hat{s} \cdot \mathbf{e}_z\right) \hat{s}, \qquad \mathbf{V_n} = \frac{-2L_{cilia} dR/dz}{3r(z)\sqrt{1 + (dR/dz)^2}} v_s \left(\hat{s} \cdot \mathbf{e}_z\right) \hat{n} \tag{5.4}$$

where L_{cilia} is the thickness of the cilia layer and is assumed to a constant measuring 14 μm. Thus the total velocity on the cilia layer in the laboratory frame can be written as $\mathbf{u}_s = V_n \hat{\mathbf{n}} + V_s \hat{\mathbf{s}}$.

5.4.6 Simulations

Since the Reynolds number for *Paramecium* swimming is Re$\sim$ 0.2 the fluid motion can be described by Stokes equations 5.1. We assume that the *Paramecium* is swimming in infinite fluid medium with an unknown swimming velocity U_{swim} along $\mathbf{z}$ direction and the surface velocities generated by the cilia are known as given in equation 5.4.

In order to stimulate the swimming a 3D Boundary element method[1] was used in which the cilia layer of the *Paramecium* was discretized using curved triangular elements whose center

[1]This work was done by Peng Zhang

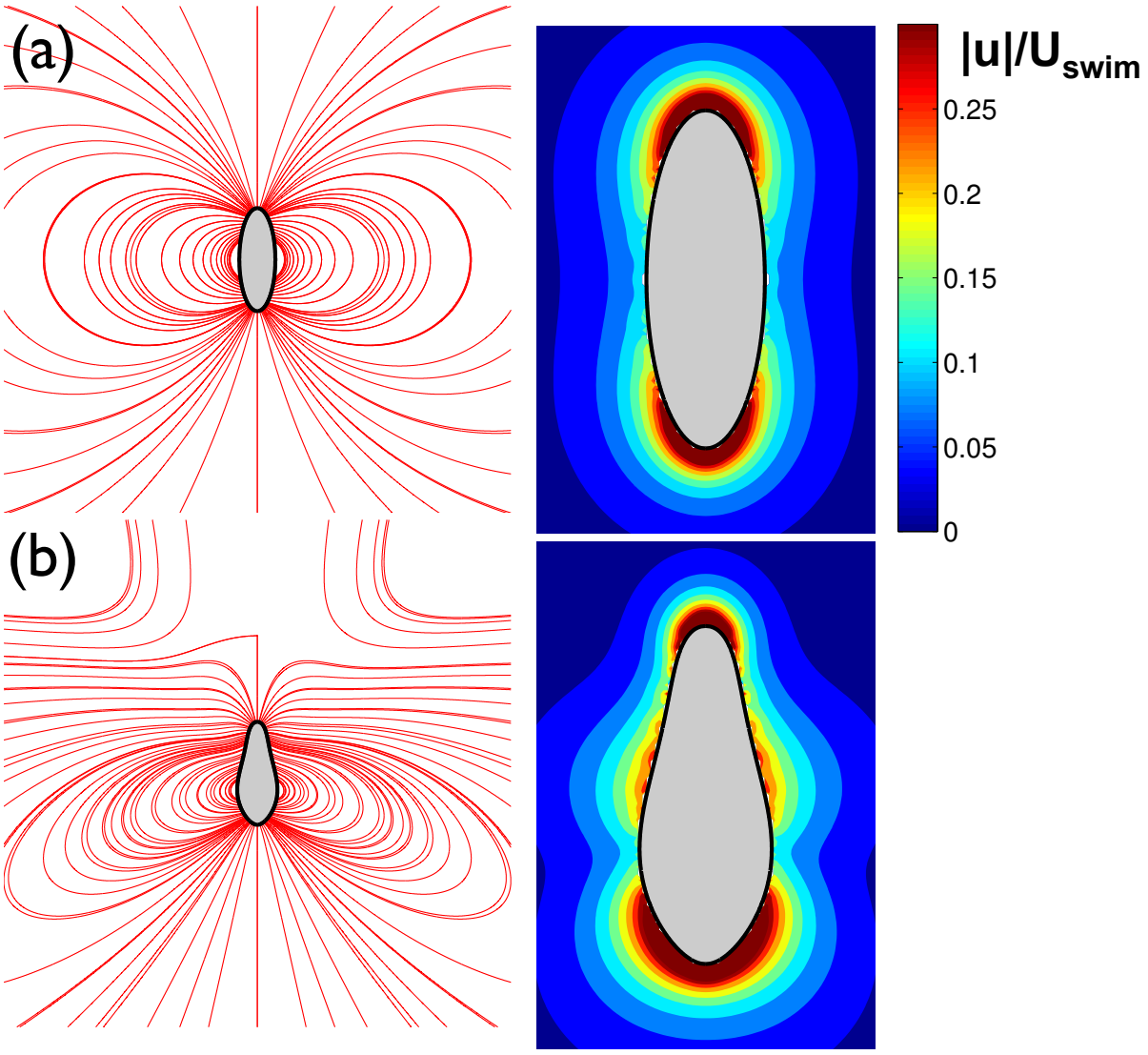

Figure 5.9: Flow field, streamlines and magnitude around the swimming *Paramecium* (a) for a non-deformed body ($\epsilon/b = 0$) (b) deformed body ($\epsilon/b = 0.05$). The streamlines for he deformed case are bent towards the posterior end of the body as compared to the non-deformed case. The surface velocities are the same as defined in equation 5.4.

is denoted by $\mathbf{x}_c$. The velocity at the center of these points is given by:

$$\mathbf{u}(\mathbf{x}_c) = -\frac{1}{8\pi\mu}\int_{\partial D} \mathbf{U}(\mathbf{x}_c, \mathbf{x})\mathbf{f}(\mathbf{x})\, dS(\mathbf{x}), \tag{5.5}$$

, where $\mathbf{U}$ is the velocity of a 3D Stokeslet. Integration of equation 5.5 yields a linear system $\mathbf{u} = A\mathbf{f}$.

By substituting equation 5.3 we get an expression of $\mathbf{f}$ in terms of the unknown swimming speed (U_{swim}). Since the *Paramecium* is swimming freely in the fluid the total force and torque must be zero:

$$\mathbf{F} = \int_{\partial D} \mathbf{f}\, dS = 0, \qquad \mathbf{L} = \int_{\partial D} \mathbf{x} \times \mathbf{f}\, dS = 0 \tag{5.6}$$

where $\mathbf{f}$ is the surface force at a point on the surface of the body. Numerical integration of equation 5.6 gives us the swimming speed of the organism U_{swim} and finally the variable $\mathbf{f}$. Once the variables have been determined; the velocity at any point in the fluid media ($\mathbf{x}_0$) is given by equation 5.7:

$$\mathbf{u}(\mathbf{x}_0) = -\frac{1}{8\pi\mu}\int_{\partial D} \mathbf{U}(\mathbf{x}_0, \mathbf{x})\mathbf{f}(\mathbf{x})\, dS(\mathbf{x}), \tag{5.7}$$

By knowing the velocities of the fluid elements one can plot the streamlines and the magnitude of velocities around the body. Simulations were run for constant eccentricities $e = 0.937$ (measured from experimental shapes) and undeformed $\epsilon/b = 0$ as well as deformed bodies $\epsilon/b = 0.05$. Figure 5.9 shows the variation in streamlines as well as the magnitude of velocities from simulations. We can see that for the deformed body the streamlines are shifted towards the posterior side.

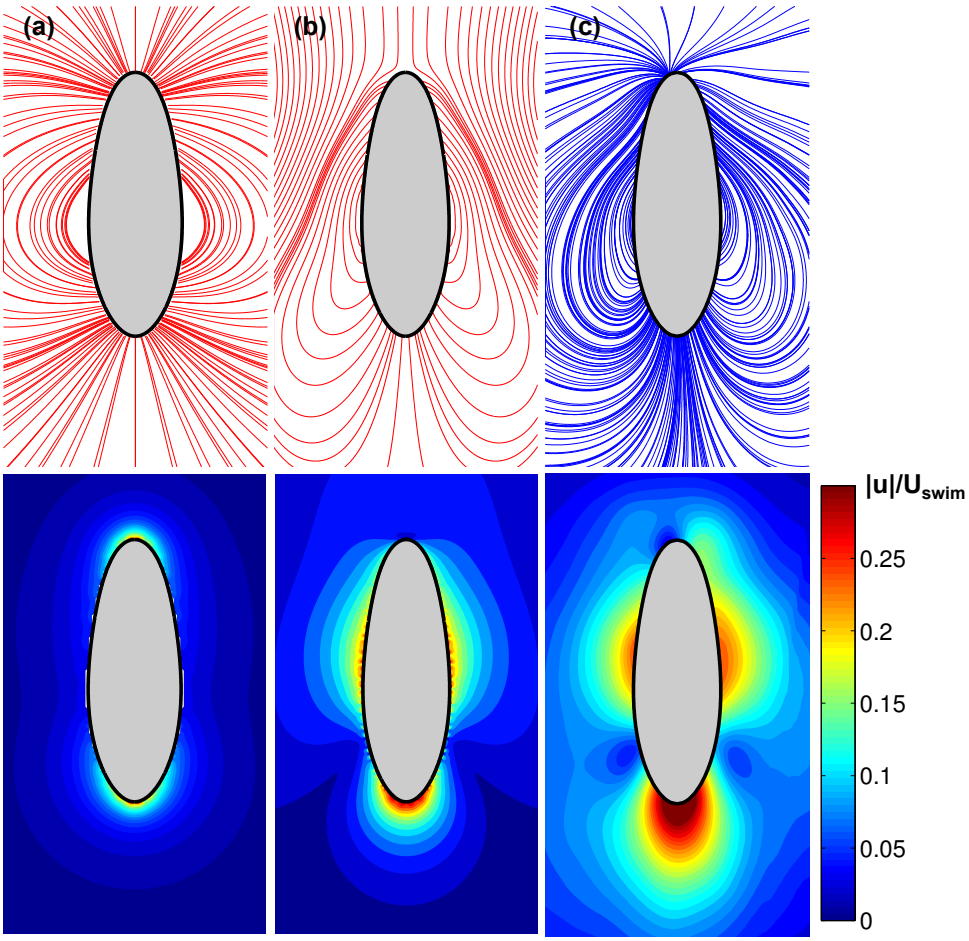

Figure 5.10: Comparison of streamlines and velocity magnitude from (a) simulation with surface velocity defined by equation (5.4); (b) simulation with surface velocity measured from experiment and (c) experimental data. Deformation parameter in all cases are $\epsilon/b = 0.05$.

5.4.7 Comparison: Simulation and experiments

Figure 5.10 shows the direct comparison of magnitude of velocities and the streamlines for deformation parameter $\epsilon/b = 0.05$ in simulations and experiments. In case of simulations we find that the magnitude of velocity decays rapidly from the center of the body as compared to experiments.

If the surface velocities from the experiments are directly used for simulations we find that the magnitudes of velocity are very similar around the body. The streamlines also show a

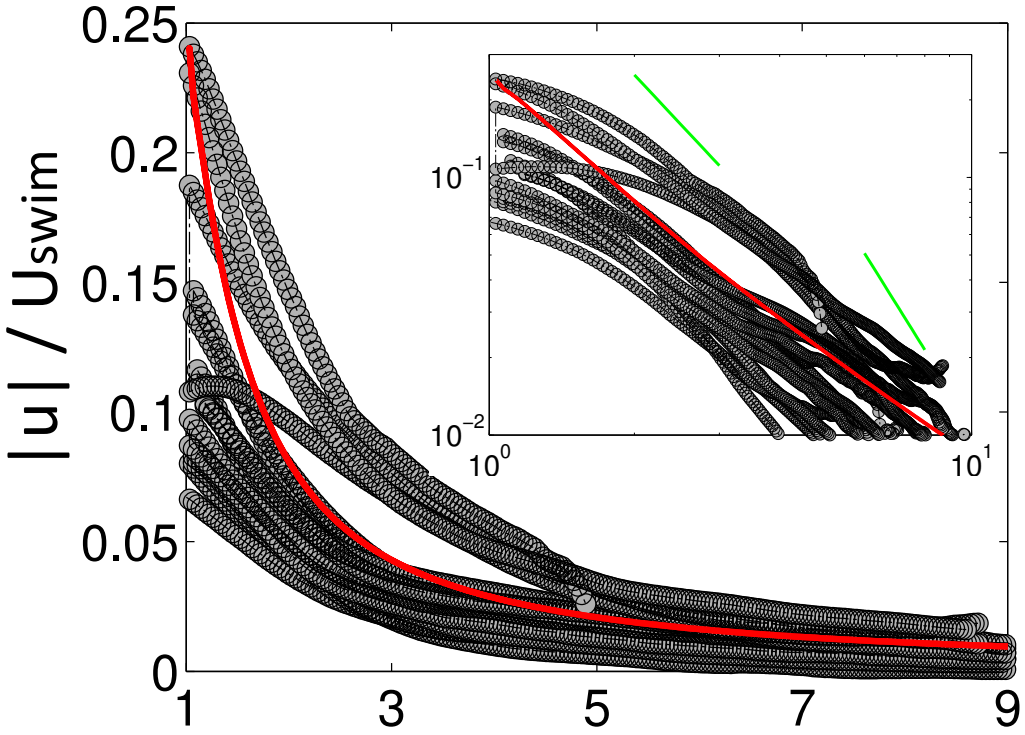

Figure 5.11: Comparison of the decay rate of normalized velocity along the equatorial line. Black dots represent the different experiments. Red line represents the decay rate when the cilia layer velocity from experiments is used as an input in simulations.

similar pattern as compared to the experiments. The decay rates from simulations decay faster when compared to the experiments and can be seen in figure 5.11.

5.4.8 Efficiencies of *Paramecium*

The energy dissipation of a swimming and the swimming efficiency *Paramecium* can be calculated from simulations as:

$$P = \int_{\partial D} \mathbf{f} \cdot \mathbf{v}\, dS, \qquad \eta_{swim} = \frac{\mu |U_{swim}|^2 a}{P} \tag{5.8}$$

We would like to measure the feeding efficiency and study the competition of the two effi-

ciencies as a function of the deformation parameter. The oral groove of the *Paramecium* is roughly located at the center of the major axis with the groove pointing towards the anterior end. It is therefore possible that all the fluid normal to the cilia layer can get transported into the oral groove. To quantify this parameter we define feeding velocity and the corresponding efficiency as:

$$U_{feed} = \frac{\int_{\partial D_{z>0}} -\mathbf{u}_s \cdot \hat{\mathbf{n}} \quad dS}{\int_{\partial D_{z>0}} dS}, \qquad \eta_{feed} = \frac{\mu |U_{feed}|^2 a}{P} \tag{5.9}$$

The different efficiencies are evaluated for the different deformation parameters. The plot showing the variation of swimming efficiency vs deformation (Fig. 5.12(a)) parameter shows a peak for $\epsilon/b = 0$ indicating the fact that a symmetric body is most efficient for swimming purpose.

However if we increase the deformation parameter ϵ/b from -0.4 to 0.4 we find that the feeding efficiency increases (Fig. 5.12(b)). This means that as the body shape of the organism changes from bulky anterior-slender posterior to slender anterior-bulky posterior the feeding efficiency increases.

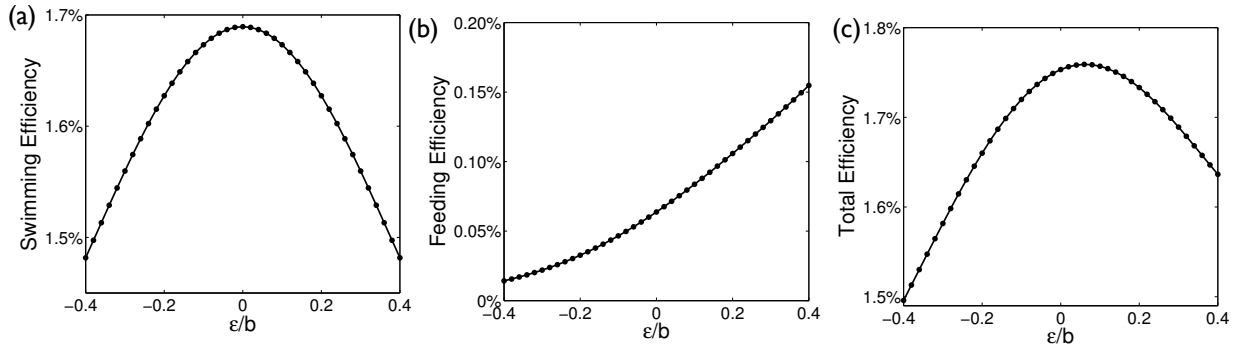

Figure 5.12: (a) swimming efficiency (b) feeding efficiency (c) total efficiency(sum of swimming and feeding) as a function of different deformation parameters.

If we consider the total efficiency as linear sum of swimming and feeding efficiency we find that it peaks for $\epsilon/b \sim 0.04$. In experiments we measured the deformation parameter to be ~ 0.05 which is very close to the values predicted in simulations.

5.5 Conclusions

We have investigated the flow fields around swimming *Paramecia* and investigated the feeding efficiency. We find that the top bottom deformation of the body causes the streamlines to be shifted towards the posterior end and observed it qualitatively both in experiments and simulations. By studying the swimming and feeding performance we find that *Paramecium* has an optimal tradeoff value of deformation parameter $\epsilon/b \sim 0.04$. The surface velocity around the *Paramecium* is complicated and hence an exact match between experiments and theory is very hard. Additionally our expression for the feeding velocity is based on location of the oral groove and hence all the fluid from the upper half may not be taken up by the *Paramecium*.

Chapter 6

Discussion and Future directions

6.1 Discussion

Our investigations were undertaken to explore the locomotion strategies of *Paramecium* in their natural habitat. By subjecting the *Paramecia* to different kind of confinements as they would feel in there natural habitat we are able to show that organism can switch between the three different swimming modes. In semi-infinite 3D fluid media the swimmers execute directed motion with large displacements from its original position. In thin 2D films the directed swimmers transition to meandering motion due to successive collisions with the walls. While swimming in channels *Paramecium* touches both walls and bends its body within the channel. The self bending represents a surprising phenomena, that allows the cells to completely change their direction of swimming due to the flexible body.

While boundaries cause and trigger the different swimming modes of *Paramecium*, the exact origin of the behaviors remains unexplored. The physical touch with the boundary causes a small deformation of the cell body which further creates an imbalance in the ionic potentials

in the cell body as compared to the ambient fluid. This has been known to trigger the avoidance behavior which has been found to be dominant mode in 2D fluid films. The mechano-sensation effects (ion gating through the membrane) have been recently explored in a theoretical paper, which considers the deformation of the cell body in a linear shear flow and finds that membrane pre-stress plays an important role by controlling the ion gating in cells and affects the swimming and sensing[126] of eukaryotic cell. It is also possible that the cilia interact with the boundaries that allows them to produce the forces necessary to buckle the cell and such behavior along with the ion-channel gating might explain why the cell choses to bend in a characteristic direction.

Secondly, we also studied the swimming of *Paramecia* in glass capillaries of varying diameter; that mimics their motion in pores of soil. Due to the finite size of the organism, swimming in a confined geometry the *Paramecium* a pressure gradient exists between its ends. By taking this fact into account we developing an envelop model for locomotion in capillaries and are able to predict their swimming speeds in confined capillaries.

The envelop model, which is developed in this thesis is a simplistic model that assumes that the metachronal wave of the *Paramecium* propagates longitudinally along the body of the organism. Such assumptions of longitudinal waves was pioneered by Blake; but it doesn't portray the reality. For helically swimming *Paramecia*, the cilia have been found to organize into helical strands which points to the fact that the metachronal waves are helically wrapped around the body of the organism. By taking this fact into account one can do full scale numerical simulation to reveal the helical patterns of path that were observed in the larger diameter tubes. It was also observed in experiments that the cell body pitches as *Paramecium*swims in tubes of larger diameter; however the exact cause of this behavior cannot be explained. Recent simulations considering a squirmer model (traveling waves on a sphere) have captured the subtleties of helical motion of the ciliates[127], but there still

remains many avenues (described in the lines above) that are yet to be explored.

Finally, using high-resolution μ-Particle Image Velocimetry we quantified the flows created by directionally swimming *Paramecium*. By taking into account the fore-aft asymmetry we are able to predict the existence of the normal velocity on ciliary layer of organism. We numerically calculate the swimming and feeding efficiencies and find that a symmetric body is optimal for swimming, while slender anterior bulky posterior is optimal for feeding. *Paramecium* possibly optimizes both these effects to have a little bulky posterior which is suggested from simulations.

While studying the flow field round the cell we only considered the case of directed swimming which manifests as helices well defined amplitude and wavelengths. We neglect the rotational motion along the longitudinal axis of the body; which causes the particles to drop in and out of the field of view and possibly causes some change in the flow-field. As a starting point we only considered the directed swimming; but have not quantified the meandering and circling motion. The ciliary motion around the body of the organism is of utmost importance in these investigations and hence direct visualizion of cilia should be undertaken along with μ-PIV experiments. The variability of the cilia motion which creates the different flows can then be understood as superposition of the different singularities. Compared to the other organisms it is amazing that the multitude of cilia can create a variety of flow-fields. Furthermore the differences in flows while locomoting near boundaries can enhance our understanding of the ciliary locomotion.

The work in totality sheds light on some of the different aspects of locomotion of ciliates near boundaries.

6.2 Future Directions

While our studies have focussed on the effect of geometries on the locomotion parameters of *Paramecium*, there are many possible areas that show promise.

We have only studied the locomotion parameters of the organism in quiescent fluid. While this has revealed interesting and surprising results; the natural environment always consists of water currents of varying shear rates. By allowing the cells to swim in millimeter sized channels and subjecting them to varying shear rates; one can understand how such effects cause a change in their swimming dynamics. This can also possibly explain the preferential accumulation of the organisms in certain regions of freshwater ponds.

An emerging area is the mechanism of flagellar/ciliary synchronization in cells, and its role in locomotion of the cells. While the synchronization creates metachronal waves that propel the cell; their distribution over the cell body remains unexplored. Furthermore the fact that synchronization leads to directed motion and during the asynchronous state causes the cell to meander is yet to be verified experimentally. Such work can also help in developing accurate mathematical model for locomotion of ciliates.

The use of microorganisms as mechanical workhorses have been demonstrated before in a variety of different situations [128, 129]. Since *Paramecia* are amongst the fastest swimmers in the micro-world their cilia can be used to enhance the mixing of two fluids which otherwise mix only through molecular diffusion. The idea is to tether the organisms in a magnetic field by feeding them nano-particles and controlling their trapping location in a fluidic channel. By making the liquids flow through the channel we can selectively enhance mixing at locations of ones choice. The idea is currently being pursued and has shown promise.

Initial investigations of elasticity indicates that the cell body of the *Paramecium* is much softer as compared to bacteria. Soft cells like *Paramecia* can also be used as active probes to

measure the elasticity of gel networks. By measuring the deformation of cells in the polymer networks; their stiffness can be estimated signifying their use a bio-mechanical probes.

Bibliography

[1] P. Falkowski. Ocean science: The power of plankton. *Nature*, 483(7387):S17–S20, 2012.

[2] L. Hall-Stoodley, J. W. Costerton, and P. Stoodley. Bacterial biofilms: from the natural environment to infectious diseases. *Nature Reviews Microbiology*, 2(2):95–108, 2004.

[3] S.L. Tamm. Ciliary motion in *Paramecium*: A scanning electron microscope study. *The Journal of Cell Biology*, 55(1):250–255, 1972.

[4] C. Brennen and H. Winet. Fluid mechanics of propulsion by cilia and flagella. *Annual Review of Fluid Mechanics*, 9(1):339–398, 1977.

[5] S. Dryl and A. Grebecki. Progress in the study of excitation and response in ciliates. *Protoplasma*, 62(2):255–284, 1966.

[6] Y. Hyon, T.R. Powers, R. Stocker, and H.C. Fu. The wiggling trajectories of bacteria. *Journal of Fluid Mechanics*, 1(1):1–19, 2012.

[7] T. Kiørboe, H.P. Grossart, H. Ploug, K. Tang, and B. Auer. Particle-associated flagellates: swimming patterns, colonization rates, and grazing on attached bacteria. *Aquatic Microbial Ecology*, 35(2):141–152, 2004.

[8] R.N. Bearon. Helical swimming can provide robust upwards transport for gravitactic

single-cell algae; a mechanistic model. *Journal of Mathematical Biology*, pages 1–19, 2012.

[9] H. Machemer and K. Sugino. Electrophysiological control of ciliary beating: a basis of motile behaviour in ciliated protozoa. *Comparative Biochemistry and Physiology Part A: Physiology*, 94(2):365–374, 1989.

[10] A. Seminara, T.E. Angelini, J.N. Wilking, H. Vlamakis, S. Ebrahim, R. Kolter, D.A. Weitz, and M.P. Brenner. Osmotic spreading of bacillus subtilis biofilms driven by an extracellular matrix. *Proceedings of the National Academy of Sciences*, 109(4):1116–1121, 2012.

[11] J.E. Cloern, B.E. Cole, and S.W. Hager. Notes on a mesodinium rubrum red tide in san francisco bay (california, usa). *Journal of plankton research*, 16(9):1269–1276, 1994.

[12] L. Margulis. Archaeal-eubacterial mergers in the origin of eukarya: phylogenetic classification of life. *Proceedings of the National Academy of Sciences*, 93(3):1071–1076, 1996.

[13] C. Claycomb and J. Tran. *Introductory Biophysics: Perspectives on the Living State: Perspectives on the Living State*. Jones & Bartlett Learning, 2010.

[14] R. Wichterman. *The biology of Paramecium*. Plenum Press New York/London, 1986.

[15] R.D. Hinrichsen and J.E. Schultz. Paramecium: a model system for the study of excitable cells. *Trends in neurosciences*, 11(1):27–32, 1988.

[16] H.S. Jennings. *Behavior of the lower organisms*, volume 10. Columbia University Press, 1906.

[17] M.A. Sleigh. *Cilia and flagella*. Academic Press, 1974.

[18] M.J. Sanderson and M.A. Sleigh. Ciliary activity of cultured rabbit tracheal epithelium: beat pattern and metachrony. *Journal of Cell Science*, 47(1):331–347, 1981.

[19] M.R. Marino and E. Aiello. Cinemicrographic analysis of beat dynamics of human respiratory cilia. *Cell Motility*, 2(S1):35–39, 1982.

[20] E.W. Knight-Jones. Relations between metachronism and the direction of ciliary beat in metazoa. *Quarterly Journal of Microscopical Science*, 3(32):503–521, 1954.

[21] H. Machemer. Ciliary activity and the origin of metachrony in *Paramecium*: effects of increased viscosity. *Journal of Experimental Biology*, 57(1):239–259, 1972.

[22] A. Vilfan and F. Jülicher. Hydrodynamic flow patterns and synchronization of beating cilia. *Physical Review Letters*, 96(5):58102, 2006.

[23] R.E. Goldstein. Evolution of biological complexity. *Biological Physics*, pages 123–139, 2011.

[24] R. Eckert. Bioelectric control of ciliary activity. *Science*, 176(4034):473, 1972.

[25] Y. Naitoh and H. Kaneko. Reactivated triton-extracted models of *Paramecium*: modification of ciliary movement by calcium ions. *Science*, 176(4034):523–524, 1972.

[26] H. Machemer, R. Bräucker, S. Machemer-Röhnisch, U. Nagel, D.C. Neugebauer, and M. Weskamp. The linking of extrinsic stimuli to behaviour: roles of cilia in ciliates. *European Journal of Protistology*, 34(3):254–261, 1998.

[27] A. Van-Leeuwenhoek. Green weeds growing in water, and some animalcula found about them. *Philosophical Transactions*, 23(277-288):1304–1311, 1702.

[28] A. Van-Leeuwenhoek. Worms in sheeps livers, gnats, and animalcula in the excrements of frogs. *Philosophical Transactions*, 22(260-276):509–518, 1700.

[29] A. Van-Leeuwenhoek. Letter of october 9, 1676 to the royal society. *Philosophical Transactions of Royal Society B*, 12:821–831, 1677.

[30] K.E. Machin. Wave propagation along flagella. *Journal of Experimental Biology*, 35(4):796–806, 1958.

[31] L. Rothschild. Non-random distribution of bull spermatozoa in a drop of sperm suspension. *Nature*, 198(1221-1222), 1963.

[32] C. J. Brokaw. Mechanisms of sperm movement. In *Symposia of the Society for Experimental Biology*, volume 22, page 101, 1968.

[33] C.J. Brokaw. Non-sinusoidal bending waves of sperm flagella. *Journal of Experimental Biology*, 43(1):155–169, 1965.

[34] P. Denissenko, V. Kantsler, D.J. Smith, and J. Kirkman-Brown. Human spermatozoa migration in microchannels reveals boundary-following navigation. *Proceedings of the National Academy of Sciences*, 109(21):8007–8010, 2012.

[35] D.M. Woolley, R.F. Crockett, W.D.I. Groom, and S.G. Revell. A study of synchronisation between the flagella of bull spermatozoa, with related observations. *Journal of Experimental Biology*, 212(14):2215–2223, 2009.

[36] G.J. Elfring and E. Lauga. Hydrodynamic phase locking of swimming microorganisms. *Physical Review Letters*, 103(8):88101, 2009.

[37] Y. Yang, J. Elgeti, and G. Gompper. Cooperation of sperm in two dimensions: synchronization, attraction, and aggregation through hydrodynamic interactions. *Physical Review E*, 78(6):061903, 2008.

[38] D.M. Woolley. Motility of spermatozoa at surfaces. *Reproduction*, 126(2):259–270, 2003.

[39] D.J. Smith, E.A. Gaffney, J.R. Blake, and J.C. Kirkman-Brown. Human sperm accumulation near surfaces: a simulation study. *Journal of Fluid Mechanics*, 621(1):289–320, 2009.

[40] J. Elgeti, U.B. Kaupp, and G. Gompper. Hydrodynamics of sperm cells near surfaces. *Biophysical Journal*, 99(4):1018–1026, 2010.

[41] E.A. Gaffney, H. Gadêlha, J.R. Blake, D.J. Smith, and J.C. Kirkman-Brown. Mammalian sperm motility: observation and theory. *Annual Review of Fluid Mechanics*, 43:501–528, 2011.

[42] H.C. Berg and R.A. Anderson. Bacteria swim by rotating their flagellar filaments. *Nature*, 245:380 – 382, 1973.

[43] H.C. Berg. Chemotaxis in bacteria. *Annual review of Biophysics and Bioengineering*, 4(1):119–136, 1975.

[44] H.C. Berg. The rotary motor of bacterial flagella. *Biochemistry*, 72(1):19, 2003.

[45] E. Lauga, W.R. DiLuzio, G.M. Whitesides, and H.A. Stone. Swimming in circles: motion of bacteria near solid boundaries. *Biophysical journal*, 90(2):400–412, 2006.

[46] A.P. Berke, L. Turner, H.C. Berg, and E. Lauga. Hydrodynamic attraction of swimming microorganisms by surfaces. *Physical Review Letters*, 101(3):38102, 2008.

[47] Z. Liu and K.D. Papadopoulos. Unidirectional motility of *Escherichia coli* in restrictive capillaries. *Applied and Environmental Microbiology*, 61(10):3567–3572, 1995.

[48] J. Männik, R. Driessen, P. Galajda, J.E. Keymer, and C. Dekker. Bacterial growth and motility in sub-micron constrictions. *Proceedings of the National Academy of Sciences*, 106(35):14861–14866, 2009.

[49] H.H. Tuson, G.K. Auer, L.D. Renner, M. Hasebe, C. Tropini, M. Salick, W.C. Crone, A. Gopinathan, K.C. Huang, and D.B. Weibel. Measuring the stiffness of bacterial cells from growth rates in hydrogels of tunable elasticity. *Molecular Microbiology*, 2012.

[50] W.R. DiLuzio, L. Turner, M. Mayer, P. Garstecki, D.B. Weibel, H.C. Berg, and G.M. Whitesides. *Escherichia coli* swim on the right-hand side. *Nature*, 435(7046):1271–1274, 2005.

[51] K. Drescher, J. Dunkel, L.H. Cisneros, S. Ganguly, and R.E. Goldstein. Fluid dynamics and noise in bacterial cell-cell and cell-surface scattering. *Proceedings of the National Academy of Sciences*, 108(27):10940, 2011.

[52] I. Rushkin, V. Kantsler, and R.E. Goldstein. Fluid velocity fluctuations in a suspension of swimming protists. *Physical Review Letters*, 105(18):188101, 2010.

[53] K.C. Leptos, J.S. Guasto, J.P. Gollub, A.I. Pesci, and R.E. Goldstein. Dynamics of enhanced tracer diffusion in suspensions of swimming eukaryotic microorganisms. *Physical Review Letters*, 103(19):198103, 2009.

[54] X.L. Wu and A. Libchaber. Particle diffusion in a quasi-two-dimensional bacterial bath. *Physical Review Letters*, 84(13):3017–3020, 2000.

[55] L.H. Cisneros, J.O. Kessler, S. Ganguly, and R.E. Goldstein. Dynamics of swimming bacteria: transition to directional order at high concentration. *Physical Review E*, 83(6):061907, 2011.

[56] H.P. Zhang, A. Be'er, E.L. Florin, and H.L. Swinney. Collective motion and density fluctuations in bacterial colonies. *Proceedings of the National Academy of Sciences*, 107(31):13626–13630, 2010.

[57] A. Baskaran and M.C. Marchetti. Statistical mechanics and hydrodynamics of bacterial suspensions. *Proceedings of the National Academy of Sciences*, 106(37):15567–15572, 2009.

[58] R. Aditi-Simha and S. Ramaswamy. Hydrodynamic fluctuations and instabilities in ordered suspensions of self-propelled particles. *Physical Review Letters*, 89(5):058101_1–058101_4, 2002.

[59] R. Eckert and P. Brehm. Ionic mechanisms of excitation in *Paramecium*. *Annual Review of Biophysics and Bioengineering*, 8(1):353–383, 1979.

[60] M.A. Sleigh. Adaptations of ciliary systems for the propulsion of water and mucus. *Comparative Biochemistry and Physiology Part A: Physiology*, 94(2):359–364, 1989.

[61] H. Winet. Wall drag on free-moving ciliated micro-organisms. *Journal of Experimental Biology*, 59(3):753–766, 1973.

[62] H. Winet. Ciliary propulsion of objects in tubes: wall drag on swimming *Tetrahymena* (ciliata) in the presence of mucin and other long-chain polymers. *Journal of Experimental Biology*, 64(2):283–302, 1976.

[63] S.R. Keller and T.Y. Wu. A porous prolate-spheroidal model for ciliated micro-organisms. *Journal of Fluid Mechanics*, 80(2):259–278, 1977.

[64] J. Kim, Y. Jang, D. Byun, M. Kim, S.W. Nam, and S. Park. Quantitative measurement of dynamic flow induced by *Tetrahymena pyriformis* (*T. pyriformis*) using micro-particle image velocimetry. *Journal of Visualization*, pages 1–10, 2011.

[65] T. Ishikawa and M. Hota. Interaction of two swimming *Paramecia*. *Journal of Experimental Biology*, 209(22):4452–4463, 2006.

[66] G.I. Taylor. Analysis of the swimming of microscopic organisms. *Proceedings of the Royal Society of London. Series A. Mathematical and Physical Sciences*, 209(1099):447–461, 1951.

[67] J. Gray and G.J. Hancock. The propulsion of sea-urchin spermatozoa. *Journal of Experimental Biology*, 32(4):802–814, 1955.

[68] J.R. Blake. Infinite models for ciliary propulsion. *Journal of Fluid Mechanics*, 49(02):209–222, 1971.

[69] J.R. Blake. A spherical envelope approach to ciliary propulsion. *Journal of Fluid Mechanics*, 46(1):199–208, 1971.

[70] J.R. Blake. A model for the micro-structure in ciliated organisms. *Journal of Fluid Mechanics*, 55(1):1–23, 1972.

[71] J.R. Blake. A finite model for ciliated microorganisms. *Journal of Biomechanics*, 6(2):133–140, 1973.

[72] E.M. Purcell. Life at low reynolds number. *American Journal of Physics*, 45(1):3–11, 1977.

[73] G.K. Batchelor. The stress system in a suspension of force-free particles. *Journal of Fluid Mechanics*, 41(3):545–570, 1970.

[74] A.T. Chwang and T.Y. Wu. Hydromechanics of low-reynolds-number flow. part 2. singularity method for stokes flows. *Journal of Fluid Mechanics*, 67:787–815, 1 1975.

[75] A.T. Chwang and T.Y. Wu. Hydromechanics of low-reynolds-number flow. part 1. rotation of axisymmetric prolate bodies. *Journal of Fluid Mechanics*, 63(3):607–622, 1974.

[76] R.E. Johnson and T.Y. Wu. Hydromechanics of low-reynolds-number flow. part 5. motion of a slender torus. *Journal of Fluid Mechanics*, 95:263–277, 1979.

[77] A.T. Chwang and T.Y. Wu. Hydromechanics of low-reynolds-number flow. part 4. translation of spheroids. *Journal of Fluid Mechanics*, 75(4):677–689, 1976.

[78] J.R. Blake and A.T. Chwang. Fundamental singularities of viscous flow. *Journal of Engineering Mathematics*, 8(1):23–29, 1974.

[79] J.R. Blake, S.R. Otto, and D.A. Blake. Filter feeding, chaotic filtration, and a blinking stokeslet. *Theoretical and Computational Fluid Dynamics*, 10(1):23–36, 1998.

[80] M. Sauzade, G.J. Elfring, and E. Lauga. Taylor's swimming sheet: Analysis and improvement of the perturbation series. *Physica D: Nonlinear Phenomena*, 240(20):1567–1573, 2011.

[81] C. Wollin and H. Stark. Metachronal waves in a chain of rowers with hydrodynamic interactions. *The European Physical Journal E: Soft Matter and Biological Physics*, 34(4):1–10, 2011.

[82] B. Guirao and J.F. Joanny. Spontaneous creation of macroscopic flow and metachronal waves in an array of cilia. *Biophysical Journal*, 92(6):1900–1917, 2007.

[83] D.J. Smith, E.A. Gaffney, and J.R. Blake. Mathematical modelling of cilia-driven transport of biological fluids. *Proceedings of the Royal Society A: Mathematical, Physical and Engineering Science*, 465(2108):2417–2439, 2009.

[84] A.T. Chwang and T.Y. Wu. A note on the helical movement of micro-organisms. *Proceedings of the Royal Society of London. Series B. Biological Sciences*, 178(1052):327–346, 1971.

[85] T.W. Su, L. Xue, and A. Ozcan. High-throughput lens-free 3d tracking of human sperms reveals rare statistics of helical trajectories. *Proceedings of the National Academy of Sciences*, 2012.

[86] B.M. Friedrich and F. Jülicher. Chemotaxis of sperm cells. *Proceedings of the National Academy of Sciences*, 104(33):13256–13261, 2007.

[87] T. Fenchel. How dinoflagellates swim. *Protist*, 152(4):329–338, 2001.

[88] J. Sheng, E. Malkiel, J. Katz, J. Adolf, and R. Belas. Digital holographic microscopy reveals prey-induced changes in swimming behavior of predatory dinoflagellates. *Proceedings of the National Academy of Sciences*, 104(44):17512, 2007.

[89] F. Bartumeus, F. Peters, S. Pueyo, C. Marrasé, and J. Catalan. Helical lévy walks: adjusting searching statistics to resource availability in microzooplankton. *Proceedings of the National Academy of Sciences*, 100(22):12771–12775, 2003.

[90] H.C. Crenshaw. Kinematics of helical motion of microorganisms capable of motion with four degrees of freedom. *Biophysical Journal*, 56(5):1029–1035, 1989.

[91] H.C. Crenshaw. Orientation by helical motion—i. kinematics of the helical motion of organisms with up to six degrees of freedom. *Bulletin of Mathematical Biology*, 55(1):197–212, 1993.

[92] H.C. Crenshaw and L. Edelstein-Keshet. Orientation by helical motion—ii. changing the direction of the axis of motion. *Bulletin of Mathematical Biology*, 55(1):213–230, 1993.

[93] G. Jékely, J. Colombelli, H. Hausen, K. Guy, E. Stelzer, F. Nédélec, and D. Arendt. Mechanism of phototaxis in marine zooplankton. *Nature*, 456(7220):395–399, 2008.

[94] P.R. Jonsson and M. Johansson. Swimming behaviour, patch exploitation and dispersal capacity of a marine benthic ciliate in flume flow. *Journal of Experimental Marine Biology and Ecology*, 215(1):135–153, 1997.

[95] J.F. Darbyshire. The use of soil biofilms for observing protozoan movement and feeding. *FEMS microbiology Letters*, 244(2):329–333, 2005.

[96] L. Cisneros, C. Dombrowski, R.E. Goldstein, and J.O. Kessler. Reversal of bacterial locomotion at an obstacle. *Physical Review E*, 73(3):030901, 2006.

[97] J.S. Guasto, R. Rusconi, and R. Stocker. Fluid mechanics of planktonic microorganisms. *Annual Review of Fluid Mechanics*, 44(1), 2012.

[98] S. Takeuchi, W.R. DiLuzio, D.B. Weibel, and G.M. Whitesides. Controlling the shape of filamentous cells of *Escherichia coli*. *Nano Letters*, 5(9):1819–1823, 2005.

[99] N. Minc, A. Boudaoud, and F. Chang. Mechanical forces of fission yeast growth. *Current Biology*, 19(13):1096–1101, 2009.

[100] T.J. Pedley and S.J. Hill. Large-amplitude undulatory fish swimming: fluid mechanics coupled to internal mechanics. *Journal of Experimental Biology*, 202(23):3431–3438, 1999.

[101] E.D. Tytell and G.V. Lauder. Hydrodynamics of the escape response in bluegill sunfish, *Lepomis macrochirus*. *Journal of Experimental Biology*, 211(21):3359–3369, 2008.

[102] R. Hara and H. Asai. Electrophysiological responses of *Didinium nasutum* to *Paramecium* capture and mechanical stimulation. *Nature*, 283(5750):869–870, 1980.

[103] A. Hamel, C. Fisch, L. Combettes, P. Dupuis-Williams, and C.N. Baroud. Transitions between three swimming gaits in *Paramecium* escape. *Proceedings of the National Academy of Sciences*, 108(18):7290, 2011.

[104] Y. Xia and G.M. Whitesides. Soft lithography. *Annual Review of Materials Science*, 28(1):153–184, 1998.

[105] M. Arroyo, L. Heltai, D. Millán, and A. DeSimone. Reverse engineering the euglenoid movement. *Proceedings of the National Academy of Sciences*, 109(44):17874–17879, 10 2012.

[106] C. Spoon and W. Grant. Biomechanics of hair cell kinocilia: experimental measurement of kinocilium shaft stiffness and base rotational stiffness with euler–bernoulli and timoshenko beam analysis. *Journal of Experimental Biology*, 214(5):862–870, 2011.

[107] T.G. Kuznetsova, M.N. Starodubtseva, N.I. Yegorenkov, S.A. Chizhik, and R.I. Zhdanov. Atomic force microscopy probing of cell elasticity. *Micron*, 38(8):824–833, 2007.

[108] Y. Deng, M. Sun, and J.W. Shaevitz. Direct measurement of cell wall stress stiffening and turgor pressure in live bacterial cells. *Physical Review Letters*, 107(15):158101, 2011.

[109] S.A. Baba. Flexural rigidity and elastic constant of cilia. *Journal of Experimental Biology*, 56(2):459–467, 1972.

[110] E. Lauga and T.R. Powers. The hydrodynamics of swimming microorganisms. *Reports on Progress in Physics*, 72:096601, 2009.

[111] R. Stocker and W.M. Durham. Tumbling for stealth? *Science*, 325(5939):400–402, 2009.

[112] H. C. Berg and L. Turner. Chemotaxis of bacteria in glass capillary arrays. *Biophysical Journal*, 58(4):919–930, 10 1990.

[113] C. Giuffre, P. Hinow, R. Vogel, T. Ahmed, R. Stocker, T.R. Consi, and J.R. Strickler. The ciliate *Paramecium* shows higher motility in non-uniform chemical landscapes. *PLoS ONE*, 6(4):e15274, 04 2011.

[114] S.A. Biondi, J.A. Quinn, and H. Goldfine. Random motility of swimming bacteria in restricted geometries. *AIChE Journal*, 44(8):1923–1929, 1998.

[115] W. Wang, L.M. Shor, E.J. LeBoeuf, J.P. Wikswo, and D.S. Kosson. Mobility of protozoa through narrow channels. *Applied and environmental microbiology*, 71(8):4628–4637, 2005.

[116] D.F. Katz. On the propulsion of micro-organisms near solid boundaries. *J. Fluid Mech*, 64(1):33–49, 1974.

[117] C. Brennen. An oscillating-boundary-layer theory for ciliary propulsion. *Journal of Fluid Mechanics*, 65(04):799–824, 1974.

[118] K. Fukui and H. Asai. Spiral motion of *Paramecium caudatum* in a small capillary glass tube. *Journal of Eukaryotic Microbiology*, 23(4):559–563, 1976.

[119] A.H. Shapiro, M.Y. Jaffrin, and S.L. Weinberg. Peristaltic pumping with long wavelengths at low reynolds number. *Journal of Fluid Mechanics*, 37(4):799–825, 1969.

[120] M.Y. Jaffrin and A.H. Shapiro. Peristaltic pumping. *Annual Review of Fluid Mechanics*, 3(1):13–37, 1971.

[121] L.G. Leal. *Advanced transport phenomena: fluid mechanics and convective transport processes*. Cambridge University Press, 2007.

[122] J.S. Guasto, K.A. Johnson, and J.P. Gollub. Oscillatory flows induced by microorganisms swimming in two dimensions. *Physical Review Letters*, 105(16):168102, 2010.

[123] D. Tam and AE Hosoi. Optimal feeding and swimming gaits of biflagellated organisms. *Proceedings of the National Academy of Sciences*, 108(3):1001–1006, 2011.

[124] M. Roper, M. J. Dayel, R. E. Pepper, and M. A. R. Koehl. Cooperatively generated stresslet flows supply fresh fluid to multicellular choanoflagellate colonies. *Physical Review Letters*, 110:228104, May 2013.

[125] S.E. Spagnolie and E. Lauga. Hydrodynamics of self-propulsion near a boundary: predictions and accuracy of far-field approximations. *Journal of Fluid Mechanics*, 700:105–147, 2012.

[126] R. Bouffanais, J. Sun, and D.K.P. Yue. Physical limits on cellular directional mechanosensing. *Physical Review E*, 87(5):052716, 2013.

[127] L. Zhu, E. Lauga, and L. Brandt. Low-reynolds-number swimming in a capillary tube. *Journal of Fluid Mechanics*, 726:285–311, 6 2013.

[128] D.B. Weibel, P. Garstecki, D. Ryan, W.R. DiLuzio, M. Mayer, J.E. Seto, and G.M. Whitesides. Microoxen: Microorganisms to move microscale loads. *Proceedings of the National Academy of Sciences of the United States of America*, 102(34):11963–11967, 2005.

[129] A. Sokolov, M.M. Apodaca, B.A. Grzybowski, and I.S. Aranson. Swimming bacteria power microscopic gears. *Proceedings of the National Academy of Sciences*, 107(3):969–974, 2010.